Universitetet i Stavanger

FACULTY OF SCIENCE AND TECHNOLOGY

MASTER'S THESIS

Study programme/specialisation: Petroleum Technology, Reservoir Engineering	Spring semester, 2017 Open
Author: Marco Utsetø	…… (signatur forfatter)
Faculty Supervisor: Prof. Dag Chun Standnes	
Title of master's thesis: **Numerical simulation of co-current and counter-current imbibition**	
Credits: 30	
Keywords: Naturally fractured reservoirs Spontaneous Imbibition Core scale simulation Relative permeability ECLIPSE	Number of pages: 80 + Enclosure: 15 Stavanger, 15.06.2017

This page is intentionally left blank

Numerical simulation of co-current and counter-current imbibition

Marco Utsetø
University of Stavanger
Spring 2017

Supervisors:
Dag Chun Standnes, UiS and Statoil ASA

This page is intentionally left blank

Abstract

Spontaneous imbibition (SI) is a very important mechanism for oil recovery in naturally fractured reservoirs. Several studies have indicated that counter-current oil production is much slower and give lower ultimate oil recovery than that of co-current production. This thesis presents an investigation of the relationship between co-current and counter-current relative permeabilities and their effect on production rates and ultimate oil recovery.

SI into strongly water-wet low-permeability chalk has been investigated by numerical simulations using ECLIPSE 100. Two independent experimental studies have been considered, dividing this thesis into two parts. In part 1 counter-current relative permeability curves obtained by history matching experimental data by Standnes (2004) were used in co-current simulations. Unexpected results were found, in which simulations showed too fast oil recovery rates when counter-current relative permeabilities were included in the model. Further investigation showed inconsistency within experimental data and certain SI tests were considered unrepresentative. As further comparison would give inconsistent results, part 2 was introduced.

For part 2, counter-current simulations were run with co-current relative permeability curves established by history matching experimental data by Bourbiaux and Kalaydjian (1990). Too fast oil recovery rates were observed. The half-recovery time was underestimated by approximately 50 %, which is in agreement with results found by Bourbiaux and Kalaydjian (1990). Exact prediction of counter-current experimental data was obtained by reducing both oil and water relative permeabilities including endpoints, by 50 % or by increasing the Corey exponents for oil and water by 45 %, however, with fixed endpoints. Since SI is described by a diffusion equation model, a relationship between the capillary diffusivity coefficient (CDC) and oil recovery curves for certain SI tests was investigated. A relationship is proposed were the oil recovery curve is expressed as a function of CDC value and curve shape (when plotted against normalized water saturation). The numerical investigation in this thesis underlines the importance of considering both co-current and counter-current conditions when evaluating the oil recovery potential on reservoir rocks experimentally, as inconsistencies may arise when results are scaled to reservoir conditions.

This page is intentionally left blank

Acknowledgements

The work in this thesis was performed at the University of Stavanger, in which I am very thankful for providing the necessary simulation software and computational capacity.

I wish to extend my gratitude to Professor Dag Chun Standnes, who has been my professional supervisor at the University of Stavanger, for giving me the opportunity to write this thesis based on his previous work. Thanks to his exceptional guidance, enthusiasm and level of expertise, the writing of this thesis has been a great learning process.

Table of contents

List of figures

List of tables

1 Introduction and background

1.1 Background

Only a fraction of the original oil in place (OOIP) can be produced by the natural driving mechanisms in a reservoir. This has resulted in a range of methods developed to maintain the reservoir pressure during production. For reservoirs with a natural water drive or expanding gas cap, injection of water is considered as an efficient way to increase oil recovery. This will conventionally displace oil from the pores and towards the production well. However, in the case of a naturally fractured reservoir, the water will flow through the high permeability fracture system and leave most of the oil behind in the matrix blocks. It was not before the 1950s that the process of spontaneous imbibition (SI) was recognized as an important mechanism for increased oil recovery in fractured reservoirs (Brownscombe & Dyes, 1952). If the reservoir is water-wet, the injected water will spontaneously imbibe from the fracture into the matrix due to capillary forces. The imbibition process is sensitive to a range of underlying parameters such as wettability, permeability, viscosity, interfacial tension (IFT) and confining fluid distribution of the matrix.

During water injection, the fracture water level (FWL) will advance and increasingly cover the matrix blocks, dividing the SI process into two modes: counter-current and co-current imbibition (Mattax & Kyte, 1962). Counter-current SI will occur if the rock is totally submersed in water, by which oil is produced from the same surface as water enters the porous medium. On the other hand, for a case where the rock is in contact with an oil phase, water and oil will flow towards the oil-covered surface, by which the oil phase can be produced. Thus, the two fluid phases flow in the same direction, also known as co-current flow. Figure 1.1 illustrates the difference between counter-current and co-current SI into a cubic rock sample.

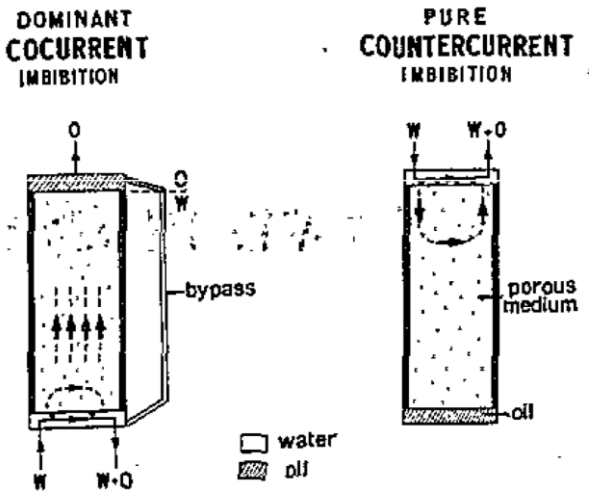

Figure 1.1: Illustration of boundary conditions for co-current and counter-current SI (Bourbiaux & Kalaydjian, 1990)

Counter-current SI is regarded as the most important driving mechanism of the two modes and has received more attention through experimental and numerical papers (Hamon & Vidal, 1986; Ma, Morrow, & Zhang, 1997; Mattax & Kyte, 1962; Torsæter, 1985; Zhang, Morrow, & Ma, 1995). Of the reported literature, a great quantity is related to qualitative investigations of the effects of boundary conditions and sample shape. Lately, more attention has been directed towards the difference between the two SI modes, in which observations have showed both faster recovery rates and higher ultimate oil recovery for co-current SI than for counter-current SI.

Pooladi-Darvish and Firoozabadi (2000); Pooladi-Darvish and Firoozabadi (1998) investigated differences between co-current and counter-current imbibition into matrix blocks of Berea and Kansas chalk. They found that when a water-wet porous medium is partially in contact with oil, co-current imbibition will be the dominant production mechanism, not counter-current. It was also observed that co-current imbibition is more efficient than counter-current imbibition, in relation to recovery rates and ultimate recovery.

In 1990 Bourbiaux & Kalaydjian performed an experimental study on co-current and counter-current flows in natural porous medium. The results showed that the rate of co-current oil production is much faster than for counter-current production. They also compared simulated and experimental oil recoveries for the two SI modes, in which co-current relative permeability curves did not give exact prediction of counter-current recvoery rates. However, good prediction was obtained by reducing the co-current relative permeability curves by 30 %. Bourbiaux & Kalaydjian also discovered higher ultimate recoveries for co-current oil production, yet emphasized the need for further ivestigation of this point.

Standnes (2004) studied the impact of boundary conditions on oil recovery by co-current and counter-current spontaneous imbibition. Not only did he discover that oil recovery induced by both SI modes is highly dependent on sample shape, size and boundary conditions, but also that counter-current SI tests showed significantly lower production rates and ultimate oil recoveries. Similar results were found by (Unsal, Mason, Morrow, & Ruth, 2009) and (Karimaie, Torsæter, Esfahani, Dadashpour, & Hashemi, 2006).

Sherafati and Jessen (2017) investigated the impact of mobility changes due to reversals from co-current to counter-current flow on the displacement performance of water alternating gas (WAG) injection preocesses. They concluded that using a single set of relative permeability curves for the simulation of WAG processes may not provide sufficient physical detail for accurate design of such processes. This suggests that the relationship between co-current and counter-current flow could be important for many aspects of displacement dynamics

1.2 Objective

For optimal reservoir simulation, it is essential to have detailed knowledge about the underlaying mechanisms critical to the problem under consideration. Input parameters must be properly understood in order to model their effect. Since laboratory measurments in most cases are carried out on co-current flow conditions, this may overestimate both production rate and ultimate oil recovery if counter-current SI is the dominating production mechanism. Hence, to prevent a optimistic oil prediction, theoretical interpretations of the imbition process must taken into account when performing numerical simulations. This will provide a better understanding of the real difference between co-current and counter-current relative permeabilites, both qualitatively and quantitatively.

The main objective of this thesis is to investigate the relationship between co-current and counter-current relative permeabilities and their effect on oil recovery curves.

Objectives of this thesis:

- Establish capillary pressure curve and a set of relative permeability curves for a basecase by history matching experimental data with ECLIPSE 100 simulation software.
- Use the obtained capillary pressure curve and relative permeability curves in simulations of further SI tests and compare with experimental data.

Part 1

- Quantitatively test if simulations with counter-current relative permeabilities will reproduce co-current experimental data. Referring to part 1, experimental data by Standnes (2004)
- Qualitatively test if co-current experimental data can be reproduced by increasing counter-current relative permeabilities. Referring to part 1, experimental data by Standnes (2004)

Part 2

- Quantitatively test if simulations with co-current relative permeabilities will reproduce counter-current experimental data. Referring to part 2, experimental data by Bourbiaux and Kalaydjian (1990)
- Quantitatively test how much co-current relative permeabilities must be reduced to match counter-current experimental data. Referring to part 2, experimental data by Bourbiaux and Kalaydjian (1990)
- Qualitatively test different combinations of relative permeability inputs to obtain approximately the same response (recovery rates). Compare results when endpoint relative permeabilities are reduced or kept constant. Referring to part 2, experimental data by Bourbiaux and Kalaydjian (1990)
- Qualitatively test the relationship between oil recovery and CDC, both with respect to value and shape. Referring to part 2, experimental data by Bourbiaux and Kalaydjian (1990)

1.3 Organization of this thesis

The thesis is divided into two parts. Part 1 is based on the work by Standnes (2004), in which a set of relative permeability curves and capillary pressure curves were established from history matching counter-current experimental results with ECLIPSE 100. Furthermore, the counter-current relative permeability curves were used to simulate co-current SI tests, in which results were compared to co-current experimental data. Counter-current relative permeability curves were then adjusted to match co-current experimental data.

Part 2 is based on a study by Bourbiaux and Kalaydjian (1990). Here, counter-current simulations were run with co-current relative permeability curves obtained from history matching. Furthermore, the simulations were compared with counter-current experimental data and adjusted until a match was obtained. The adjustment factors were compared with results found by Bourbiaux and Kalaydjian (1990). The procedure of adjusting relative permeability curves was further studied, in which two methods were compared: reduce relative permeability curve including endpoint values or keep the endpoint values constant by only increasing the Corey exponents. Lastly, a relationship between oil recovery curves and the CDC for certain SI tests was investigated. Figure 1.2 shows the procedure of investigation performed in this thesis.

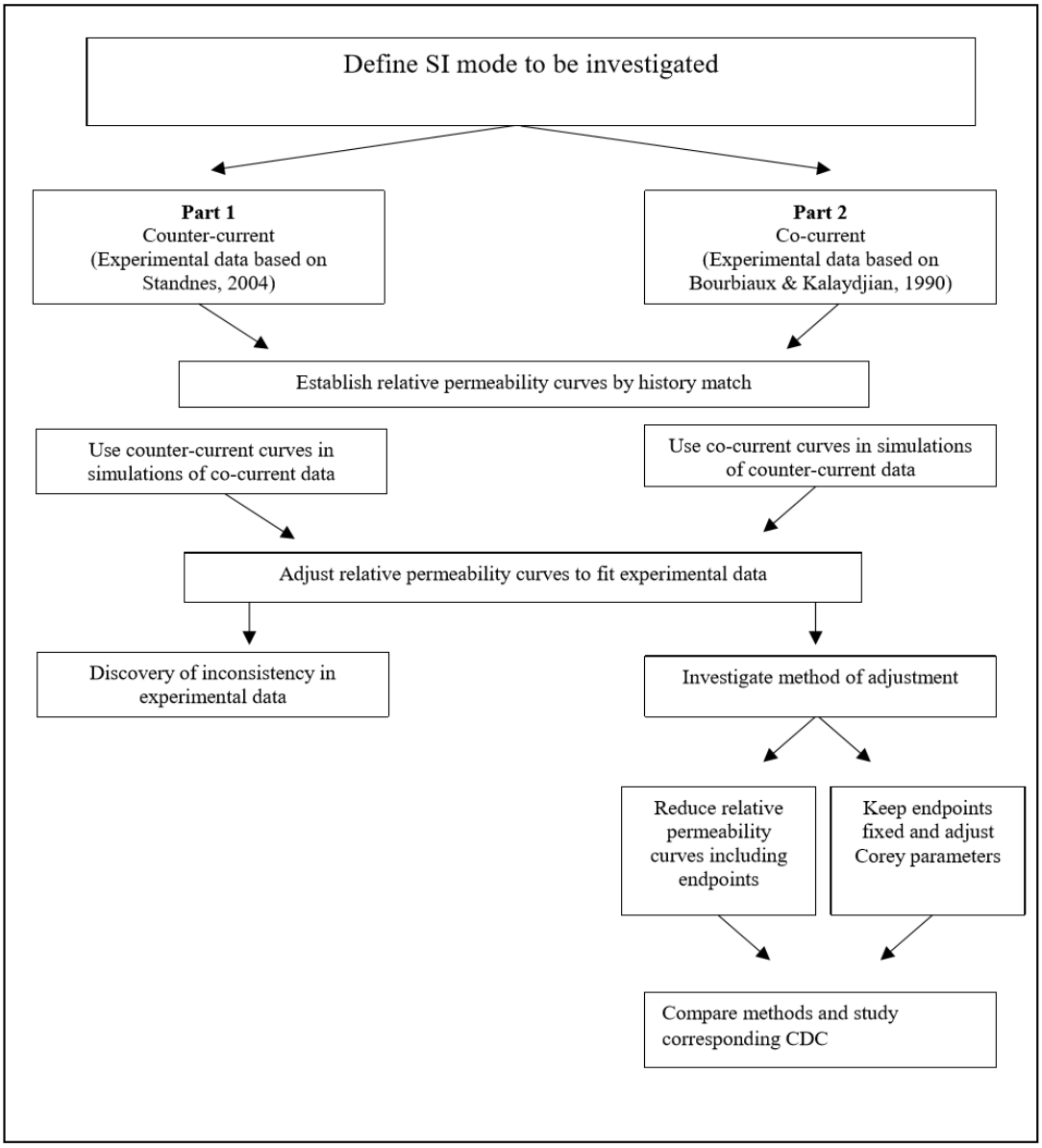

Figure 1.2: Procedure of investigation performed in this thesis.

2 Theory

2.1 Modelling of fractured reservoirs

The understanding and modelling of naturally fractured reservoirs present the idea of a reservoir that is divided into two different media; matrix and fractures. The matrix is described as the main source for hydrocarbons, with high storage capacity, but low permeability. On the other hand, fractures are recognised for having low storage capacity, but high permeability. As the two media exhibit such opposing characteristics, it will encourage a matrix-fracture fluid exchange. To describe this fluid exchange in a fractured porous medium, the concept of dual-porosity is arguably the most recognized model in the history of petroleum reservoir engineering.

The first developments of the dual-porosity model was introduced in the 1960s by Warren and Root (1963) and further incorporated into a numerical model for fluid flow on a large scale by Kazemi, Merrill Jr, Porterfield, and Zeman (1976). In later time, much research has been performed to further improve numerical modelling of naturally fractured reservoirs using dual-porosity models (Uleberg & Kleppe, 1996). Special attention has been directed towards the challenge of properly representing the imbibition process and gravity drainage. Some authors have tried to represent correct behaviour with formulations including a gravity term that assumes a simplified fluid distribution in the matrix (Gilman & Kazemi, 1988; Sonier, Souillard, & Blaskovich, 1988). Others have focused on pseudo-capillary-pressure for the matrix, fracture or both, in which a simplified matrix fluid distribution is assumed, or obtained through history matching with a fine-grid model of a single matrix block (Dean & Lo, 1988; Rossen & Shen, 1989; Thomas, Dixon, & Pierson, 1983).

To illustrate the complex behaviour of a naturally fracture reservoir, Warren and Root (1963) proposed a simplified idealization where the reservoir is modelled as numerous discrete volumetric elements to represent the matrix, coupled by surrounding interconnected voids for the fractures. The concept of dual porosity can now be related to this simplified idealization, in which the matrix represents primary porosity and the fractures represent secondary porosity. Figure 2.1 depicts an illustration of the simplified idealization of the heterogenous porous medium (Warren & Root, 1963).

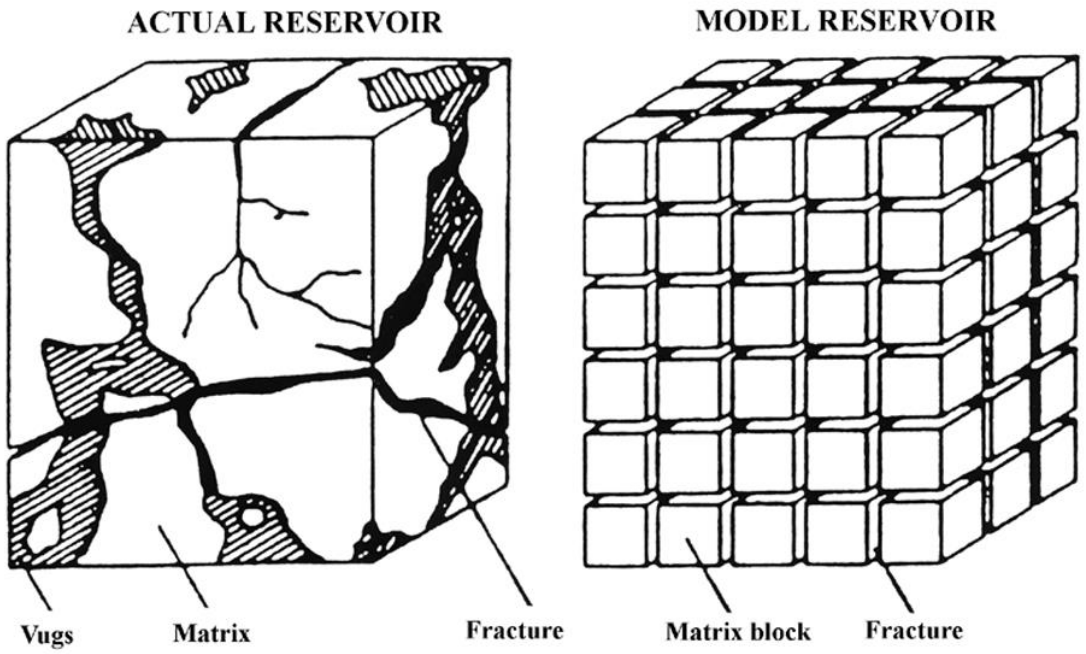

Figure 2.1: idealization of the heterogenous porous medium (Warren & Root, 1963).

The fluid exchange between matrix and fractures in the apparent dual-porosity model are calculated by so called transfer functions. However, due to the extensive number of grid blocks employed in today's reservoir simulators, an individual computation for each block would be impossible. Hence, various attempts have been made to find a solution for this challenge. As a result, Uleberg and Kleppe (1996) presented in 1996, a new concept for improving the simulation of fractured reservoirs. They further developed the idea of having multiple grids to represent the reservoir model. The idea was to introduce large-scale coarse grid blocks, each with a number of small matrix blocks inside. Then, by selecting the large-scale grid blocks such that all the matrix blocks inside exhibit similar behaviour, the calculated results from one small matrix block could be multiplied with the number of matrix blocks present in the large grid block (Uleberg & Kleppe, 1996). This suggests that data from laboratory experiments on small core samples could implemented into large scale simulators for actual reservoirs. An illustration of the multiple grid concept is shown in Figure 2.2.

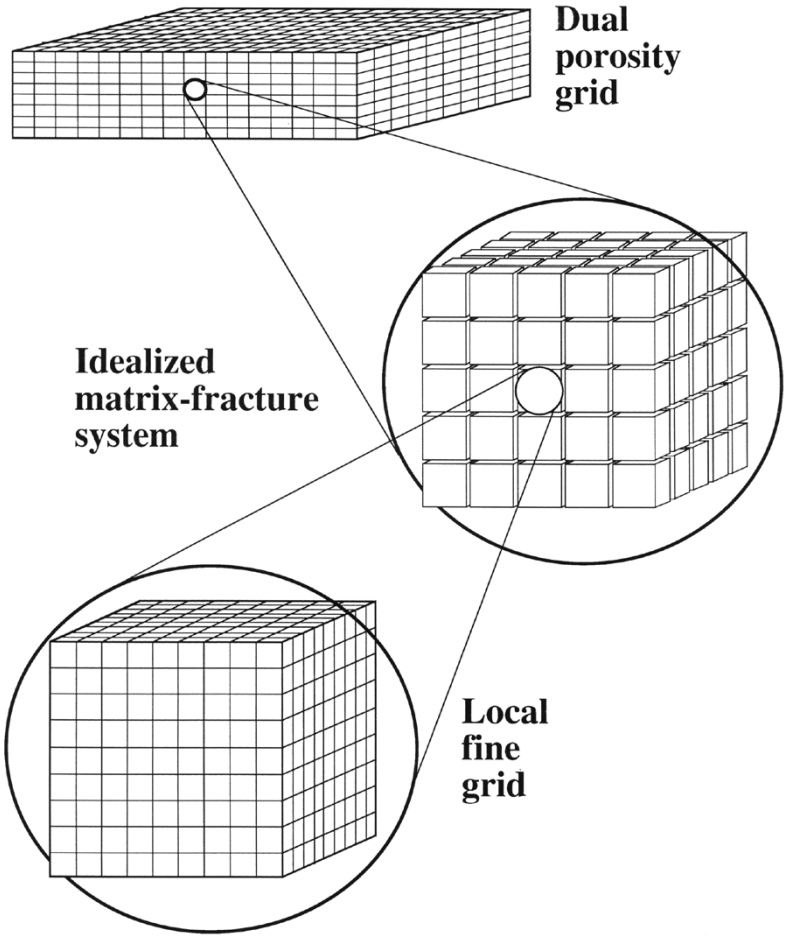

Figure 2.2: Multiple grid concept for fractured reservoir simulation (Warren & Root, 1963).

In a natural fractured reservoir, the fracture-matrix fluid exchange is not always straightforward. Because water follows the path of least resistance, oil tends to be bypassed and left behind in the matrix blocks. This would naturally result in lower ultimate oil recoveries. However, if the reservoir rock exhibit water-wet characteristics the water will imbibe spontaneously into the matrix blocks due to capillary forces and simultaneously expel oil to the fracture system. This mechanism, referred to as spontaneous imbibition (SI), did not receive much attention before the 1950s in relation to the highly fractured Spraberry field in west Texas (Brownscombe & Dyes, 1952). Since then, the subject has undergone numerous investigations which is reflected in the number of publications. Today, spontaneous imbibition is regarded as one of the most important driving mechanisms for oil recovery in fractured reservoirs, yet, with great potential for further research. The SI process is very complex and is effected by a range of different parameters. This includes wettability, permeability, shape and size of the reservoir rock (matrix) in addition to viscosities and interfacial tension (IFT) of the fluids involved. It can be argued that the understanding of a bigger picture depends on the understanding of the basic concepts. Hence, to facilitate further discussion of spontaneous imbibition, a review of the parameters controlling the process may be helpful.

2.2 Wettability

Wettability is defined as "*the tendency of one fluid to spread on or adhere to a solid surface in the presence of other immiscible fluids*" (Craig, 1971). Understanding the wettability preference of a reservoir is of great importance where it directly impacts the driving forces in hydrocarbon recovery (Anderson, 1986; Morrow et al., 2006; Ursin & Zolotukhin, 1997). The wettability of the reservoir rock is controlled by interfacial tension acting on fluid-fluid and fluid-rock interface of the reservoir rock and strongly influences the distribution and flow of oil and water during production. The reason for this can be explained by the effect of contact angles between fluids, which was introduced by Young (1805).

For an oil drop floating in water, where the densities are equal and no external forces exist, the interface of the oil drop tends to take a spherical shape, to minimize the surface area, Figure 2.3 (Ursin & Zolotukhin, 1997).

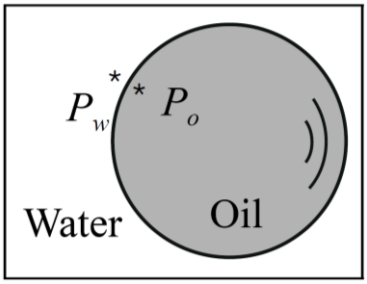

Figure 2.3: Pressure difference between two fluids across a curved interphase (Ursin & Zolotukhin, 1997).

On the other hand, for a system where two immiscible fluids are placed on some surface, a contact angle will be developed when the fluids come in contact with each other, if none of the fluids are spreading on the surface. The equilibrium that the droplet exhibits will depend on the surface tensions between all three phases and will be a direct measurement of the wettability preference of the surface. For such a system, the wetting angle can be determined from the following equation:

$$\sigma_{ow} \cos\theta = \sigma_{so} - \sigma_{sw} \quad \textbf{(1)}$$

where θ is the contact angle at the oil-water-solid interface measured through the water and σ_{ow}, σ_{so}, σ_{sw} are the surface tensions between oil-water, surface-oil and surface-water, respectively.

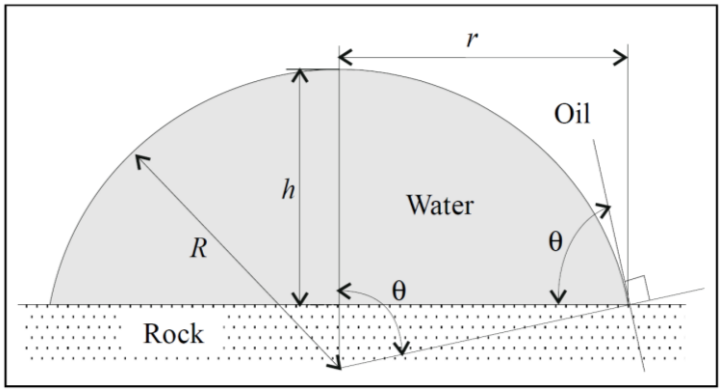

Figure 2.4: Geometry of the water droplet in oil, placed in a contact with a water-wet reservoir rock (Ursin & Zolotukhin, 1997).

The wettability of a solid surface can be divided into three preferences; water-wet, neutral-wet and oil-wet, for which a corresponding contact-angle interval exists. For angles between 0° and 90°, the surface favours water above oil and is referred to as water-wet. Furthermore, a neutrally water-wet system corresponds to a contact angle of 90°, signifying that both fluids have equal preferences for the surface. Finally, for contact angles above 90°, the system is oil-wet and that the surface favours oil rather than water. Figure 2.5 illustrates the three wettability situations with corresponding contact-angle intervals, respectively.

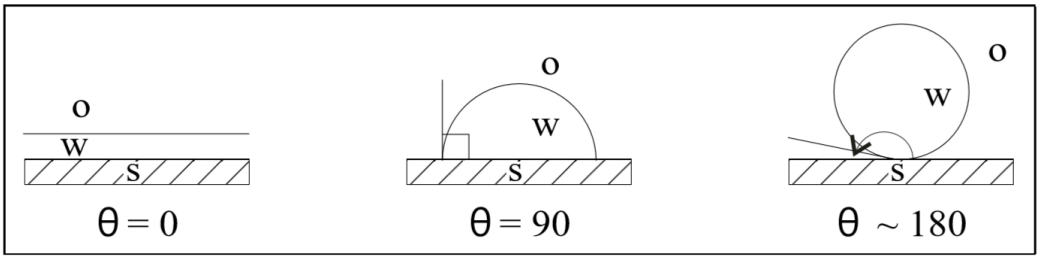

Figure 2.5: Example of wetting phase (Ursin & Zolotukhin, 1997).

2.2.1 Wettability measurements

In 1986, Anderson (1986) published an extensive literature survey on wettability measurement where three quantitative methods were discussed; the contact angle, Amott method and the USBM (United States Bureau of Mines) method. It was concluded that each of the three methods have their advantages and disadvantages for certain experimental designs. It can be argued that the extended Amott-Harvey method (Anderson, 1986) based on Amott (1959) is the most celebrated method for quantitative wettability measurements used in the petroleum industry. Compared to the contact angle method, the Amott-Harvey method is more practical where it is based on measuring the amount of fluid imbibed spontaneously or by force. The method can be described as a procedure consisting of the five following steps: Establish the initial water saturation (S_{wi}) of the core sample; immerse the core in water and let

the water imbibe spontaneously into the rock sample until S_{ws} is reached; flood the core with water in order to reach residual oil saturation; immerse the core in oil and let oil imbibe spontaneously into the rock sample S_{os} is reached; flood the core with oil until residual water saturation is reached. Figure 2.6 depicts an illustration of the parameters involved in the five-step procedure for determining wettability with the Amott-Harvey test.

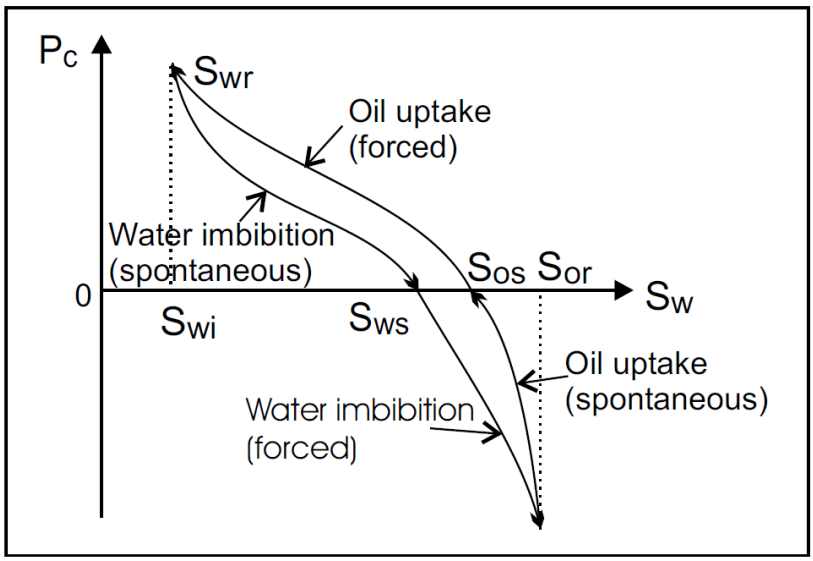

Figure 2.6: Capillary pressure vs. water saturation, illustrating the parameters needed to calculated Amott-Harvey (Standnes, 2001).

The measured fluid saturations are then used to calculate the water index, I_w, and the oil index, I_o by the following formulas:

$$I_w = \frac{S_{ws} - S_{wi}}{S_{or} - S_{wi}} \qquad I_o = \frac{S_{or} - S_{os}}{S_{or} - S_{wr}}$$

which ultimately gives the Amott-Harvey wettability index, $I_{A\text{-}H}$:

$$I_{A-H} = I_w - I_o$$

where S_{wi} =Initial water saturation; S_{ws} =Water saturation after SI; S_{or} =Water saturation after forced imbibition; S_{os} =Water saturation after spontaneous imbibition of oil; S_{wr} =Water saturation after forced imbibition of oil. For a strongly water-wet system, $I_{A\text{-}H}$ will be equal to +1, while strongly oil-wet systems will give a value of -1. Table 1 depicts a more detailed description of the wettability index, introduced by Cuiec (1984).

Table 1: Wettability preference expressed by Amott-Harvey index, I_{A-H} (Cuiec, 1984).

Wettability preference	Amott-Harvey wettability index, I_{A-H}
Water-wet	$+0.3 \leq I_{A-H} \leq +1$
Intermediate	$-0.3 \leq I_{A-H} \leq +0.3$
Oil-wet	$-0.3 \leq I_{A-H} \leq -1$

2.3 Capillary pressure

Capillary pressure is defined as the pressure difference across a curved interface between two immiscible fluids in a porous medium. The interface which separates the two immiscible fluids is characterized by some surface energy. In order to balance the equilibrium pressures of the two fluids when passing over this interface, a pressure difference will be observed. It is in fact this pressure difference that is called the capillary pressure, which is given by Laplace equation (1806):

$$P_c = P_o - P_w = \sigma_{ow}\left(\frac{1}{R_1} + \frac{1}{R_2}\right) \quad \textbf{(2)}$$

where in this thesis, oil is considered the non-wetting phase. Then: P_c = Capillary pressure; P_o =Pressure in oil phase; P_w =Pressure in water phase; σ_{ow} =Interfacial tension (IFT) between oil and water; R_1, R_2 =radii of the curved interface separating oil and water.

To describe the process of fluid displacement in a porous medium, a capillary tube can be used as a simplified representation of a single pore throat in the reservoir rock. Furthermore, when the radii of the curved interface between water and oil are equal, $R_1 = R_2 = R$, the radius of the capillary tube can be written in terms of the radius of the interfacial tension surface:

$$R_{tube} = R * \cos\theta \quad \textbf{(3)}$$

where θ is the contact angle and R_{tube} is the radius of the capillary tube. Subsequently, it follows that the relationship between capillary pressure, interfacial tension, contact angle and tube radius can be expressed by the following equation:

$$P_c = P_o - P_w = \frac{2\,\sigma_{ow} \cdot \cos\theta}{R_{tube}} \quad \textbf{(4)}$$

Then, by using an example where oil and water are placed in a water-wet capillary tube, the capillary pressure is given as the pressure in the oil phase minus the pressure in the water phase. Moreover, it is

the wettability preference of the surface of the porous medium that will determine the shape of the oil-water interface. This phenomenon is illustrated in Figure 2.7 where the fluid of which exhibit the greatest attraction towards the porous medium will displace the other fluid. Consequently, the pressure will always be lower in the fluid phase that occupies the concave side of the interface.

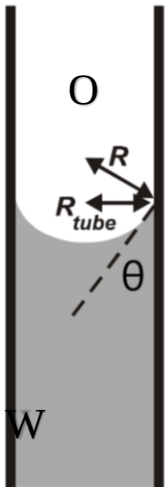

Figure 2.7: Capillary tube model, illustrating the curved interface between oil and water due to wettability preference of the tube wall (Glover, 2002).

By extending the capillary tube analogy, the reservoir can be conseptualized as a bundle of capillary tubes with varying radii and identical wettability preference. The pressure that exist inside each of the capillary tubes tend to pull the water up to a height h above the free water level. This concept is known as capillary rise, where the height h of which the water rises can be directly related to the pressure that is needed for the non-wetting fluid to displcae the wetting fluid at a given pore radius. Because the capillary pressure is inversly proportinal to the tube radius, it signifies that higher capillary pressures are needed in order to invade the smallest pores in the reservoir. The pore size distribution will therefore define the equlibrium saturation distribtuion of a reservoir after oil has migrated from source rock into water filled pore space. This process is also known as drainage, which occurs when the pressure in the oil phase exceeds the pressure in the water phase by a specific value. The value is called the reservoir treshold pressure P_{cd}, which is the pressure needed for oil to enter the largest pores in the distribution (Szymkiewicz, 2012). Furthermore, as the capillary pressure inreases, the water saturation will approach irreducable water saturation S_{ir}, in which no more water will be displaced. The drainage process described corresponds to the so-called primary drainage curve, depicted in Figure 2.8.

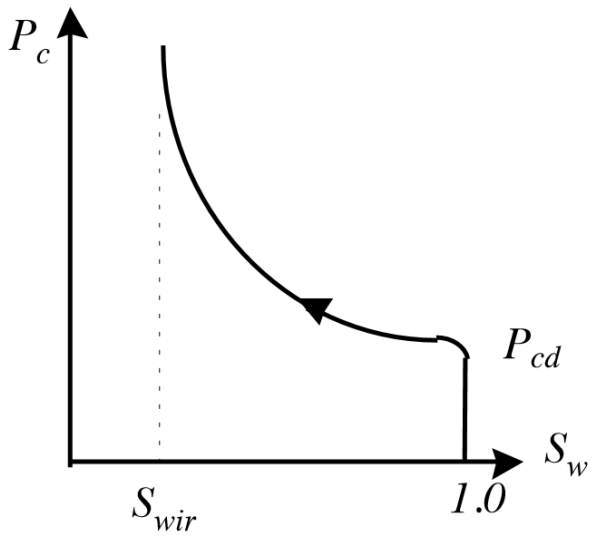

Figure 2.8: Illustration of the drainage process (J. Kleppe, 2014).

A complementary relationship exists for the process of which the water invades the pore space of an initially oil filled reservoir, also known as imbibition. If no external force is apllied to the system, the imbibition process is defined as spontaneous. The capillary pressure is greatest at irreducible water saturation S_{wir} (or $S_{wr)}$, in which only the smallest pores of the core is filled with water. This is the water that could not be displaced by the oil during drainage. As the water starts to invade largest pores of the core, the water saturation increases and the capillary pressure starts to decrease. The rate of which the water will spontaneously imbibe will be directly proportional to the strength of capillary forces (Cuiec, 1984). The water will spontaneously imbibe into the rock until the capillary pressure approaches zero and S_{ws} is reached. Then, if external forces are applied to the system, forced imbibition will continue until ultimate water saturation $1\text{-}S_{or}$ is reached. At this stage, no more oil will be displaced and a residual oil saturation is left in the reservoir rock. The spontaneous imbibition curve is illustrated in Figure 2.9.

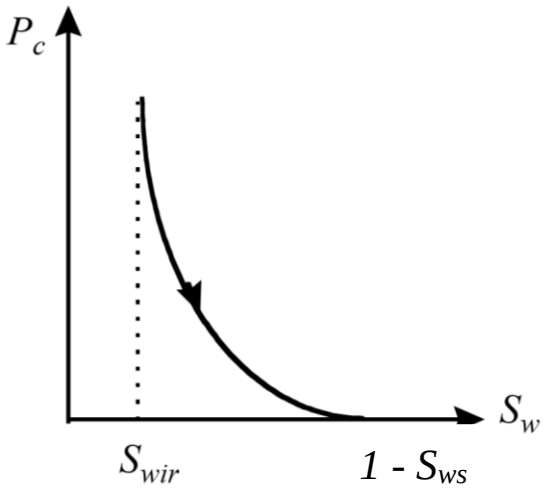

Figure 2.9: : Illustration of the imbibition process (J. Kleppe, 2014).

By combining the drainage- and imbibition curve in the same figure, a total capillary curve is obtaned. It is the total capillary pressure curve that is used to describe how the water saturation will vary throughout the reservoir as a function of the capillary pressure. Hence, much information about the quality of the reservoir can be obtained by studying the shape of the curve. For example, if the reservoir has very homogeneous pore size distribution, most of the pores will be invaded at the same time and the capillary curve will be very steep. On the other hand, a much more gradual curve will be observed where the pores show large heterogeneity. It can be seen from Figure 2.10 that the drainage curve shows greater values than for the imbibition curve at a given water saturation. This phenomenon is termed hysteresis and is explained by variations in the wetting angle between the fluid entering the pore channel and the fluid being expelled (Pinder & Gray, 2008). The fact that the capillary pressure is larger for drainage than for imbibition is because the drainage process is controlled by the small diameter pores whereas the larger diameter pores control imbibition.

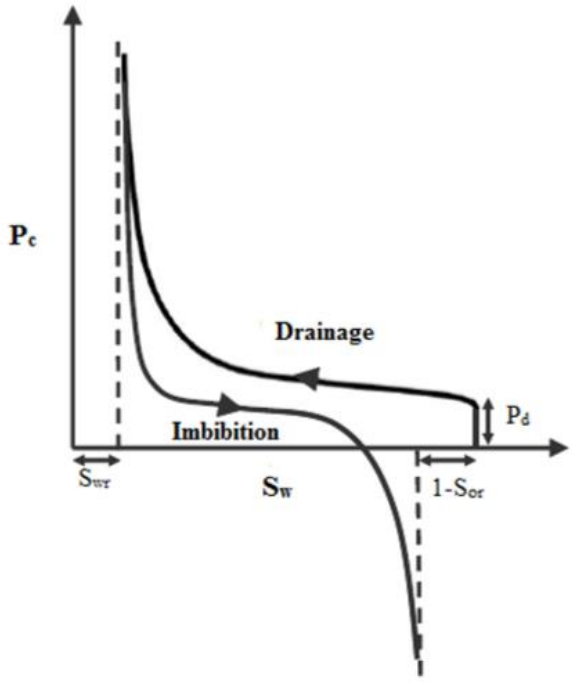

Figure 2.10: illustration of total capillary curve, showing drainage- and imbibition process (Espevold, 2015).

There are several ways of obtaining a capillary pressure curve based on laboratory measurements, which includes centrifuge-, mercury- and porous-plate methods. However, for numerical investigation it would be convenient to express the capillary curve as an analytical function. Today, several analytical models are available, where the input parameters depend on the problem under consideration. For this thesis, the primary topic of interest is to investigate the process of imbibition with ECLIPSE simulation

software. In order to do so, the capillary pressure curve is included into the model as tabulated values for corresponding water saturation. Consequently, it was decided that model developed by Skjaeveland (1998) was the most suitable option to obtain accurate simulation of the porous medium. The capillary pressure is given by the Skjaeveland expression:

$$P_c = \frac{C_w}{\left(\frac{S_w - S_{wr}}{1 - S_{wr}}\right)^{a_w}} + \frac{C_o}{\left(\frac{S_o - S_{or}}{1 - S_{or}}\right)^{a_o}} \quad \textbf{(5)}$$

where P_c =Capillary pressure (atm); S_w =Water saturation; S_{wr} =Irreducible water saturation; S_o =Oil saturation; S_{or} =Residual oil saturation; C_w and a_w =Constants adjusting contribution from water to P_c; C_o and a_o =Constants adjusting contribution from oil to P_c. The correlation described above is originally designed for a mixed-wet system, where the C_o constant is a negative value. The model can however easily be applied for completely water-wet systems by using small values for the constants adjusting the contribution from the oil to the capillary pressure.

2.4 Flow functions

As the capillary pressure curve describes how water vary throughout the reservoir, another relationship is needed to describe the relative fractions of fluid saturations in a system occupied by more than one fluid phase. This introduces the concept of relative permeability, which is defined as the effective permeability of a fluid l, relative to the absolute permeability of a porous medium:

$$k_{rl} = \frac{k_l}{K} \quad \textbf{(6)}$$

where l denotes the fluid type (oil, water) and K is the absolute permeability of the porous medium. Given a process where water spontaneously displaces oil in a water-wet system, the relative permeabilities can be expressed as a function of fluid saturations. For a porous medium with initial oil saturation equal to S_{oi}, the water relative permeability will vary from k_{rw} =0 for S_w =S_{wir} to k_{rw} =k_{rw}* (maximum water relative permeability) at S_w =1-S_{or}. At the same time, the oil relative permeability will vary from k_{ro} = k_{ro}* (maximum oil relative permeability) for S_o =1-S_{wir} to k_{ro} = 0 at S_o =S_{or}. This relationship is more conveniently represented by relative permeability curves, depicted in Figure 2.11.

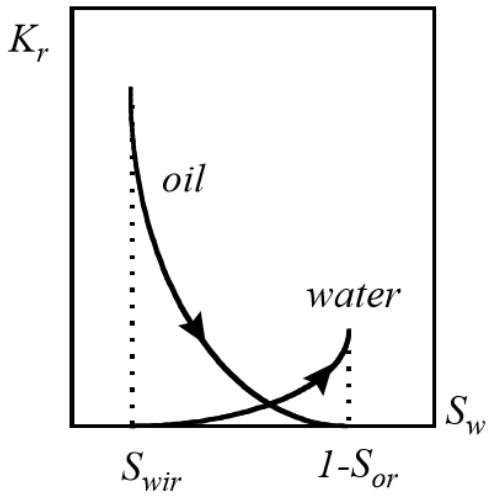

Figure 2.11: Spontaneous imbibition of water into water-wet oil filled core (J. Kleppe, 2014).

To solve the numerical model with ECLIPSE, the relative permeability functions must also be implemented as tabulated values, under the same keyword as for the capillary pressure. However, if the permeability is measured in the laboratory, only endpoint values and a few values is used to describe the relative permeability curve. Therefore, analytical models are used to obtain more complete curves which include additional data-points in between the ones measured. In this thesis, the modified Corey type expression (Standing, 1974) was used to construct relative permeability curves for oil and water:

$$k_{rw} = k_{rw}^{*} \left(\frac{S_w - S_{wi}}{1 - S_{or} - S_{wi}} \right)^{n_w} \quad \textbf{(7)}$$

$$k_{ro} = k_{ro}^{*} \left(\frac{S_o - S_{or}}{1 - S_{or} - S_{wi}} \right)^{n_o} \quad \textbf{(8)}$$

In the two equations (2) and (3), k_{rw}* =Endpoint relative permeability of water; k_{ro}* =Endpoint relative permeability of oil; S_w =Water saturation; S_{wi} =Initial water saturation; S_{or} =Residual oil saturation. Moreover, n_w and n_o are constants used to adjust the shape of the relative permeability curves for oil and water, by which the graph curvature increases with higher n_w and n_o values. It can be seen from Figure 2.11, that the water relative permeability function shows greater curvature than the oil relative permeability function. This is typical for a water-wet system, because the water will fill all the smallest pores and move along the solid surface of the porous medium during displacement. Hence, the resistance of the medium to the flow of water will be greater than for oil. As a result, the n_w constant tends to be greater than n_o

2.5 Spontaneous imbibition

The SI process can be summarized in one illustration, which relates the capillary pressure, relative permeabilities and water saturation, Figure 2.12.

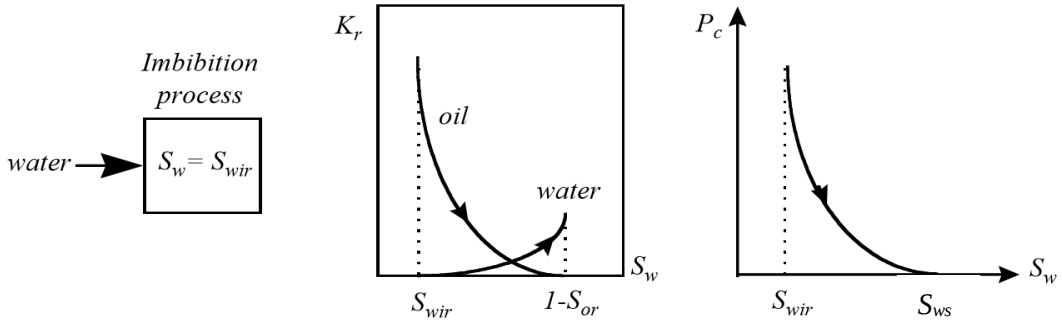

Figure 2.12: Spontaneous imbibition of water into water wet oil filled core (J. Kleppe, 2014).

Summary of SI process of water into water-wet oil filled core:

- An initially oil filled core with $S_w = S_{wir}$ is immersed in water
- Water starts to imbibe and oil is expelled, where the relationship between co-current and counter-current flow depends on the boundary conditions of the core sample
- The relative permeability of water will increase while a decreasing oil relative permeability curve is observed
- The rate of which the water saturation increases will be a function of the capillary pressure, which is controlled by several underlying parameters
- The process continues until the capillary pressure reaches zero at $S_w = S_{ws}$
- The shape of the capillary curve provides important information about reservoir quality

2.5.1 Mathematical investigation

A diffusion equation model is used to present an analytical solution for both counter-current and co-current imbibition, in strongly water-wet porous medium, where water displaces oil spontaneously under the influence of capillary pressure. Incompressible and immiscible fluids will be considered and the contribution of gravity effects (g) will be neglected (where the gravitational force due to vertical displacement of fluid is insignificant compared to capillary forces).

The transport equations for oil (o) and water (w) in porous media are given by:

$$\varphi \frac{\partial S_l}{\partial t} = -\frac{\partial v_l}{\partial x} \quad \textbf{(9)}$$

where φ =Porosity; S_l =phase saturation and v_l =Darcy velocity of each phase. Considering two-phase flow in a 1-D system along the vertical axis, the generalized Darcy law is formulated as:

$$v_w = -\frac{Kk_{rw}}{\mu_w}\left(\frac{\partial P_w}{\partial x}\right) \quad \textbf{(10)}$$

$$v_o = -\frac{Kk_{ro}}{\mu_o}\left(\frac{\partial P_o}{\partial x}\right) \quad \textbf{(11)}$$

where $v_{w/o}$ =Water and oil flux; K =Absolute permeability; k_{rw} =Relative permeability to water; k_{ro} =Relative permeability to oil; $\mu_{w/O}$ =Viscosity for water/oil and $P_{w/o}$ =Water and oil phase pressure.

The capillary pressure P_c is defined as the difference between oil and water phase pressures:

$$P_c = P_o - P_w \quad \textbf{(12)}$$

Then, the total Darcy velocity v_T is can be written on the following form:

$$v_T = v_w + v_o = -\lambda_o \frac{\partial P_c}{\partial x} - \lambda_T \frac{\partial P_w}{\partial x} \quad \textbf{(13)}$$

where the mobilities (λ_w), (λ_o) and (λ_T) are defined as:

$$\lambda_w = -K\frac{k_{rw}}{\mu_w} \qquad \lambda_o = -K\frac{k_{ro}}{\mu_o} \qquad \lambda_T = \lambda_w + \lambda_o$$

Now, equation (10) to (13) can be used to derive the water transport equation for both co-current and counter-current imbibition.

Co-current:

For co-current SI, oil and water will flow in the same direction in the porous medium. Thus, the flow of fluid out of the porous medium is the sum of the water being imbibed and the oil being expelled, which yields:

$$v_T = v_w + v_o \quad \textbf{(14)}$$

From simple algebraic operations, the water flow term can be written as:

$$v_w = f_w v_T - f_w \lambda_o \frac{\partial P_c}{\partial x} \quad \textbf{(15)}$$

where $f_w = \frac{\lambda_w}{\lambda_T}$ is the water fractional flow function. Then by combining equations (9) and (15), the water transport equation becomes:

$$\varphi A \frac{\partial S_w}{\partial t} = -\frac{\partial}{\partial x}[f_w q_T] - \frac{\partial}{\partial x}\left[f_w \lambda_o (\frac{\partial p_c}{\partial x})\right] \quad \textbf{(16)}$$

Counter-current:

For counter-current SI, the flow of water into the porous medium is equal to the flow of oil moving out of the medium, in the opposite direction, which yields:

$$v_T = 0;\ v_w = -v_o \quad \textbf{(17)}$$

Since $q_T = 0$, the water flow term can be expressed by the following term:

$$v_w = -f_w \lambda_o \frac{\partial P_c}{\partial x} \quad \textbf{(18)}$$

in which the water transport equation becomes:

$$\varphi \frac{\partial S_w}{\partial t} = -\frac{\partial}{\partial x}\left[f_w \lambda_o (\frac{\partial p_c}{\partial x})\right] \quad \textbf{(19)}$$

For the core sample of interest in this thesis, with length L, the initial and boundary conditions are:

$S_w = S_{wi} = 0,$ $t = 0,$ $0 \le x \le L,$

$S_w = 1 - S_{or,}$ $t = 0^+$ $x = 0,$

$q_w = 0,$ $t = 0^+$ $x = L$

2.5.2 Capillary diffusivity coefficient (CDC)

The flow of water and oil in a 1-D water-wet porous medium with no total velocity (counter-current flow) is described by a diffusion equation model. To express the diffusion equation model with respect to a diffusion coefficient, the water velocity can be written on the following form:

$$v_w = -f_w \lambda_o \frac{\partial P_c}{\partial x} = \frac{K k_{rw} k_{ro}}{\mu_w k_{ro} + \mu_o k_{rw}} \frac{\partial P_c}{\partial x} \quad \textbf{(20)}$$

which can be formulated in terms of saturation:

$$v_w = \frac{K k_{rw} k_{ro}}{\mu_w k_{ro} + \mu_o k_{rw}} \frac{\partial P_c}{\partial S_w} \frac{\partial S_w}{\partial x} \quad \textbf{(21)}$$

Then, by combining equations (9) and (21), the water transport equation can be expressed as follows:

$$\varphi \frac{\partial S_w}{\partial t} = -\frac{\partial}{\partial x}\left(\frac{K k_{rw} k_{ro}}{\mu_w k_{ro} + \mu_o k_{rw}} \frac{\partial P_c}{\partial S_w} \frac{\partial S_w}{\partial x} \right) \quad \textbf{(22)}$$

Furthermore, by simple algebraic operations, equation (22) can be expressed with the following form:

$$\varphi \frac{\partial S_w}{\partial t} = \frac{\partial}{\partial x}\left[D(S_w) \frac{\partial S_w}{\partial x} \right] \quad \textbf{(23)}$$

where

$$D(S_w) = -\frac{K k_{ro}(S_w)}{\mu_o} \cdot \frac{1}{1 + \frac{k_{ro}(S_w)}{k_{rw}(S_w)} \cdot \frac{\mu_w}{\mu_o}} \cdot \frac{dP_c(S_w)}{dS_w} \quad \textbf{(24)}$$

is called the capillary diffusivity coefficient (CDC) and is given in m^2/s. Moreover, S_w =Normalized water saturation; K =Absolute permeability; k_{ro} =Relative permeability to oil; k_{rw} =Relative permeability to water; μ_w =Water viscosity; μ_o =Oil viscosity; Pc =Capillary pressure and φ =fractional porosity.

By normalizing the water saturation, the Corey expressions are defined as:

$$k_{rw} = {k_{rw}}^* (S)^{n_w} \quad \textbf{(7)}$$

$$k_{ro} = {k_{ro}}^* (1 - S)^{n_o} \quad \textbf{(8)}$$

where k_{rw}* and k_{ro}* are the endpoint relative permeabilities to water and oil; n_w and n_o are the Corey exponents; S is the normalized water saturation and is defined as:

$$S = \frac{S_w - S_{wi}}{1 - S_{oR} - S_{wi}}, \qquad S_{wi} \leq S_w \leq 1 - S_{or} \tag{25}$$

where S_{wi} is the initial water saturation and S_{or} is the residual oil saturation. Then, by implementing the Corey expression for normalized water saturation into equation (24), the CDC can be modelled directly as a function of the Corey exponents:

$$D(S_w) = -\frac{k k_{ro}{}^{*}(S)^{n_o}}{\mu_o} \cdot \frac{1}{1 + \frac{k_{ro}{}^{*}(S)^{n_o}}{k_{rw}{}^{*}(S)^{n_w}} \cdot \frac{\mu_w}{\mu_o}} \cdot \frac{dP_c(S_w)}{dS_w} \tag{26}$$

The diffusion coefficient is used in investigations in chapter 4.9.

2.5.3 Extended Darcy's law

Reservoir simulation rely on the understanding and modelling of relative permeabilities. The standard Darcy equations used in existing reservoir simulation are adequate for describing steady-state processes. However, limitations have been demonstrated in more complex situations where co-current and counter-current flows components are combined (Rose, 1969; Spanos, 1981). Consequently, an extended formulation of Darcy equations has been developed and extensively discussed in literature. The common denominator of all the papers on the subject was the effects of viscous coupling or Yuster effect (Babchin, Yuan, & Nasr, 1998). "By coupling is meant a situation where the motion of elements of pore fluid reciprocally will be subject to viscous drag extending across the fluid-fluid interfaces that separate them from other contiguous element of immiscible fluid(s)..." (Rose, 1988). This signifies that the pressure gradient in each fluid is a function of the Darcy velocity in both fluids.

It is assumed that the porous medium is strongly water-wet and that the water is covering the solid surface, preventing any interaction between oil and solid surface. Furthermore, the gravity term is neglected and one-dimensional forms are considered. Then, for steady-state two-phase flow, the generalized Darcy equations can be written on the following form:

$$v_w = -\frac{k_{ww}}{\mu_w}\frac{dP_w}{dx} - \frac{k_{wo}}{\mu_o}\frac{dP_o}{dx} \tag{27}$$

$$v_o = -\frac{k_{ow}}{\mu_w}\frac{dP_w}{dx} - \frac{k_{oo}}{\mu_o}\frac{dP_o}{dx} \tag{28}$$

where v_w and v_o represent the Darcy velocity in the two fluid phases, μ_w and μ_o are fluid viscosities, dP_w/dx and dP_o/dx are the two pressure gradients. k_{ww}, k_{wo}, k_{ow} and k_{oo} are the four transport coefficients describing the contribution of one fluid phase to the flow of the other fluid phase.

In co-current imbibition, oil and water flow in the same direction, which imply that the pressure gradients of the two phases are oriented in the same direction. As a result, the displacement of the fluid with higher Darcy velocity will contribute positively to the flow of the other fluid. In other words, viscous coupling has a positive effect on co-current flow.

For counter-current imbibition, the fluids move in opposite direction of each other. This will generate a negative viscous drag on the interface between the two fluids and give a lower total velocity of the displacement process. Consequently, viscous coupling has a negative effect on counter-current flow in terms of fluid mobility.

2.6 History match procedure

History matching can be defined as the process of adjusting uncertain input parameters used in the reservoir model, in order to obtain a better match between simulated and observed reservoir responses (H. Kleppe, 2014). Since a perfect match cannot be obtained, history matching is recognised as a very time-consuming trial-and-error process. Therefore, a clear strategy must be followed to prevent that the definition of a match is restricted by factors such as time or money. Perhaps most important is that only one parameter must be adjusted at a time. In this way, the variation caused on simulations can be used to rank the significance of a certain parameter. Furthermore, by performing sensitivity analyses, it will point out which parameters are more sensitive to adjustments. Such knowledge will reduce the time needed to obtain adequate results.

Since reservoir simulation involves an extensive amount of input parameters, a history match between experimental data and simulations can be generated by almost infinite many combinations. In other words, a match is not the only match and perhaps not even the most correct one. Hence, by using representative input parameters, a more representative result will be obtained. It is namely the robustness of the model that will determine the simulators ability to predict future reservoir behaviour.

In this thesis, history matching was performed by adjusting the relative permeability curves and the capillary pressure curve. Since analytical models are used to represent the two input parameters in ECLIPSE, the adjustments were performed on the Corey- and Skjaeveland parameters (n_w, n_o, C_l, a_l).

3 Numerical investigation

3.1 ECLIPSE simulator

The numerical investigation was performed with ECLIPSE simulation software developed by Schlumberger. The software provides two separate simulators; ECLIPSE 100 for black oil modelling and ECLIPSE 300 for compositional modelling. In this thesis, ECLIPSE 100 was used, where it is designed to run fully-implicit, three phase, and three dimensional simulations.

3.1.1 Input data

A basecase DATA-file was provided by Standnes as a foundation for further modifications and history matching. The process from basecase to best match started with construction- and refinement of the grid. Moreover, relative permeability curves and the capillary pressure curve were generated. Lastly, no-flow boundaries and time step adjustments were considered.

3.1.2 Grid

First, the grid was constructed to simulate the process of spontaneous imbibition of water from the fracture system into the matrix clocks. This was achieved by using the keyword BOX to construct a cube of 10 x 10 x 10 (1000 blocks), placed in the middle of a 20 x 20 x 20 grid (8000 blocks). The cube was assigned parameter values according to the experiments performed by Standnes (2004). The confining grid was given a permeability of 100,000 mD and porosity of 0.99 to represent high porosity water-filled fractures. The no-flow boundaries were generated by setting transmissibility multipliers equal to zero. The keywords MULTX, MULTY, MULTZ were used for the representative planes. An illustration of the grid setup is depicted in Figure 3.1.

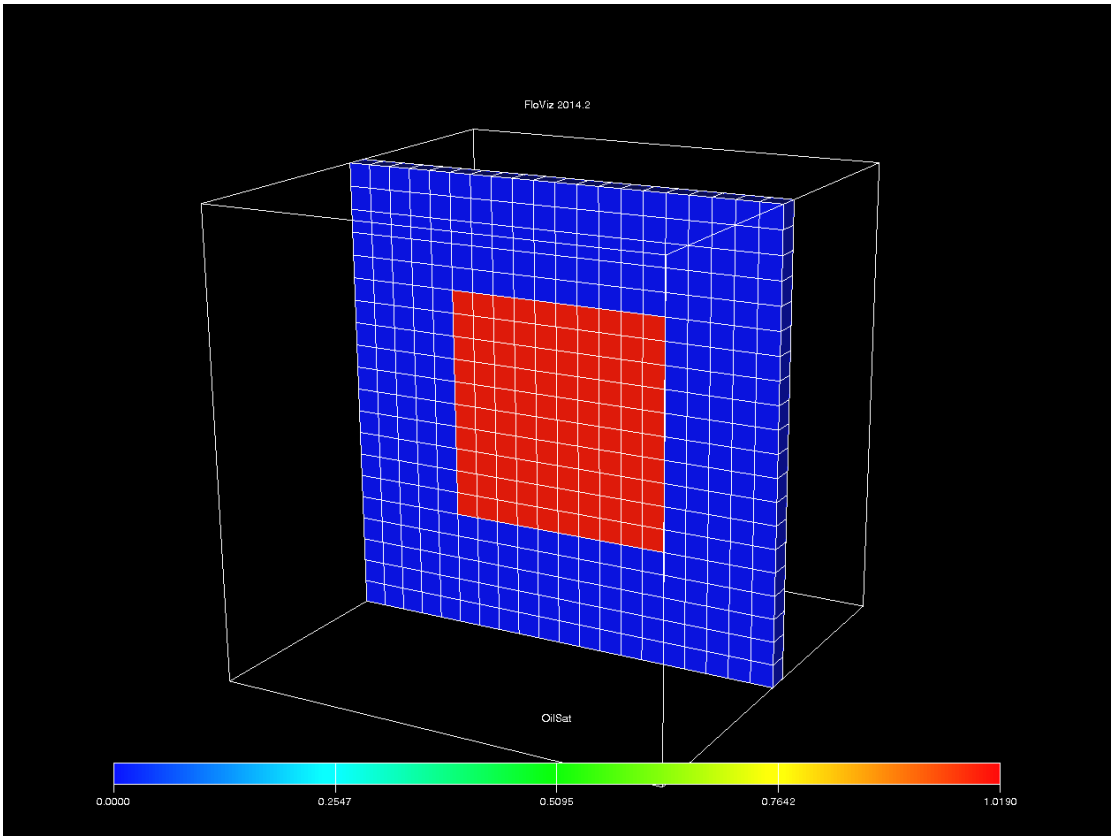

Figure 3.1: 3D plane slice of the constructed grid, where red colour illustrates the oil-filled core plug and blue colour is used for water phase.

3.1.3 Capillary pressure and relative permeability curves

Capillary pressure and relative permeability curves are defined as tabulated values, calculated by the Corey- and Skjaeveland expressions introduced in chapter 2.3 and 2.4, equations (5), (7) and (8). The keyword SWOF is used to represent relative permeability and capillary pressure as a function of corresponding water saturation, also known as the SWOF-table.

3.2 Local grid refinement (LGR)

In the process of history matching the experimental data for test 12, the simulations showed quite erroneous results in the start of the production. This was investigated by studying the grid in 3D view, by using the FloViz module in ECLIPSE. It could be seen that the cube was produced too fast, assumingly due to the coarseness of the grid. Figure 3.2 shows the difference between no grid refinement (left) and grid refinement in the two outer layers (right) for time steps 1, 3 and 30.

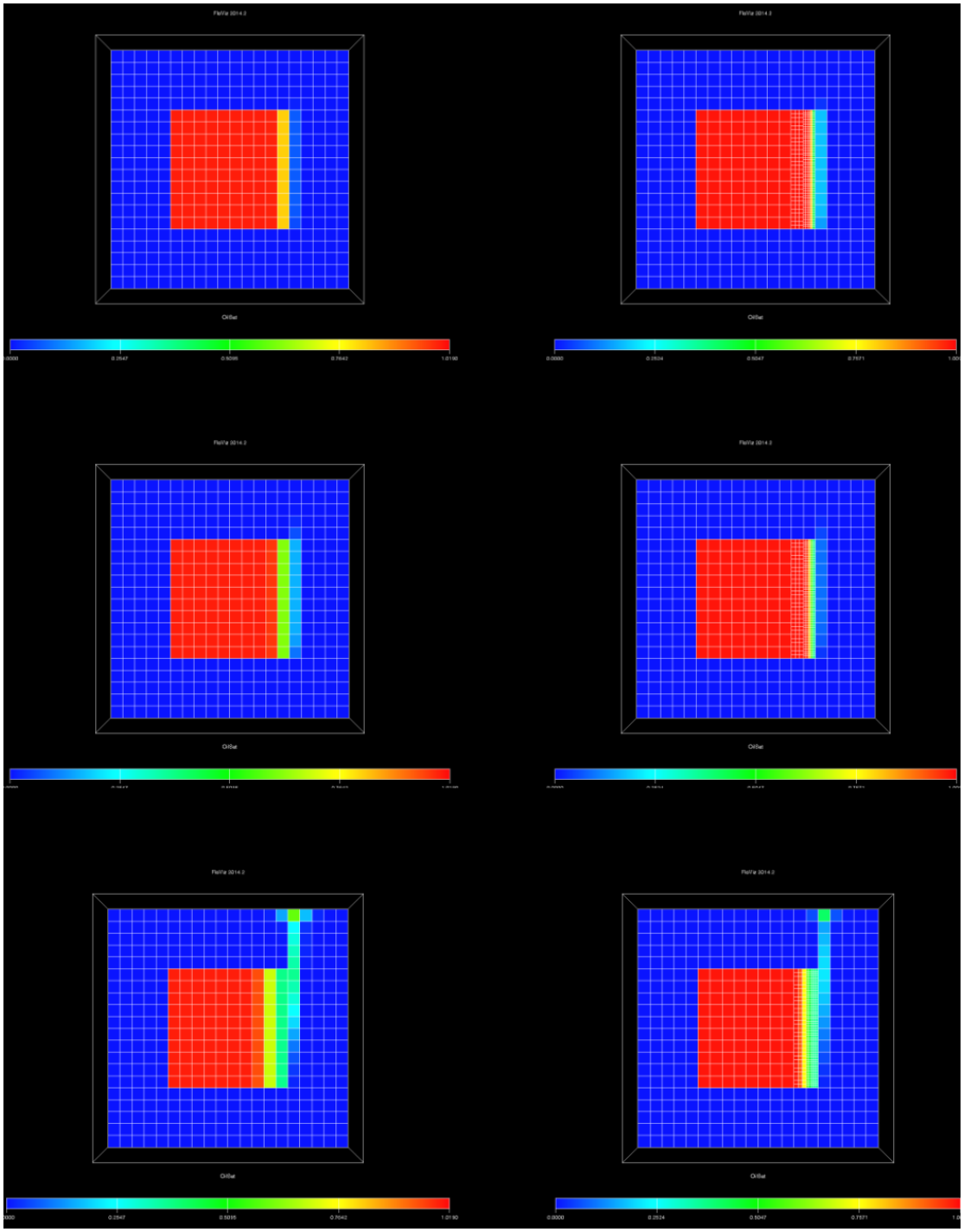

Figure 3.2: Simulations of test 12 showing impact of grid refinement in the 2 outer layers (in direction of flow) for time steps 1, 3 and 30.

By increasing the number of grid blocks in the model, the numerical dispersion decreased while the integrity and accuracy of the model increased. However, it must be considered that the necessary computational capacity for the simulation increased exponentially with the number of grid blocks. This introduced questions such as “What is the sufficient number of grid blocks?” or “to what degree ought local grid refinement to be performed?” Consequently, a compromise between computational work and model accuracy was investigated by performing a LGR sensitivity analysis.

3.2.1 LGR sensitivity

A sensitivity analysis was performed to investigate simulation results as a function of LGR. First, the case containing no grid refinements in the direction of flow was run and used as a basecase (LGR: 0 blocks). Furthermore, grid refinements were introduced in the two outer layers of the cube by using keywords CARFIN and AMALGAM in the DATA-file. The outermost layer (open to water) was refined into 5 grid blocks (in direction of flow) whereas the next layer was refined into 3 layers (in direction of flow). To test even finer grid, the outermost layer was kept refined into 5 grid blocks while constantly increasing the number of layers refined into 3 blocks (in direction of flow). A 2-D slice of the matrix grid with increasing degree of LGR is showed in Figure 3.3.

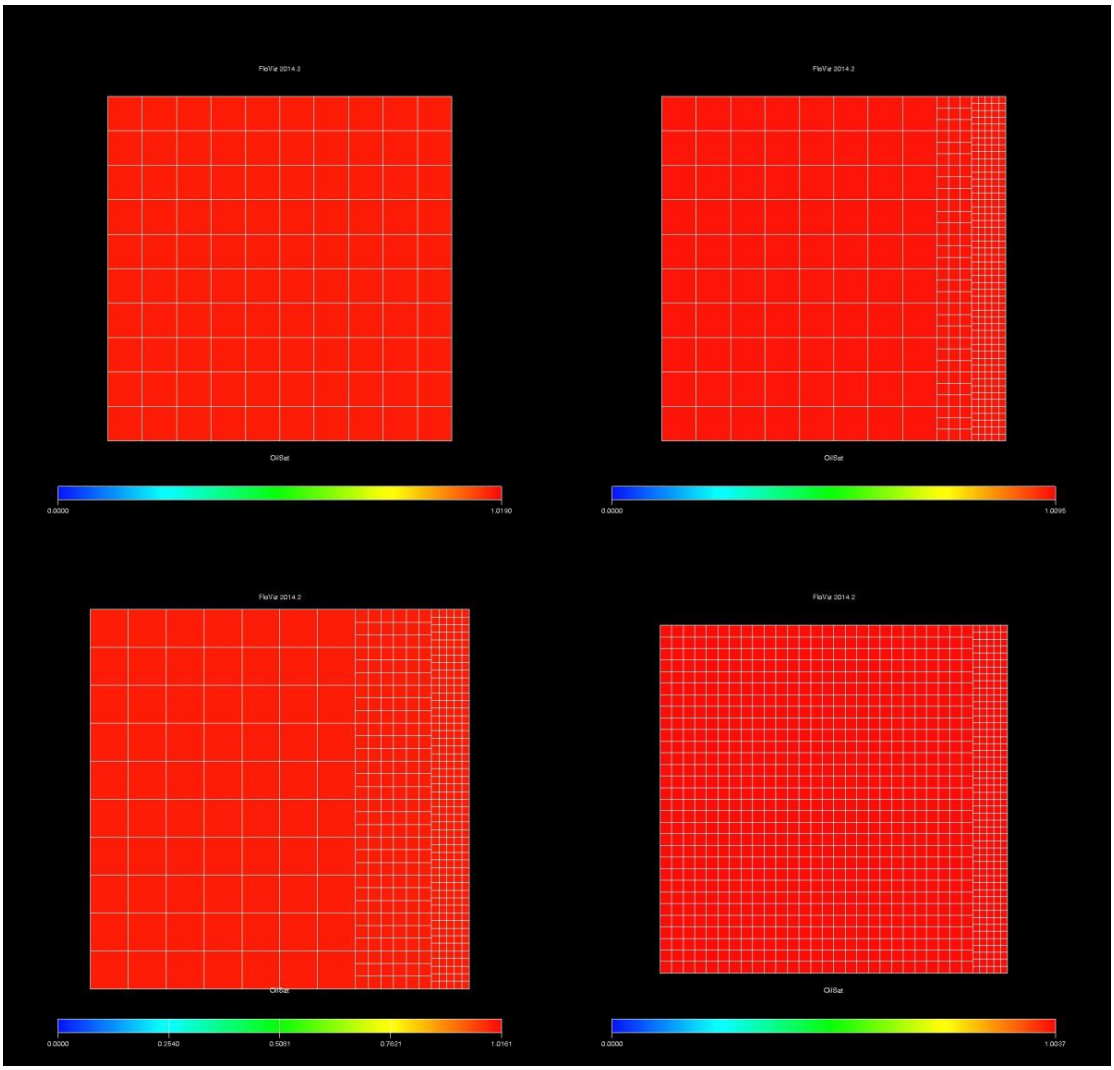

Figure 3.3: Showing simulation of test 12 at time step 0, with increasing degree of LGR from 0 to 10 blocks in direction of flow.

Simulation times ranged from a few minutes for low degree of LGR (LGR: 0 and 2 blocks) to more than an hour for the most refined case (LGR: 10 blocks). In conclusion, the optimal degree of LGR with

respect to accuracy of simulation and computational time was set to 2 blocks in the direction of flow. The outer layer refined into 5 blocks and the second layer refined into 3 blocks, both refinements in direction of flow.

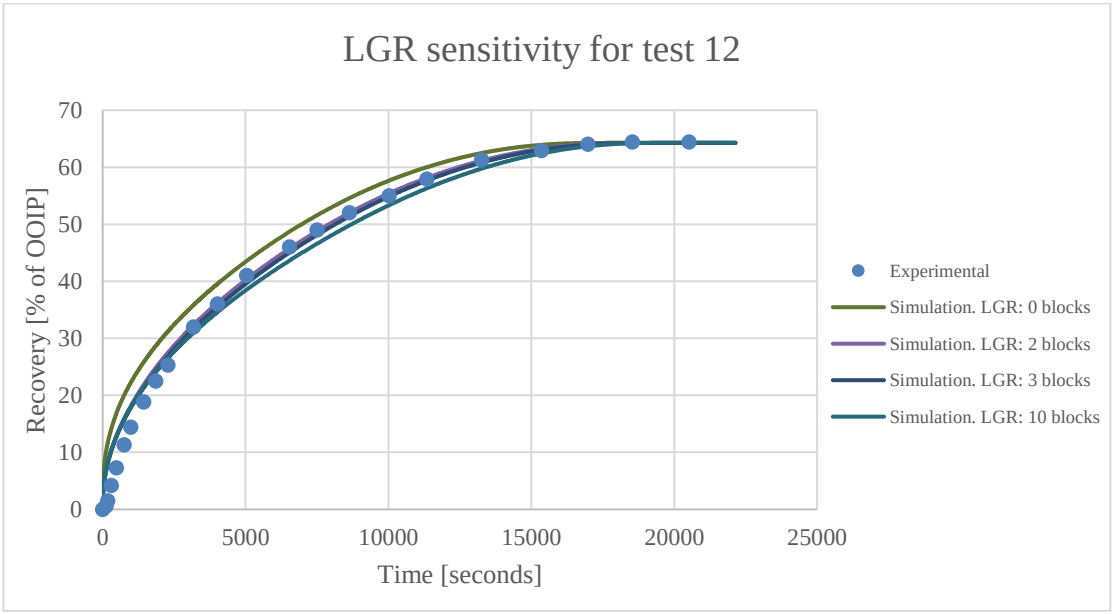

Figure 3.4: Simulation of Test 12 with increasing degree of LGR and experimental data on the y-axis plotted against time on the x-axis.

3.2.2 Error investigation

It was found that independently of the degree of LGR, the simulations did still show overproduction in early production times. To find out if this was due to grid characteristics, further adjustments in the outermost layer was investigated. The layer open to water was first coarsened into 3 blocks in the direction of flow to see if a slight reduction of grid blocks would impact simulation results. Secondly, the same layer was refined into 10 blocks in direction of flow, Figure 3.5. Yet, even by doubling the number of grid blocks in the outermost layer, it had only minimal impact on the simulation results, Figure 3.6. Hence, the deviation between simulations and experimental data in the start of production could not be reduced any further by including any more refinements. The exact reason for this deviation was not discovered, but it can be argued to be from experimental uncertainty.

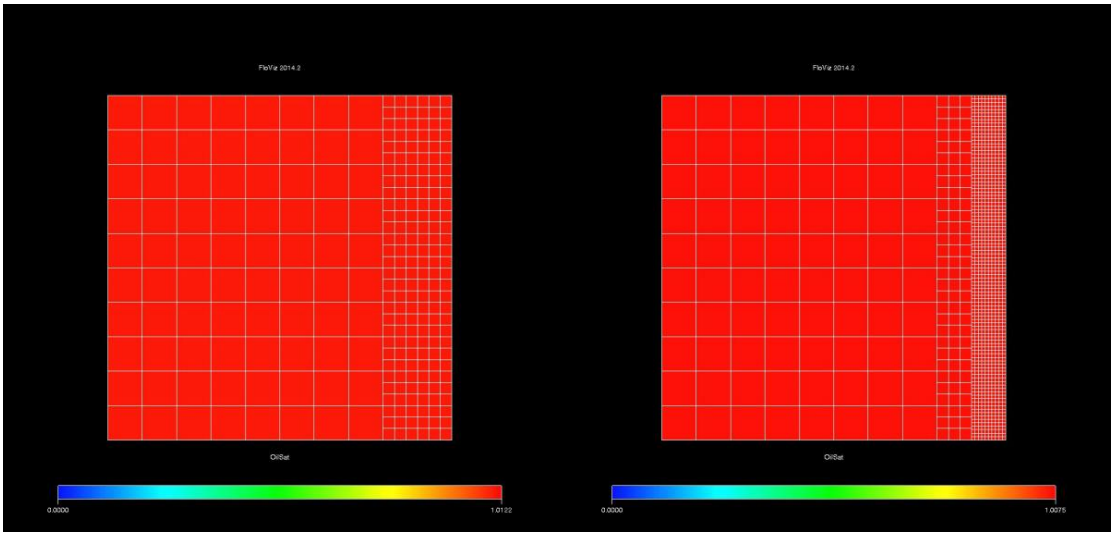

Figure 3.5: Simulation of test 12 with increasing degree of refinement in the outermost layer at time step 0.

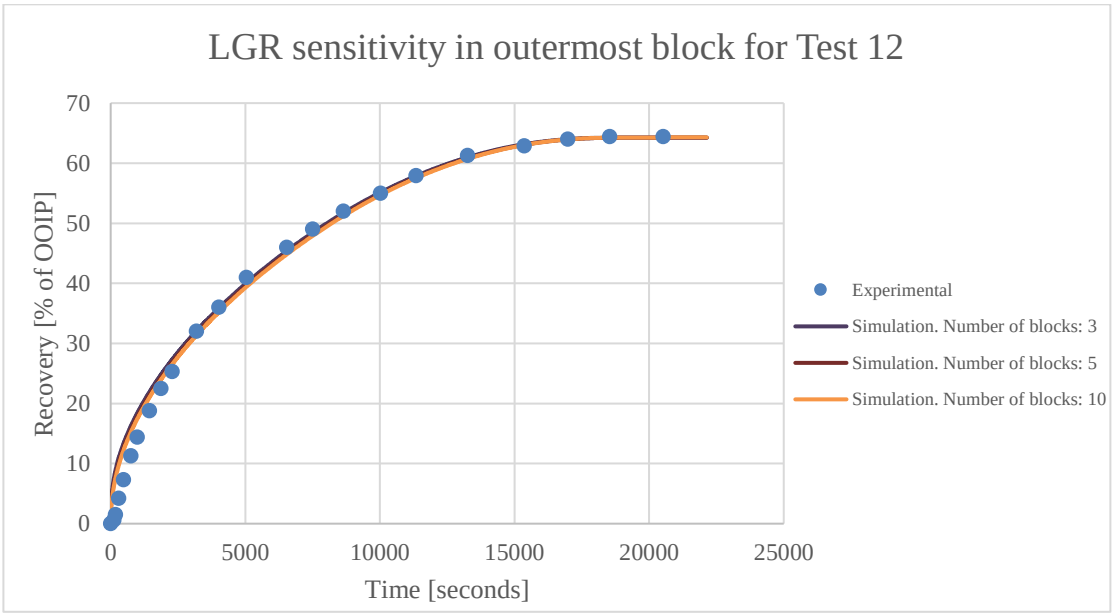

Figure 3.6: Simulation of Test 12 with increasing degree of grid refinement in the outermost layer together with experimental data on the y-axis plotted against time on the x-axis.

4 Results and discussion

4.1 Part 1 - Experimental details

Part 1 of this thesis is based on laboratory work performed by Standnes (2004). The experiments were divided into two groups with respect to the imbibition process; counter-current and co-current. All counter-current tests were performed using Amott cells in which the 100% oil saturated core plug were completely immersed in water. Oil production was measured as a function of time with an uncertainty of ± 0.1 mL.

For Co-current SI, all tests were suspended from a balance where a part of the sample was immersed into water until satisfying a certain WOAR (water-oil area-ratio). Oil production was calculated by monitoring the change of sample-weight as a function of time. This gave an uncertainty of approximately ± 0.2 mL.

All experiments were performed on outcrop chalk samples from Denmark, taken from the same block, with porosity values close to 42% and absolute permeability of approximately 2 mD. For the non-wetting phase (oil), it was used n-Decane from Riedel-deHaen with grade >95%, where this fluid does not modify the wettability of the chalk samples. Furthermore, the density of the oil phase was 0.731 g/cm^3 at standard conditions (20 °C). For the wetting phase (water) it was used distilled water with density 0.9982 g/cm^3 and IFT of 46 mN/m at ambient temperature (≈20 °C).

All tests investigated in this thesis were performed on cubical rock samples with geometry index CU (cubical) and boundary conditions defined as AFO (all face open), 1FC (1 face closed), 2FC (2 faces closed) and (O: oil; W: water; C: Coated). A summary of experimental details and boundary conditions partly reprinted from Standnes (2004) given in Table 2 and Table 3.

Table 2: Fluid properties.

Liquid phase	Density at 20 °C (g/cm^3)	Viscosity at 20 °C (mPa*s)	IFT (mN/m)
Distilled water	0.9982	1	46
n-decane	0.731	0.95	-

Table 3: Core data for SI tests performed on counter-current and co-current flow

Test no.	Boundary condition	Side length (m)	Porosity (%)
Counter-current			
7	CU-AFO	0.038	42.3
8	CU-2FC	0.038	43.4
12	CU-5FC	0.038	43.7
Co-current			
16	AFO	0.05	43.2
17	O: Top surface; W: All other surfaces; C: -	0.05	43.6
18	O: Upper half; W: Lower half; C: -	0.05	43.6
19	O: Top and lateral surfaces; W: Bottom surface; C: -	0.05	43.5
21	O: Upper half; W: Bottom surface; C: lower half lateral surfaces	0.05	42
22	O: Top surface; W: Bottom surface; C: All lateral surfaces	0.05	43.1
23	O: - ; W: One surface; C: 5 surfaces	0.05	42.9
24	O: Top surface; W: Lower half; C: Upper half lateral surfaces	0.05	42.2

4.2 History matching of test 12

For the process of history matching counter-current experimental data, test 12 CU-5FC was selected as basecase due to its favourable test results. For SI into cubic rock samples, test 12 displays the highest recovery time with a smooth curve and is also the test with most experimental data points. Such conditions will reduce uncertainty in experimental measurements. In addition, test 12 was history matched in bachelor theses by Nesvik (2016) and Moe (2016), which enabled comparison of results.

The basecase from Standnes was used as starting point. Capillary pressure (Pc) and relative permeability curves ($k_{rw,}$ k_{ro}) were constantly adjusted until a better fit could not be obtained. The final endpoint values, constants and exponents that were used are presented in Table 4. Furthermore, Table 5 shows the final values for capillary pressure and relative permeability curves.

Table 4: key input parameters used to generate final capillary pressure and relative permeability curves used in the history match of test 12.

Corey exponents and endpoint relative permeabilities		Capillary pressure constants and exponents		Endpoint saturations	
n_w	3	c_w	0.9	S_{wi}	0
n_o	1.14	c_o	-0.002	S_{or}	0.32
k_{rw}*	0.2	a_w	0.4		
k_{ro}*	1	a_o	2		

Table 5: Tabulated values (SWOF-table) for Pc, k_{rw} and k_{ro} for different water saturations used in history match of test 12 CU-5FC.

S_w [fraction]	K_{rw} [fraction]	K_{ro} [fraction]	P_c [atm]
0	0	1	8
0.02	5.08854E-06	0.96654	4.301463
0.04	4.07083E-05	0.933222	3.259251
0.06	0.000137391	0.900049	2.770799
0.08	0.000325667	0.867026	2.469192
0.1	0.000636068	0.834157	2.257949
0.12	0.001099125	0.801446	2.098748
0.14	0.001745369	0.768898	1.972848
0.16	0.002605333	0.736518	1.869825
0.18	0.003709546	0.704313	1.783338
0.2	0.005088541	0.672287	1.709275
0.22	0.006772848	0.640448	1.64483
0.24	0.008792998	0.608802	1.588011
0.26	0.011179524	0.577356	1.537357
0.28	0.013962955	0.54612	1.491763
0.3	0.017173825	0.515102	1.450376
0.32	0.020842662	0.484311	1.412518
0.34	0.025	0.45376	1.377642
0.36	0.029676369	0.423458	1.345289
0.38	0.0349023	0.393421	1.31507
0.4	0.040708325	0.363664	1.286634
0.42	0.047124975	0.334202	1.259655
0.44	0.05418278	0.305057	1.233805
0.46	0.061912274	0.27625	1.208726
0.48	0.070343985	0.247807	1.183988
0.5	0.079508447	0.219761	1.159014
0.52	0.08943619	0.192148	1.132947
0.54	0.100157745	0.165016	1.104372
0.56	0.111703643	0.138422	1.070703
0.58	0.124104417	0.112445	1.026626
0.6	0.137390596	0.087189	0.959533
0.62	0.151592713	0.062811	0.832758
0.64	0.166741299	0.039563	0.497897
0.66	0.182866884	0.017952	-1.24927
0.68	0.2	0	-6

Initial water saturation S_{wi} was set to 0 as the core plug was initially 100 % oil saturated, where residual oil saturation S_{or} was set to 0.32. Additionally, the maximum relative permeabilities were set to 0.2 for water (k_{rw}*) and 1 for oil (k_{ro}*), respectively (Høgnesen, Standnes, & Austad, 2006). To control the oil recovery endpoint, the capillary pressure was manipulated by adjusting the constants controlling the shape curve. Figure 4.1 depicts the final capillary pressure curve and relative permeability curves used in history match of test 12 CU-5FC.

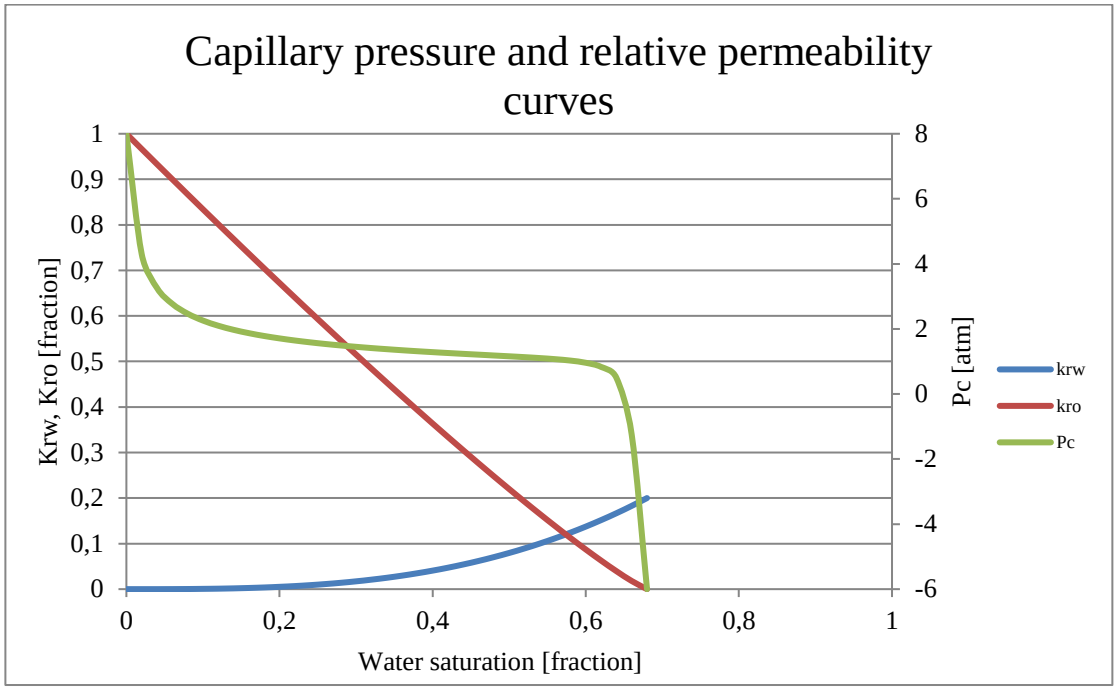

Figure 4.1: Relative permeability curves (k_{rw}, k_{ro}) on the primary y-axis, capillary pressure curve on the secondary y-axis plotted against corresponding water saturation on the x-axis.

Figure 4.1 shows a relatively straight line for k_{ro} whereas k_{rw} has a slightly more curved shape. The capillary pressure curve decreases rapidly from 8 atm to approximately 4 atm, before the slope approaches 0 at 1 atm. Furthermore, the curve shows another drop until final oil recovery is reached at a water saturation of 0.64. From that point, the capillary pressure continues to drop with a steep slope to the endpoint value of -6 atm. Both relative permeabilities and the capillary pressure show smooth curves. The final history match for test 12 with oil recovery as fraction of OOIP and normalized fraction of recoverable oil are depicted in Figure 4.2 and Figure 4.3.

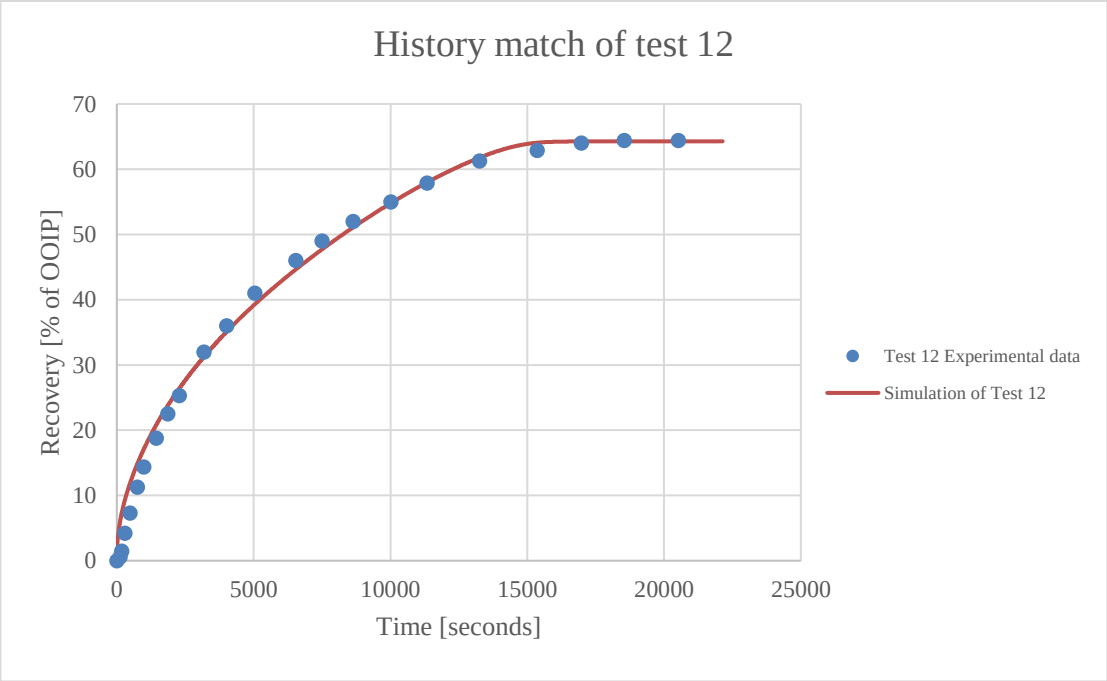

Figure 4.2: History match of test 12 CU-5FC with recovery (% of OOIP) on the y-axis and time (seconds) on the x-axis.

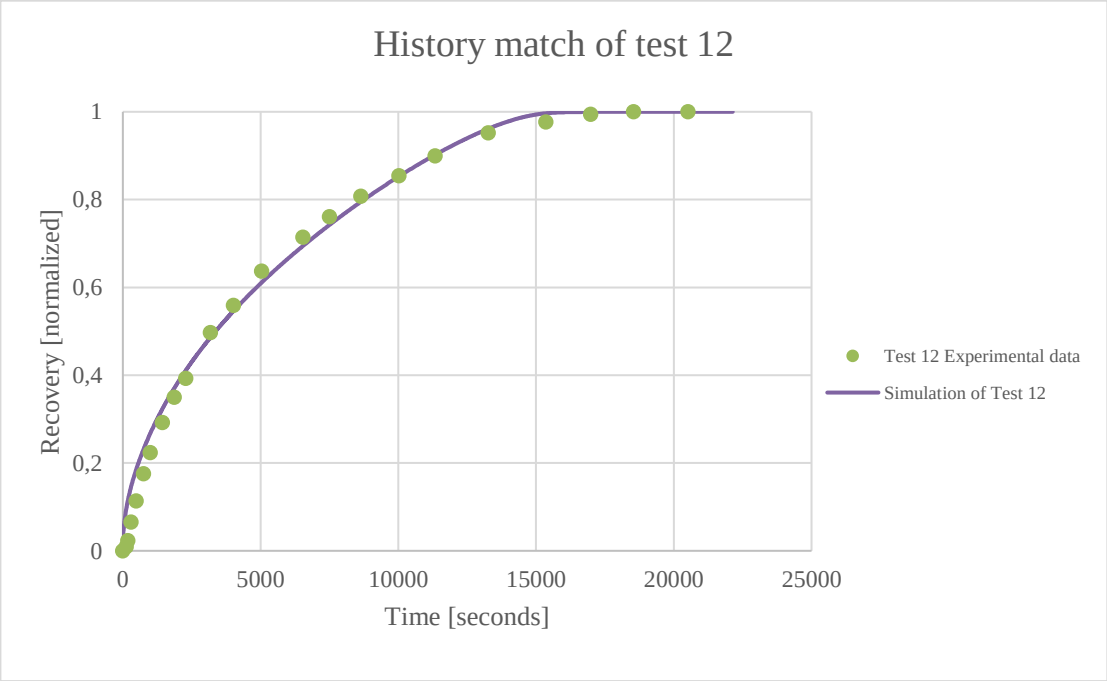

Figure 4.3: History match of test 12 CU-5FC with normalized recovery on the y-axis and time (seconds) on the x-axis.

Apart from the small deviation at early production times, the simulations match the experimental data match quite well. This deviation was discussed in section 3.2.2, where it was argued to be minimized in relation to grid refinements.

4.2.1 Sensitivity analysis

The process of history matching counter-current experimental data appeared to be quite challenging due to the number of adjustable input parameters, each with a different level of influence. The question was not only "which parameters must be adjusted?" but also "how sensitive are the parameters to adjustments?" This was investigated by performing sensitivity analyses on the constants and exponents used in the Skjaeveland- and Corey expressions. By fixing all input parameters but one, variance in simulations could be observed and related to its level of significance. Some parameters showed minimal influence while other caused great variation. A summary of selected values used in the sensitivity analysis for input parameters is given in Table 6. More to the point, Figure 4.4 and Figure 4.5 demonstrate an example of two input parameters with great variation in sensitivity.

Table 6: Summary of values used for input parameters in sensitivity analyses.

Input parameter values					
n_w	n_o	c_w	c_o	a_w	a_o
2	1.1	0.8	-0.0009	0.3	1
3	1.14	0.85	-0.002	0.35	2
4	1.2	0.9	-0.004	0.4	3
8	1.3	0.95	-0.006	0.45	4

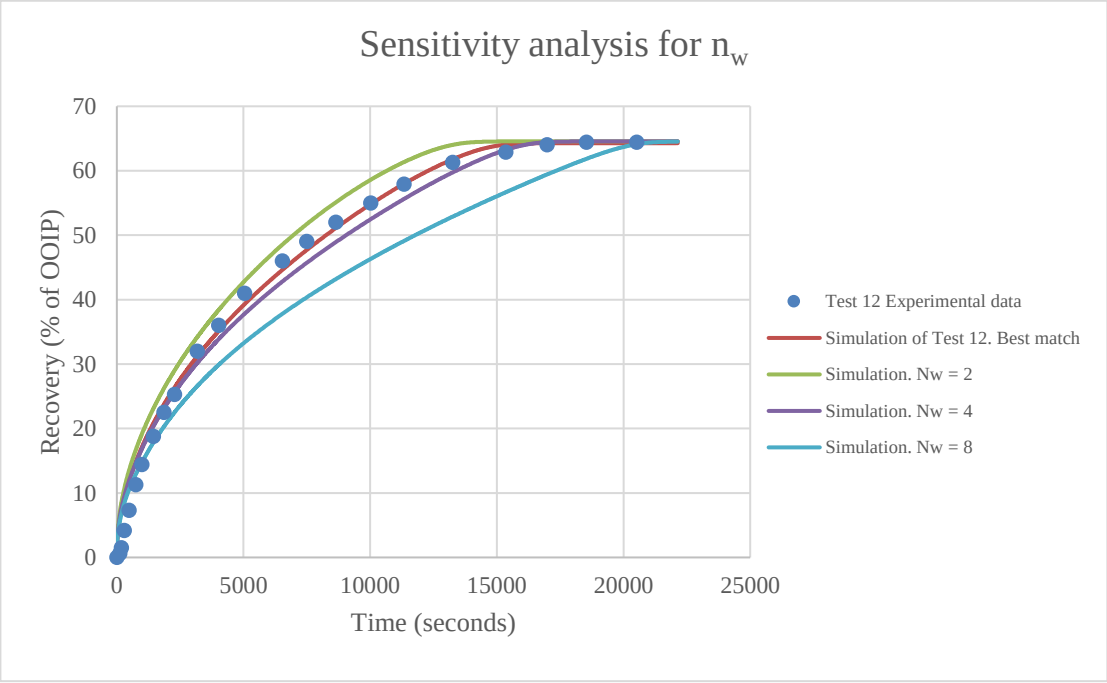

Figure 4.4: Deviation from the history match caused by adjusting n_w while keeping all other parameters fixed.

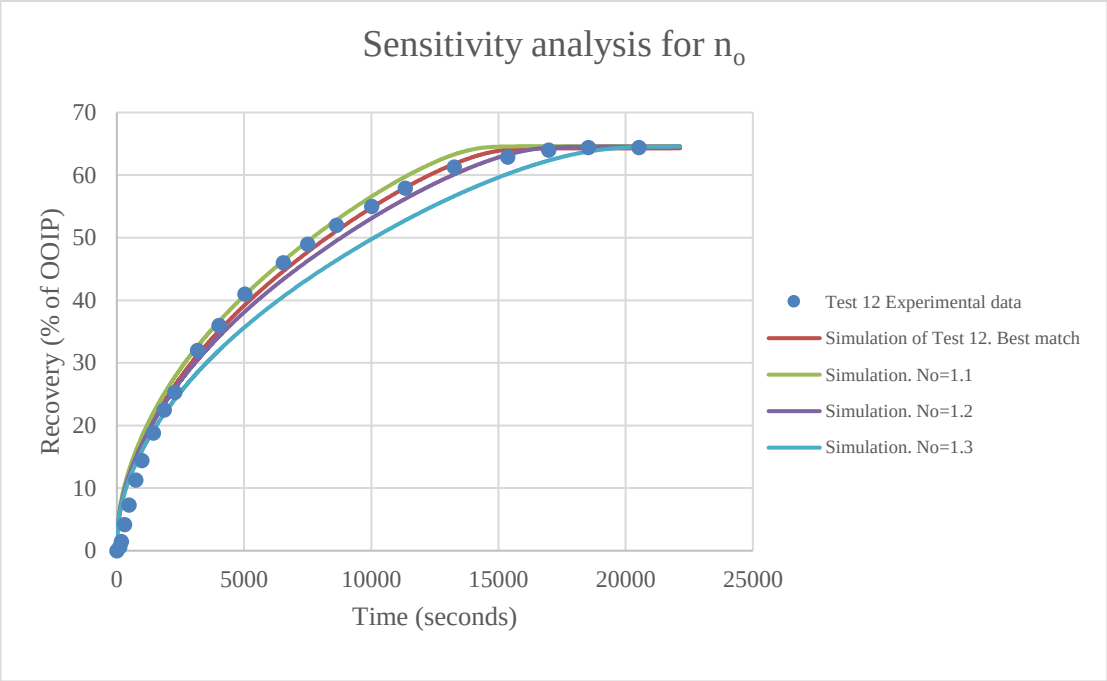

Figure 4.5: Deviation from the history match caused by adjusting n_o while keeping all other parameters fixed.

The deviation in simulations caused by adjusting n_w and n_o are quite similar, yet, caused by different relative level of adjustments. Since n_w causes the same deviation with a higher value than n_o, it signifies that n_w is the less sensitive parameter.

4.3 Co-current simulations

After a satisfactory history match was obtained for test 12 CU-5FC, capillary pressure and relative permeability curves were used in simulations of co-current SI. The aim was to investigate if the history matched counter-current relative permeability curves would recreate co-current experimental data, and if so, to what extent must the curves be adjusted.

A DATA-file designed for co-current simulations was provided by supervisor Standnes. The DATA-file was initially modified to simulate test 22 (1-D co-current SI), which was obtained by closing off the lateral faces, leaving only the lower and upper face open to flow. Compared to the DATA-file used for test 12, no grid refinement was used. Figure 4.6 shows an illustration of the grid construction for test 22.

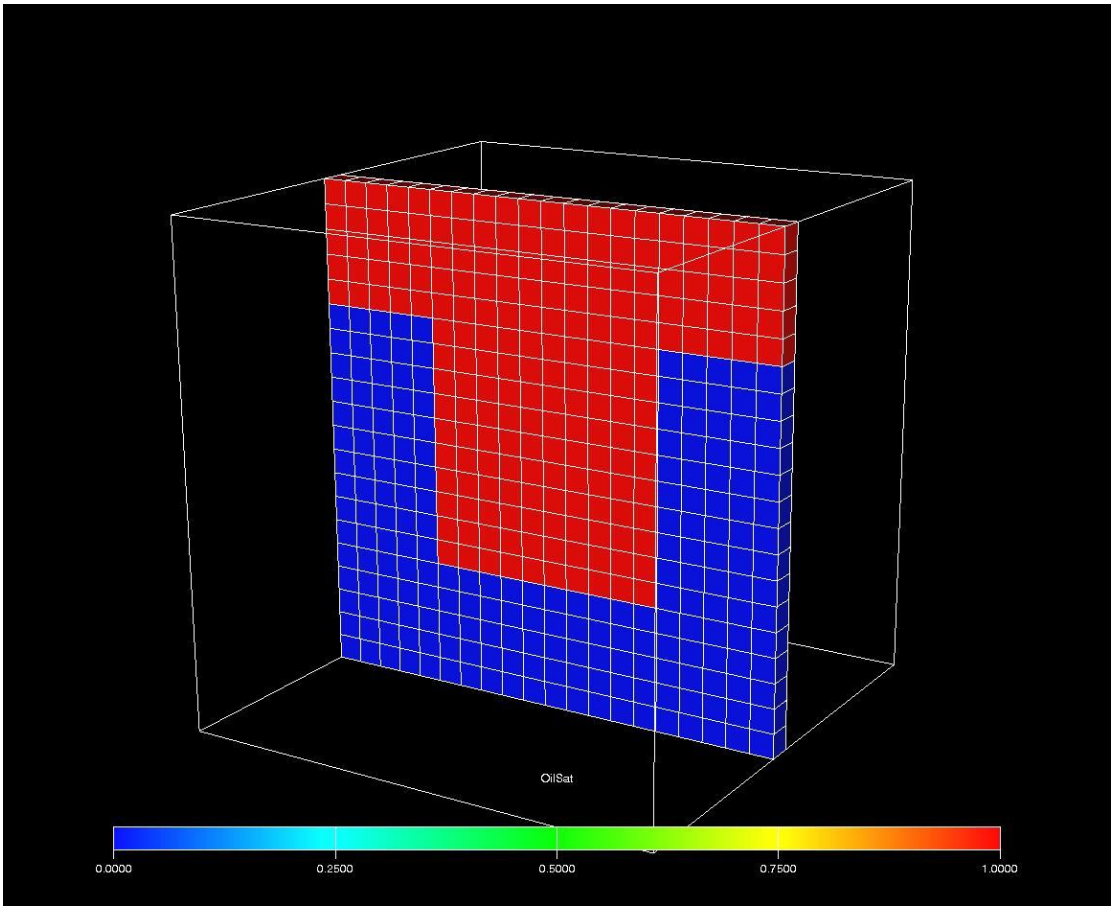

Figure 4.6: IJ plane-slice of the constructed grid for test 22, where red colour illustrates oil phase and oil-filled core plug, whereas blue colour is used for water phase.

An effect of using the same capillary pressure and relative permeability curves for test 22 as for test 12, is identical ultimate oil recoveries. Hence, normalized ultimate oil recovery is given to view differences in curve shape and recovery time. Figure 4.7 shows a comparison between simulated and experimental oil recovery curves.

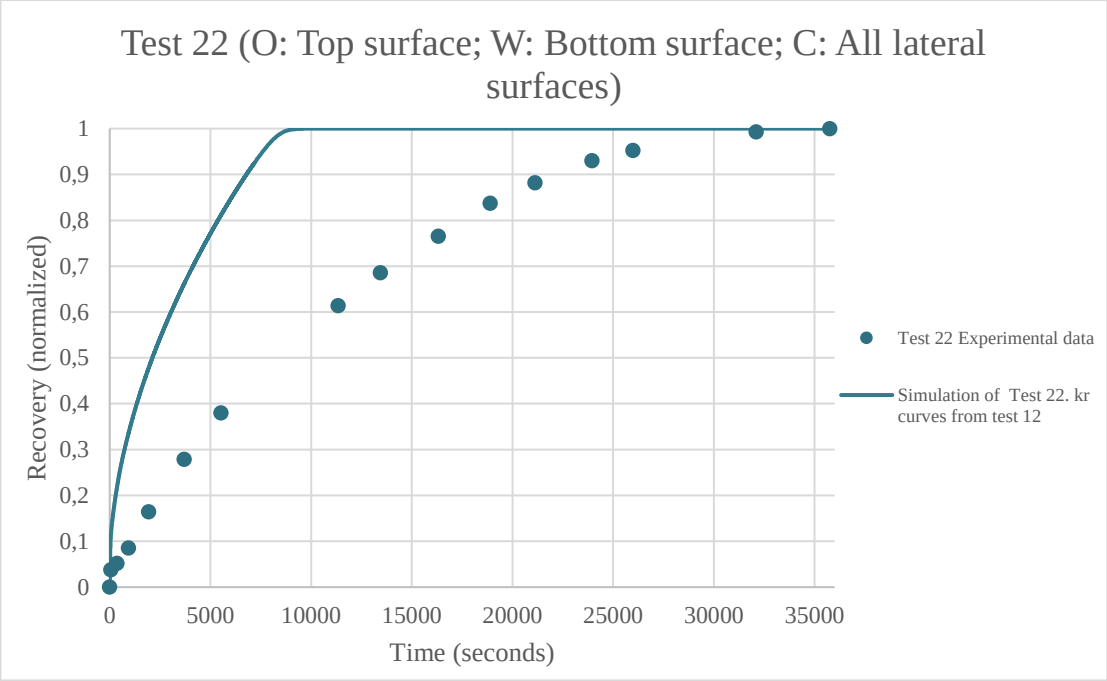

Figure 4.7: Comparison between experimental and simulated oil recovery curves for co-current imbibition test 22.

It can be seen from Figure 4.7 that neither the shape or recovery rate of the simulated recovery curve is reproduced effectively. In fact, the experimental half-recovery time is nearly 4 times higher than for the simulation. This is the opposite of what was found in experiments by (Standnes, 2004) and (Bourbiaux & Kalaydjian, 1990). They discovered that counter-current SI in general shows significantly higher recovery times than for co-current SI. Then, with counter-current relative permeability curves used for test 22, one would expect a higher simulated half-recovery time than for the co-current experimental data. To determine if test 22 was an anomaly, the remaining co-current tests performed by Standnes (2004) was also simulated and compared with experimental data. The results are depicted in Figure 4.8 to Figure 4.12 with boundary conditions explained in Table 3.

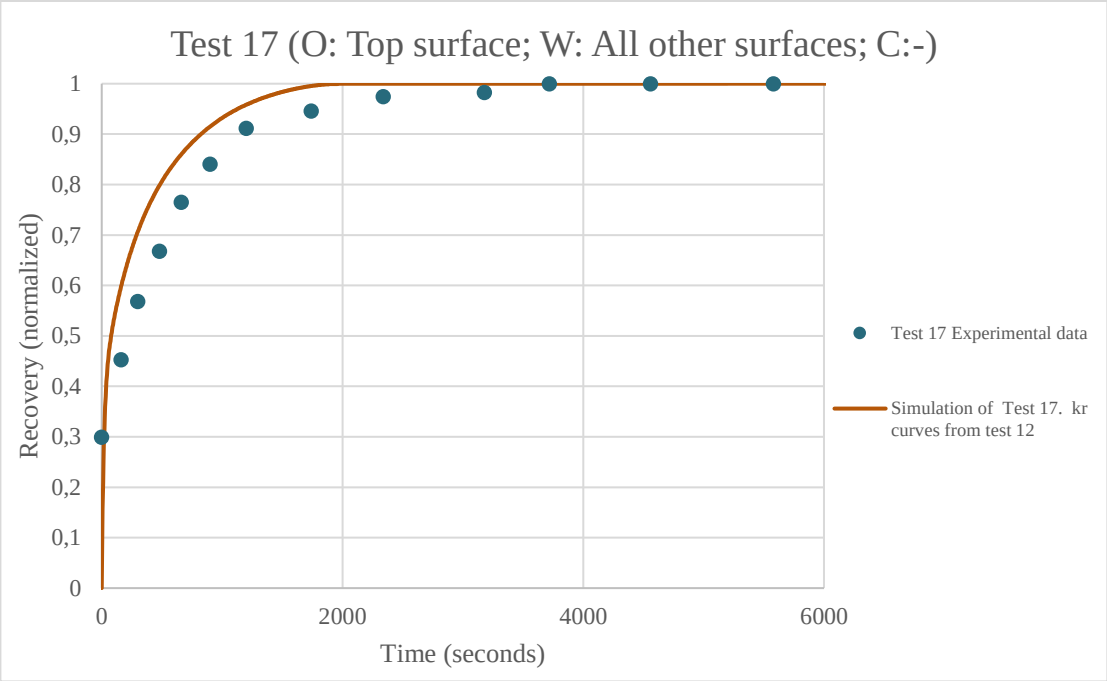

Figure 4.8: Comparison between experimental and simulated oil recovery curves for co-current SI test 17.

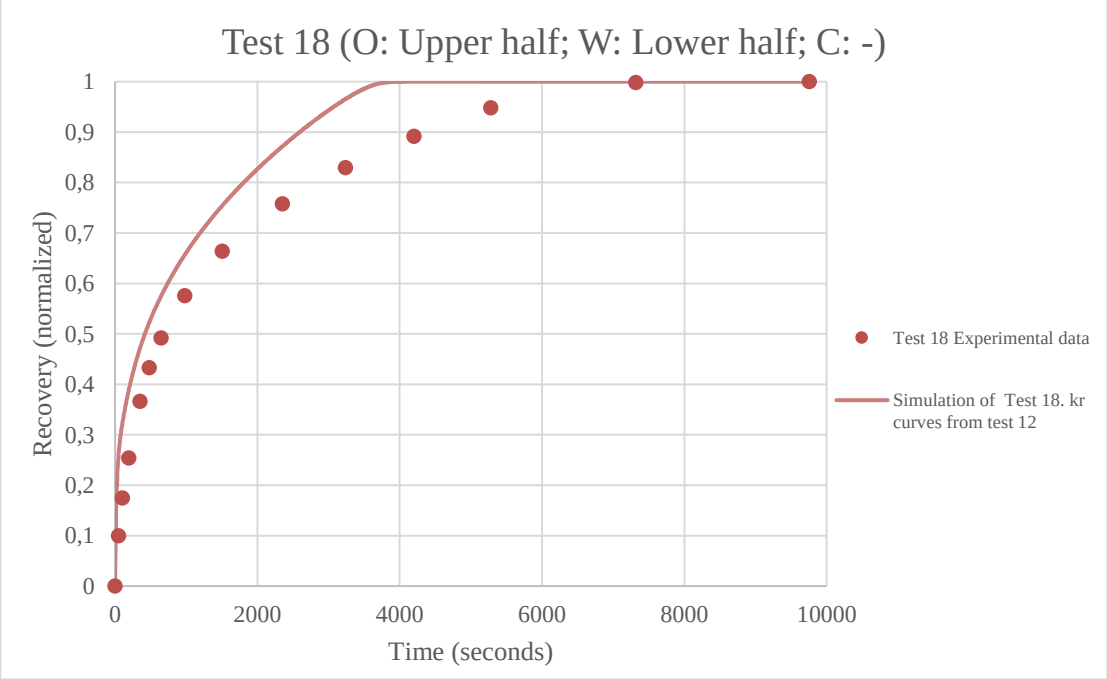

Figure 4.9: Comparison between experimental and simulated oil recovery curves for co-current SI test 18.

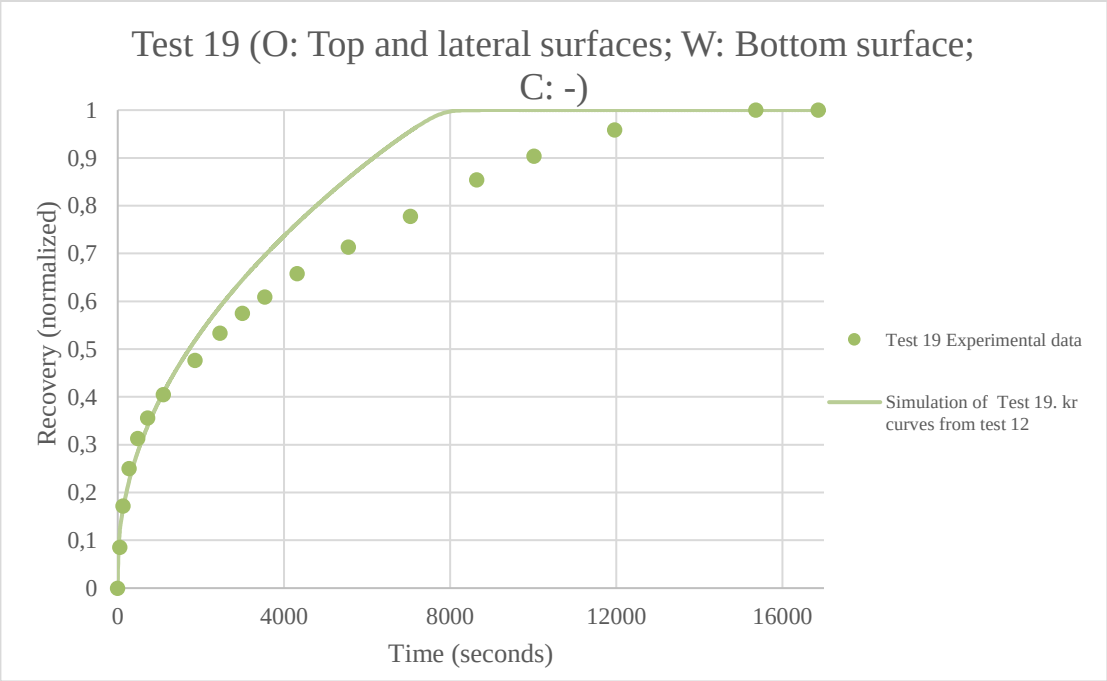

Figure 4.10: Comparison between experimental and simulated oil recovery curves for co-current SI test 19.

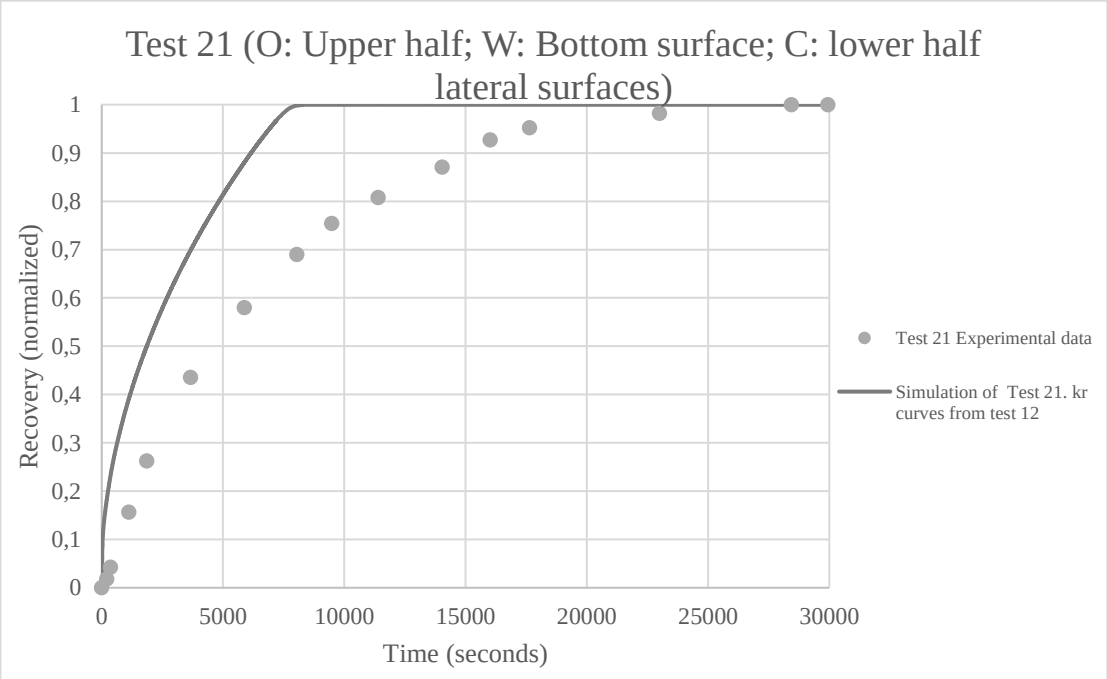

Figure 4.11: Comparison between experimental and simulated oil recovery curves for co-current SI test 21.

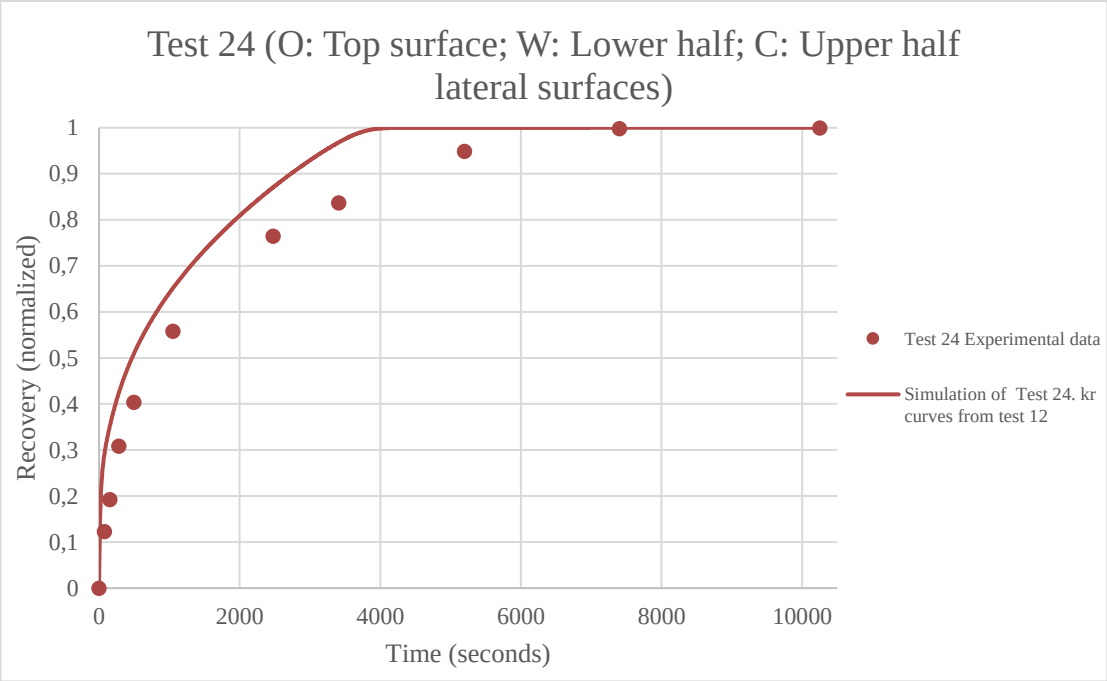

Figure 4.12: Comparison between experimental and simulated oil recovery curves for co-current SI test 24.

The 5 additional co-current tests show a consistent deviation between simulated and experimental recovery curves. As for test 22, these tests also experience higher experimental half-recovery times. It can be argued that this consistency confirms that test 22 most likely is not an isolated case. Still, the reason why all co-current simulations based on counter-current relative permeability curves consistently show reversed results (of what is expected), was unclear.

To determine if test 12 could be experimentally flawed, a simulation of test 23 based on relative permeability curves from test 12 was performed to compare results. The fact that test 12 and test 23 both are performed under the same conditions (1D counter-current SI) would suggest a close match between simulated and experimental oil recovery curves for Test 23. A comparison of simulations and experimental data for test 12 and test 23 is shown in Figure 4.13.

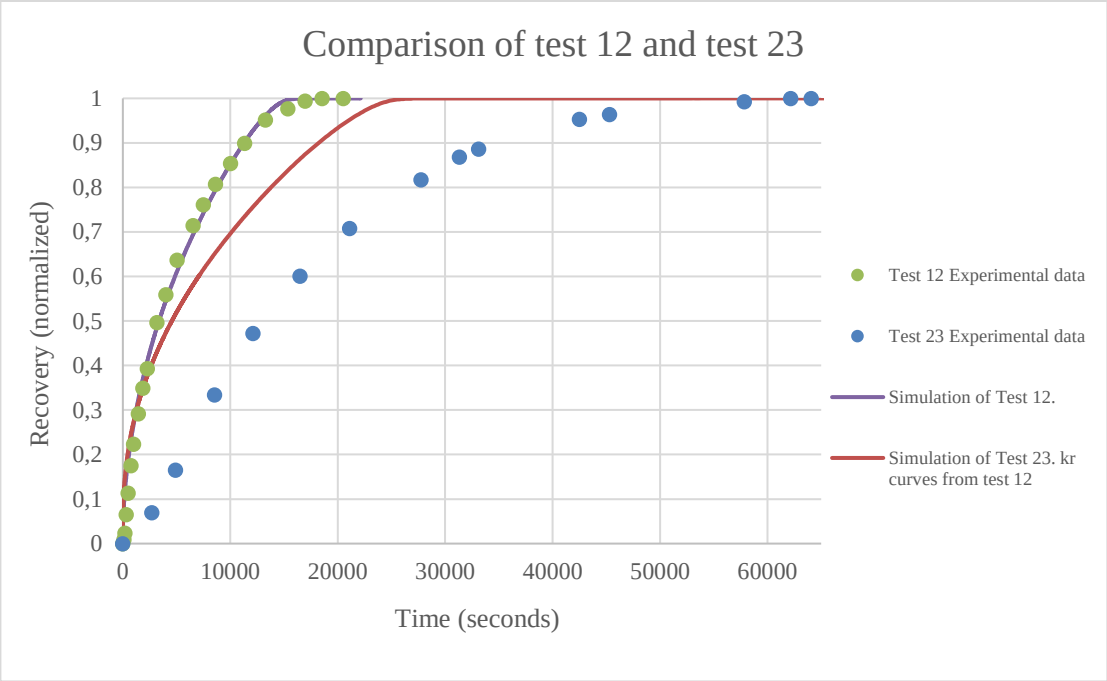

Figure 4.13: Simulations of test 12 (1-D counter current SI) and test 23 (1-D counter current SI) with relative permeability curves from test 12.

Test 23 shows a suspiciously large deviation between the simulation and experimental data. For a case where counter-current flow is the dominant production mechanism and counter-current relative permeability curves are used, the simulated oil recovery should in theory reproduce experimental data. To find an explanation for this, experimental details where closely compared and potential errors in the numerical simulation was investigated. The minor porosity difference of 43.7% (test 12) against 42.9% (test 23) was also tested, but showed no impact on the simulated results. In fact, no other significant difference than the core sample lengths could be found, which is accounted for in the DATA-file. Subsequently, one may ask what else could cause such deviation in results between two very similar experiments. A possible explanation suggests that either test 12 or test 23 must be experimentally flawed. Therefore, it was decided to further investigate the relationship between test 12 and test 23. A solution was to history match experimental data for test 23 to simulate co-current tests 17-24 with obtained relative permeability curves. This would enable a comparison with the results found with test 12.

4.4 History matching of test 23

Test 23 was history matched by using the same relative permeability curves as obtained for test 12, and multiply the capillary pressure curve with a factor of 0.76. Endpoint saturations was set equal to those used in history matching of test 12. The same was done with endpoint relative permeability values. Other differences in experimental details were adjusted in the DATA-file. The final k_{rw}-, k_{ro}- and P_c

values for corresponding water saturation can be found in Table 13 and Table 14 in appendix B. Figure 4.14 depicts the best history match for test 23.

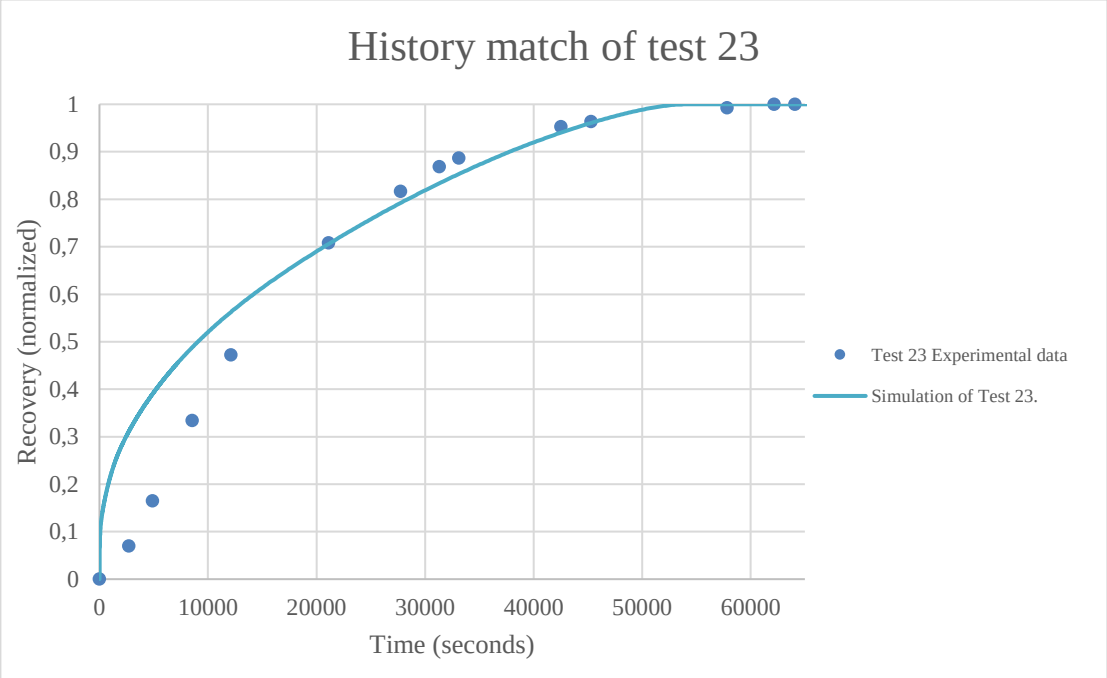

Figure 4.14: History match of test 23 with normalized recovery on the y-axis and time (seconds) on the x-axis.

The simulation of test 23 experiences some deviation at early times, but is in good agreement experimental data after approximately 20000 seconds. The deviation in early times may be due to several factors, in which no local grid refinement is one of them.

4.4.1 Co-current simulations based on test 23

After a satisfactory history match was obtained for test 23, capillary pressure and relative permeability curves were used in simulations of co-current SI to compare simulations with experimental data. At this point, the aim was to investigate if the history matched counter-current relative permeability curves from test 23, also would give reversed results when used in simulations. A comparison between simulated and experimental oil recovery curves for test 22 can be seen in Figure 4.15. The remaining simulations of co-current tests based on test 23 can be found in appendix C.

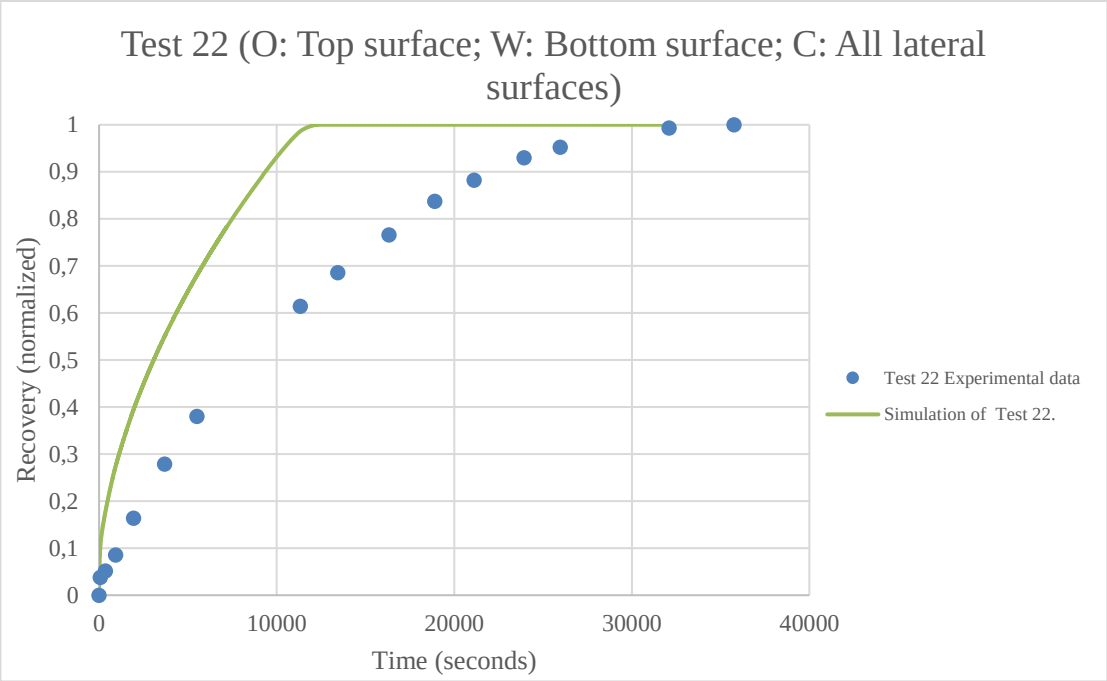

Figure 4.15: Comparison between experimental and simulated oil recovery curves for co-current imbibition test 22.

The numerical investigation of test 23 showed that not only test 22 (1-D co-current), but all co-current simulations (except test 18) showed higher experimental half-recovery times. Since the same trend was found for co-current simulations based on test 23 as for test 12, this give no information on which 1-D counter-current test is more correct.

The aim of this thesis is to investigate what extent counter-current relative permeability curves must be changed to match co-current experimental data. To perform such a study, a representative counter-current test is needed as a basecase. Subsequently, a closer investigation of experimental inconsistency was required to determine which out of test 12 and test 23 had the most representative experimental data.

4.5 Investigation of experimental inconsistency

It has been verified that oil recovery by 1-D counter-current spontaneous imbibition (before the water front reaches the end of the core sample) is proportional to the square root of the imbibition time (Fernø et al., 2013; Fischer & Morrow, 2005; Li & Horne, 2006). Hence, by plotting the square root of imbibition time against normalized oil recovery would indicate any deviations of this relationship. The straight line can be described with equation (29) where R_{SI} is ultimate oil recovery, k is the slope of the line and t is time. Figure 4.16 shows normalized oil recovery for test 12 and 23, plotted versus the square root of imbibition time.

$$R_{SI}^2 = k^2 * t \quad \textbf{(29)}$$

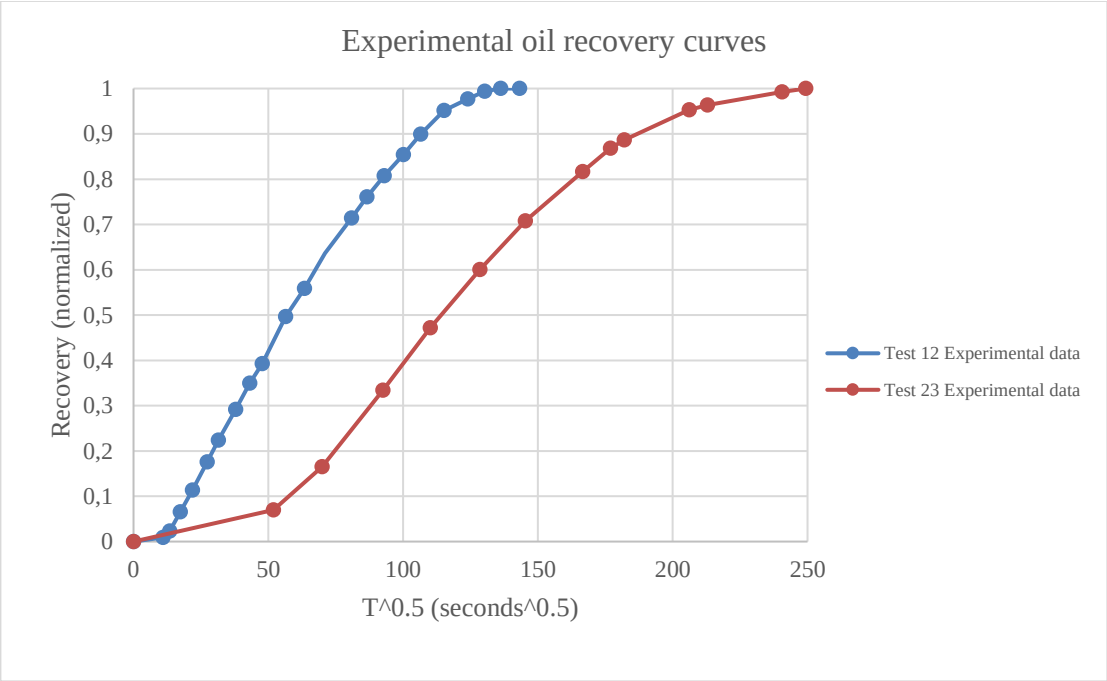

Figure 4.16: Comparison of the normalized oil recovery rates versus the square root of imbibition time for experimental data for test 12 and test 23.

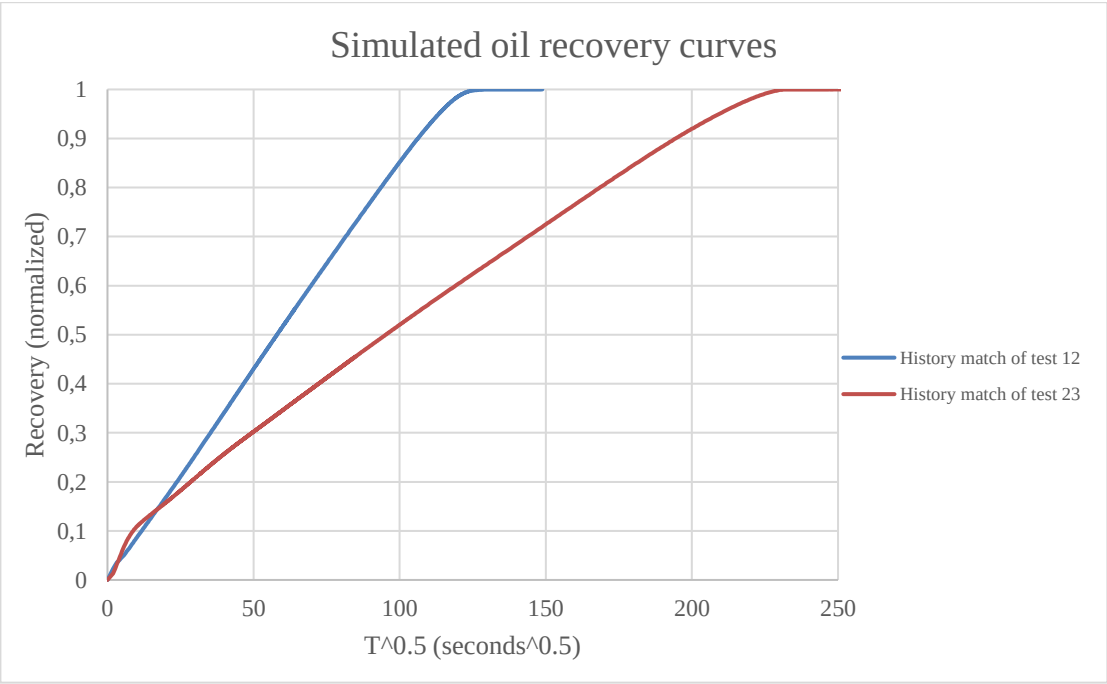

Figure 4.17: Comparison of the normalized oil recovery rates versus the square root of imbibition time for simulations of test 12 and test 23 with relative permeability curves from test 12.

It can be argued that the experimental recovery curve for test 23 exhibits greater deviation from a straight line than for test 12, when plotted against the square root of imbibition time. This is a strong indication of inconsistency between test 12 and test 23. Furthermore, Figure 4.17 was used to verify the consistency of the model used in simulations. The fact that straight lines can be seen for simulations of both tests, would suggest that the model is more correct.

4.5.1 Constant diffusion coefficient

For further verification of inconsistency between experimental data, the diffusion coefficients at oil-production plateau were calculated for both test 12 and test 23. From the relationship given by equation (29), it can be derived that the diffusion coefficient must be constant for 1-D counter-current SI to be proportional with the square root of imbibition time. Due to the results depicted in Figure 4.16, a difference in diffusion coefficients would be expected for test 12 and test 23. The calculated values were found by equation (30), where L is core sample length, k is diffusion coefficient and t is time. The diffusion coefficients for test 12 and test 23 calculated from simulated and experimental data are given in Table 7.

$$k = \sqrt{\frac{L^2}{t}} \tag{30}$$

Table 7: Comparison of diffusion coefficients for experimental data and simulations for test 12 and test 23.

Diffusion coefficient		
	Experimental	Simulation
Test 12	0.03	0.03
Test 23	0.02	0.03

The experimental diffusion coefficients show noticeable deviation, which is another sign for inconsistency between data. On the other hand, simulations show almost identical values, which again suggests that the model is more correct.

4.5.2 Simulations of counter-current test based on test 12 and test 23

It was decided to run counter-current tests 7 and 8 with input data from test 12 and test 23 to view which of the tests could better reproduce experimental data.

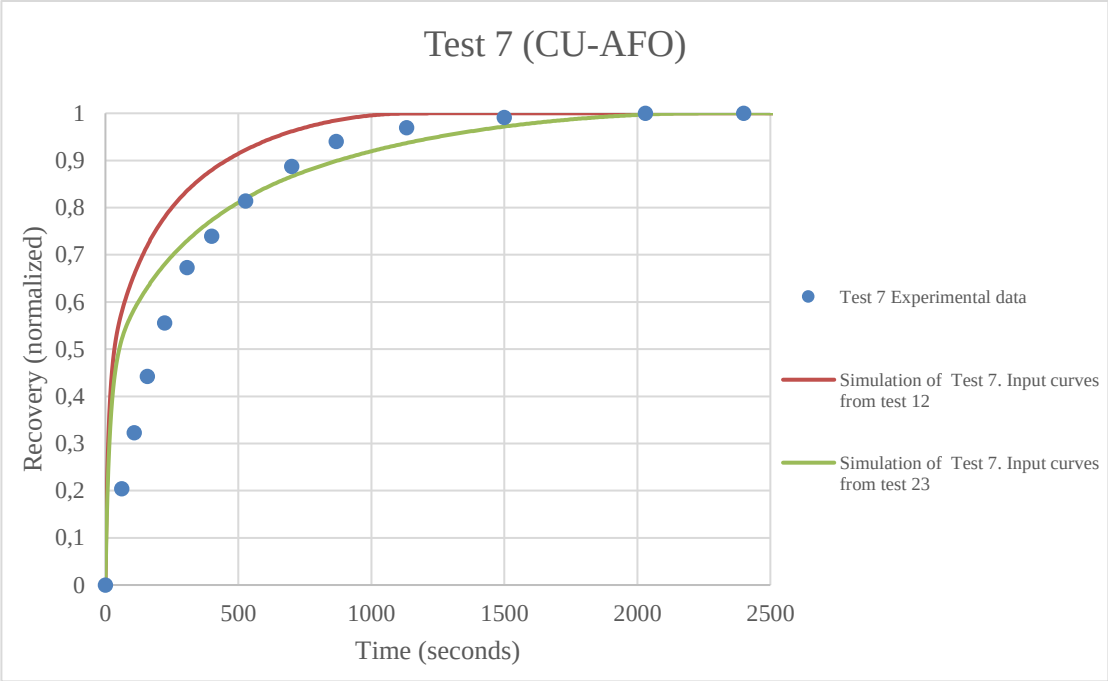

Figure 4.18: Comparison between experimental and simulated oil recovery curves for counter-current imbibition test 7, with input curves from test 12 and test 23.

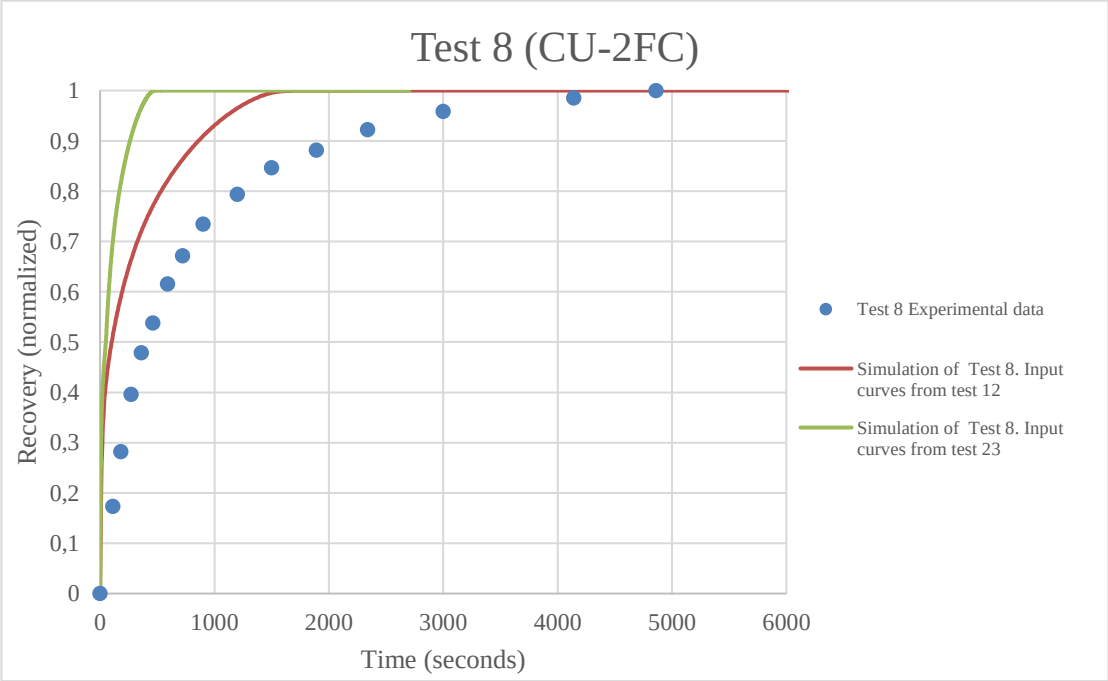

Figure 4.19: Comparison between experimental and simulated oil recovery curves for counter-current imbibition test 8, with input curves from test 12 and test 23.

It can be argued that test 12 exhibit more consistent results and better reproduce experimental data based on curve shape and oil recovery rate. The conflicting results found in this investigation confirms inconsistency between test 12 or test 23. Furthermore, based on the results that was found, it can be

argued that most of the factors indicate that test 23 is experimentally flawed. In consequence of this, test 12 will be used as the 1- D counter-current basecase for further investigation in this thesis.

4.6 Numerical investigation of co-current data

To investigate how much counter-current relative permeability curves must be changed to match co-current experimental, test 22 and test 12 were selected as the most representative experiments for comparison. As both tests were performed on very similar rock samples this enabled a comparison of 1-D co-current and 1-D counter-current SI. However, due to unexpected results for all co-current tests, this introduced new questions regarding the representativeness of the co-current experimental data as well. The fact that all co-current simulations based on counter-current relative permeability curves consistently showed lower half-recovery times may suggest that all co-current experiments show too high oil recovery rates. Then, what would be the result of reversing the procedure of numerical investigation? In other words, performing simulations of counter-current oil recovery rates based on co-current relative permeability- and capillary pressure curves. Would these results also be opposite of what is expected? These questions led to a new investigation where test 22 (1-D co-current) was history matched to study the result of counter-current simulations based on co-current relative permeability curves.

4.6.1 History match of test 22

A match between simulations and experimental data was obtained by using the relative permeability curves from test 12 while the capillary pressure curve was adjusted. The saturation interval for water was scaled up to fit the recovery factor. Furthermore, no grid refinements were used and all other experimental details were imported to the DATA-file. The final endpoint values, constants and tabulated values that were used are presented in Table 15 and Table 16, appendix D. Figure 4.20 give a picture of the best history match for test 23.

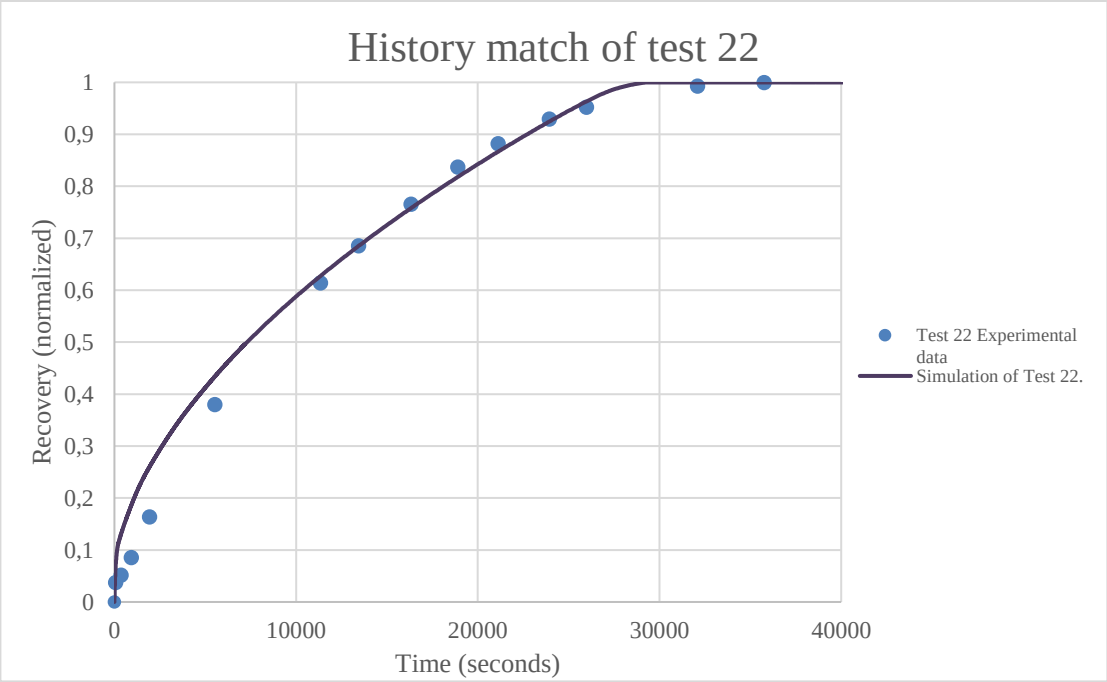

Figure 4.20: History match of test 22 with normalized recovery on the y-axis and time (seconds) on the x-axis.

The simulation of test 22 match the experimental data surprisingly well. The deviation in early time has been previously discussed.

4.6.2 Counter-current simulations based on test 22

After a satisfactory history match was obtained for test 23, final capillary pressures and relative permeability curves were used in simulations of counter-current SI to compare simulations with experimental data. At this point, the aim was to investigate if the history matched co-current relative permeability curves from test 22 would give reversed results, as found for both test 12 and test 23. If so, this would strongly question the representativeness of the experimental data of which this thesis is based on. A comparison between simulated and experimental oil recovery curves for four selected counter-current tests are plotted in Figure 4.21 to Figure 4.24.

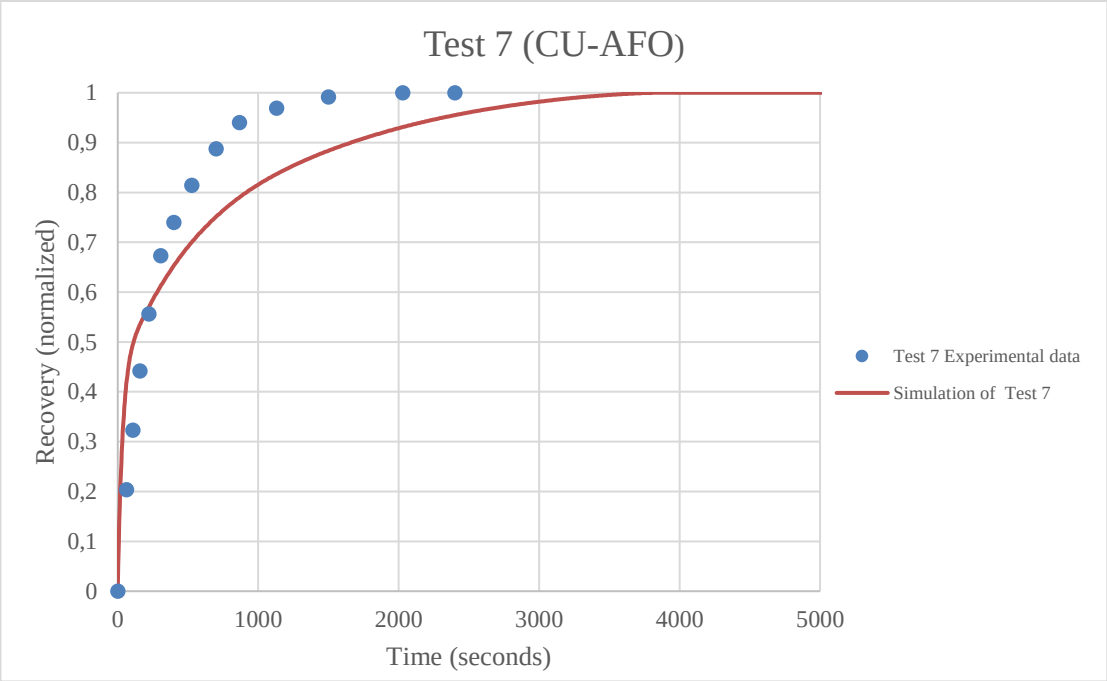

Figure 4.21: Comparison between experimental and simulated oil recovery curves for co-current imbibition test 7.

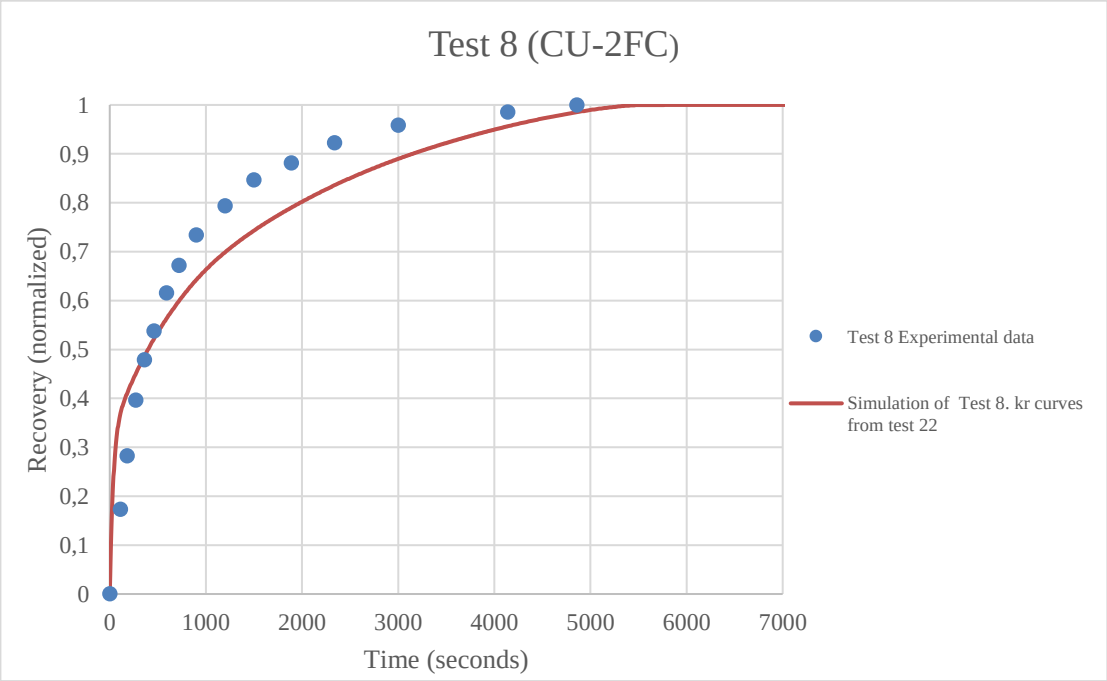

Figure 4.22: Comparison between experimental and simulated oil recovery curves for co-current imbibition test 12.

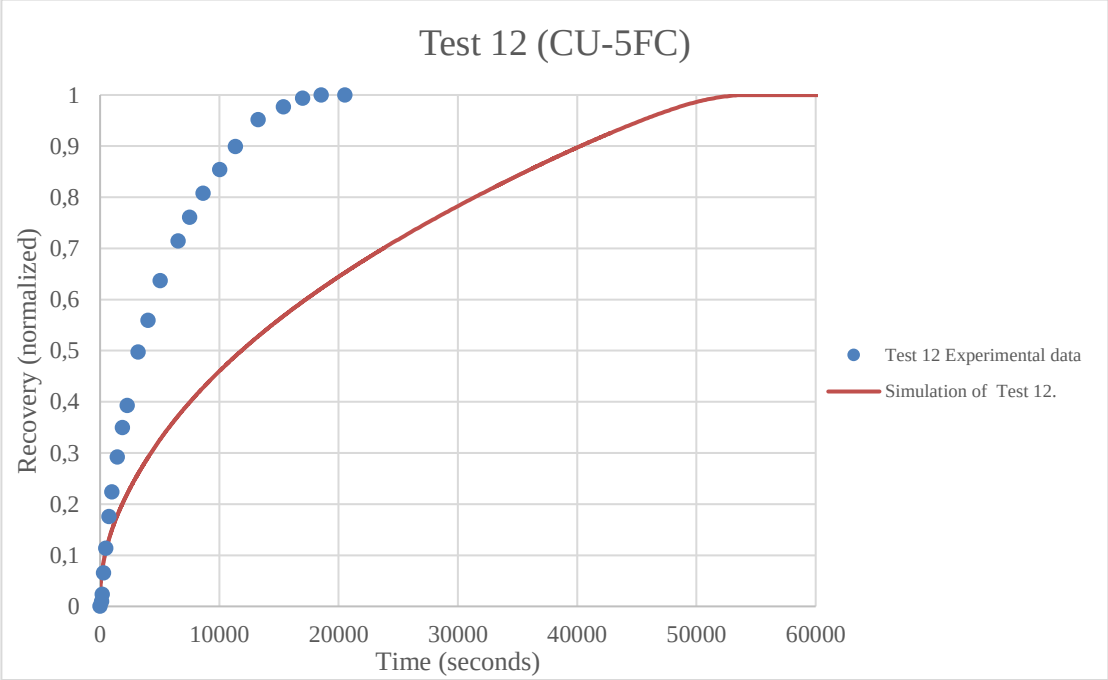

Figure 4.23: Comparison between experimental and simulated oil recovery curves for co-current imbibition test 12.

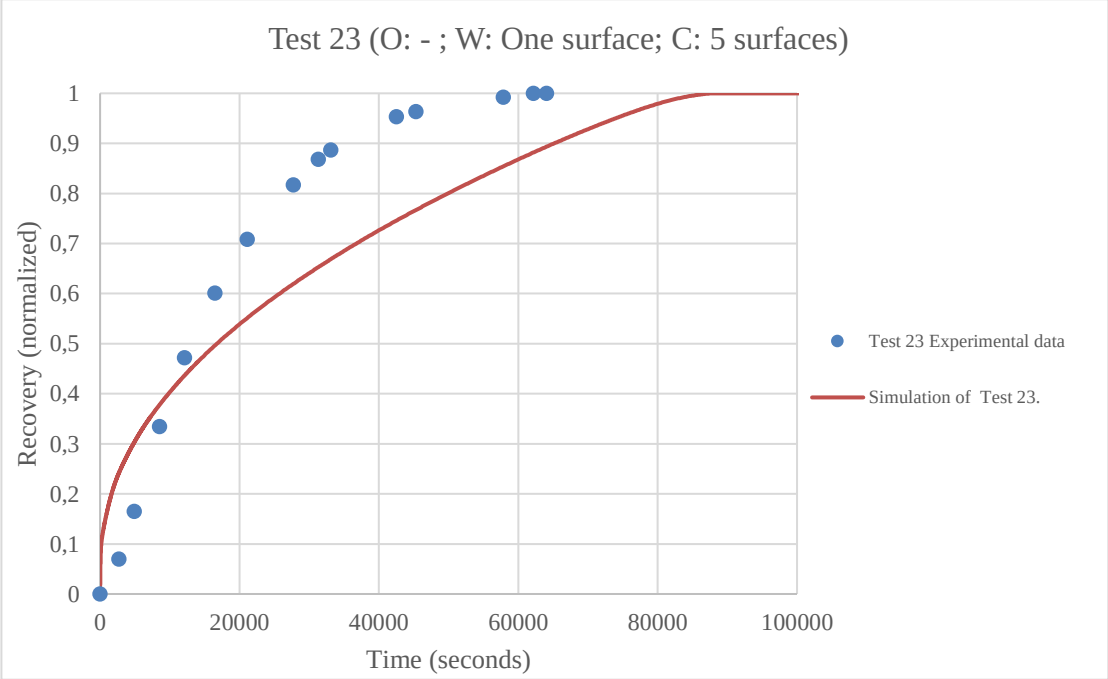

Figure 4.24: Comparison between experimental and simulated oil recovery curves for co-current imbibition test 12.

Interestingly, all co-current simulations based on counter-current relative permeability curves show faster recovery rates than the experimental data. This is the very opposite of what is theoretically

expected (Bourbiaux & Kalaydjian, 1990; Pooladi-Darvish & Firoozabadi, 2000; Standnes, 2004). With co-current relative permeability curves used for counter-current tests, one would expect a lower simulated half-recovery time than for the experimental data. The reason why all results from this numerical investigation appears to be reversed could not be confirmed with certainty. However, it suggests that certain tests may be experimentally flawed, which will cause great uncertainty and misevaluation of all further comparisons by which the flawed tests are included. In this thesis, the problem of inconsistent data was not further addressed. Instead, attention was directed towards a study performed by two French scientists, Bourbiaux & Kalaydjian, where their topic of interest is very relevant to the main subject of this thesis.

4.7 Part 2 - Experimental details

Bourbiaux & Kalaydjian also investigated the difference between calculated and experimental recovery rates. Relative permeability curves were modified to reproduce the oil recovery rate equal to experimental data.

The spontaneous imbibition experiments were performed by putting one or two ends of the core sample in in contact with water, in which the produced oil was collected in a separator. Furthermore, all experiments were performed under laboratory conditions at a constant temperature of 20 °C on fine and slightly illitic Triassic sandstone from France. The porous medium was strongly water-wet with low permeability and high porosity. With a rectangular shape, the core sample has a cross section of 13 cm^2 and length of 29 cm. A summary of fluid properties and experimental details is given in Table 8 and

Table 9. Figure 4.25 depicts the experimental setup by Bourbiaux and Kalaydjian (1990), used in measurements of co-current and counter-current SI.

Table 8: Fluid properties.

Liquid phase	Density at 20 °C (g/cm^3)	Viscosity at 20 °C (mPa*s)	IFT (mN/m)
Brine	0.9982	1	35
Paraffinic oil	0.76	1.5	-

Table 9: Experimental details for SI tests performed in in tests GVB-1, GVB-2 and GVB-4.

Test no.	Description	K (md)	Length (m)	Porosity (%)	K_{ro}*	K_{rw}*	S_{or} (% of PV)
GVB-1	Co-current	137	0.29	23.3	0.56	0.048	37.6
GVB-3	Counter-current	124	0.29	23.3	0.46	0.044	42.2
GVB-4	Total	118	0.29	23.3	0.49	0.045	39.9

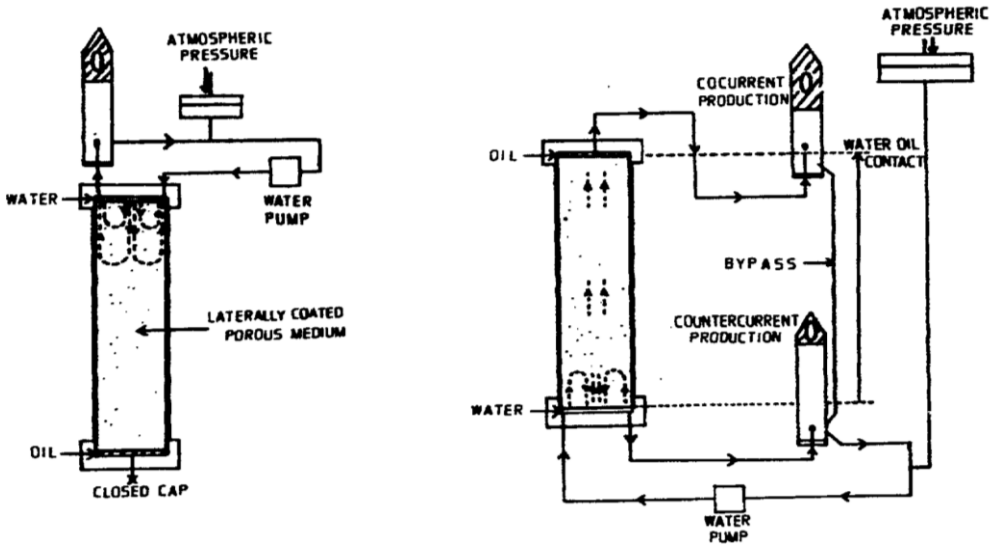

Figure 4.25: Experimental setup for counter-current and co-current SI, respectively (Bourbiaux & Kalaydjian, 1990).

4.7.1 History matching of test GVB-1

In their simulations, Bourbiaux & Kalaydjian investigated if experimentally obatined co-current relative permeability curves (test GVB-1) would reproduce experimental data for pure counter-current flow. They used a 1-D, finite difference numerical model with 29 identical blocks in vertical direction, with the following dimensions: 2.1 cm x 6.1 cm x 1.0 cm. The final capillary pressure curve was obtained by including local variations caused by porosity and absolute permeability into the experimentally found reference curves. Moreover, the shape of the relative permeability curves used in simulations was estimated from relative permeability curves (by the unsteady-state method) with other cores from the same porous medium. The endpoints of these curves were the co-current oil and brine endpoints at the end of drainage and during tertiary waterflooding.

To recreate and further investigate tests performed by Bourbiaux & Kalaydjian, the first step was to history match test GVB-1 (1-D co-current) to use the obtained relative permeability curves in simulations of test GVB-3 (1-D counter-current). In order to do so, a DATA-file was constructed based on the DATA-file used in history matching of test 12 CU-5FC. The grid consisted of 20 x 20 x 20 grid blocks in which 1000 blocks in the middle of the grid reprsented the core plug. Different from test 12, which was initially 100 % oil filled, test GVB-1 had an initial water saturation of 39 % and a residual oil saturation of 37. 6 %, indicating no more than 23.3 % mobile oil.

The relative permeability curves and capillary pressure curves were generated from the Corey type expressions and Skjaeveland equation described in chapter 2.3 and 2.4. These curves were constantly adjusted until a close match was found with the curves by Bourbiaux & Kalaydjian. The final endpoint values, constants and exponents used in the best match are presented in Table 10. Furthermore,

Table 11 shows the final tabulated values for capillary pressure and relative permeability curves for corresponding water saturation.

Table 10: key input parameters used to generate final capillary pressure and relative permeability curves used in history matching of test GVB-1.

Corey exponents and endpoint relative permeabilities		Capillary pressure constants and exponents		Endpoint saturations	
n_w	2	c_w	0.6	S_{wi}	0.39
n_o	1.5	c_o	-0.0003	S_{or}	0.376
k_{rw}*	0.048	a_w	2.9		
k_{ro}*	0.56	a_o	1.5		

Table 11: Tabulated values for Pc, k_{rw} and k_{ro} for different water saturations used in history match of test GVB-1.

S_w [fraction]	K_{rw} [fraction]	K_{ro} [fraction]	P_c [atm]
0.39	0	0.56	0.11843
0.4	8.7662E-05	0.52449	0.08441
0.42	0.00078895	0.45584	0.07327
0.44	0.00219154	0.39047	0.06402
0.46	0.00429542	0.32857	0.05627
0.48	0.00710059	0.27034	0.04973
0.5	0.01060706	0.21602	0.04417
0.52	0.01481481	0.16593	0.0394
0.54	0.01972387	0.12044	0.0353
0.56	0.02533421	0.0801	0.03173
0.58	0.03164585	0.04566	0.02858
0.6	0.03865878	0.01839	0.02566
0.62	0.046373	0.00125	0.01792
0.624	0.048	0	0

The final capillary pressure curve and relative permeability curves used in the history match of test GVB-1 compared to the curves found by Bourbiaux & Kalaydjian, are depicted in Figure 4.26 and Figure 4.27. It can be argued that the deviation is small, which resulted in a quite good match of experimental data, which is shown in Figure 4.28.

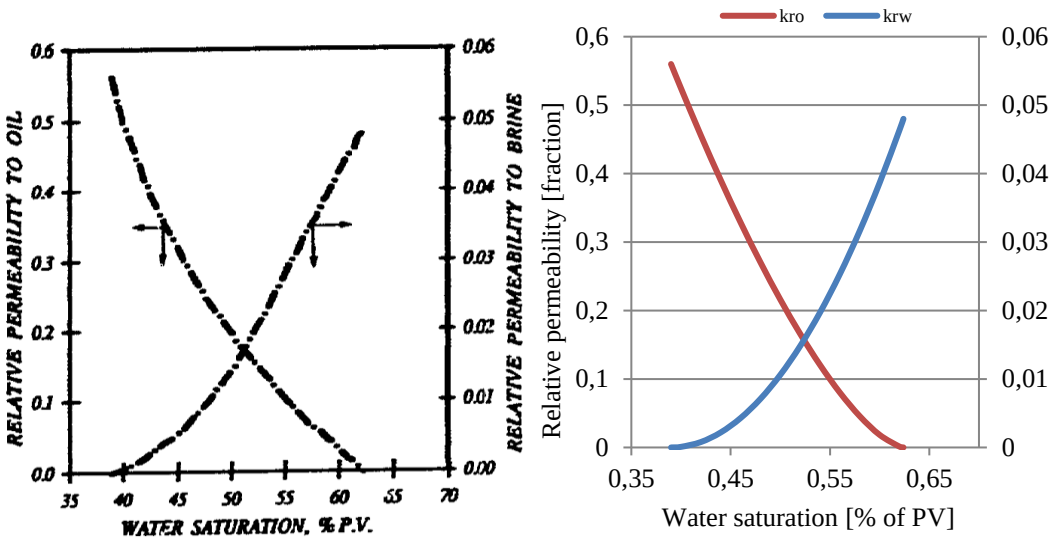

Figure 4.26: Relative permeability curves with k_{ro} on the primary y-axis, k_{rw} on the secondary y-axis plotted against corresponding water saturation on the x-axis. Left: Bourbiaux & Kalaydjian (1990). Right: Utsetø 2017

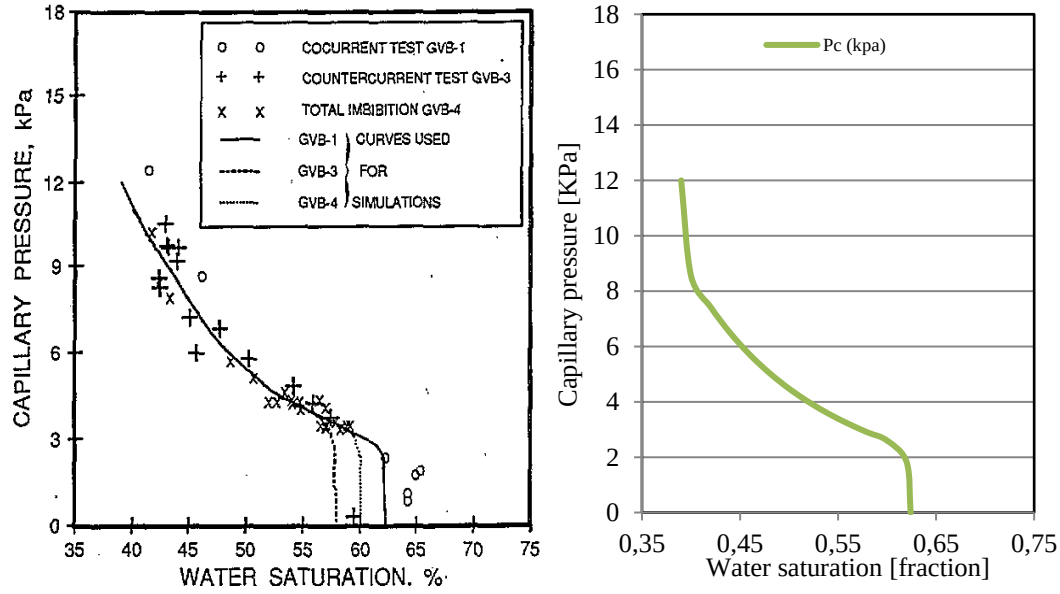

Figure 4.27: Capillary pressure curve on the y-axis plotted against corresponding water saturation on the x-axis. Left: Bourbiaux & Kalaydjian (1990). Right: Utsetø 2017

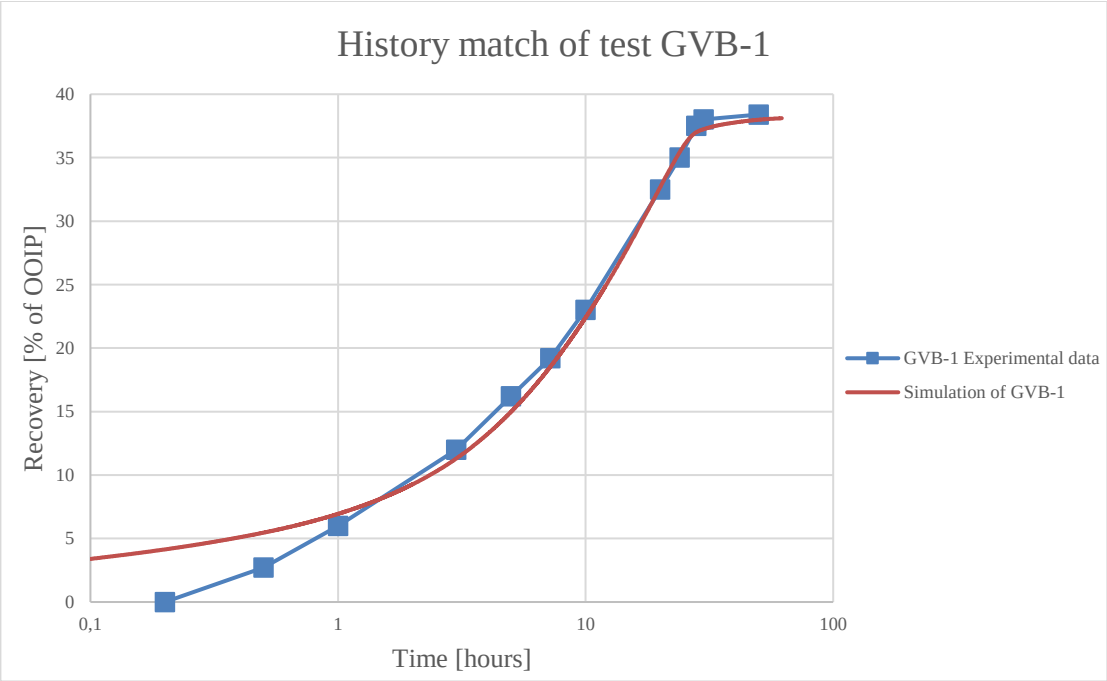

Figure 4.28: History match of test GVB-1 with recovery (% of OOIP) on the y-axis and time (hours) on the x-axis (logarithmic units).

The simulation of GVB-1 is in good agreement with experimental data and depicts quite small deviations after 1 hour (log scale). The relative permeability curves obtained from the match of test GVB-1 could now be used in simulations of test GVB-3.

4.7.2 Simulation of GVB-3

The DATA-file used in simulations of co-current test GVB-1 needed only simple adjustments to enable counter-current simulations (test GVB-3). The SWOF-table was completed with capillary pressure and relative permeability curves obtained from history match of test GVB-1. Moreover, boundary conditions were updated by closing off the bottom surface of the core sample. This would enable a 1-D counter-current simulation with co-current input curves for capillary pressure and relative permeability for brine and oil. Due to unexpected (reversed) results for all simulations of experiments by Standnes (2004), it remained interesting to see if different results would be obtained based on a different dataset. A comparison of experimental and simulated oil recovery curves can for test GVB-3 is depicted in Figure 4.29.

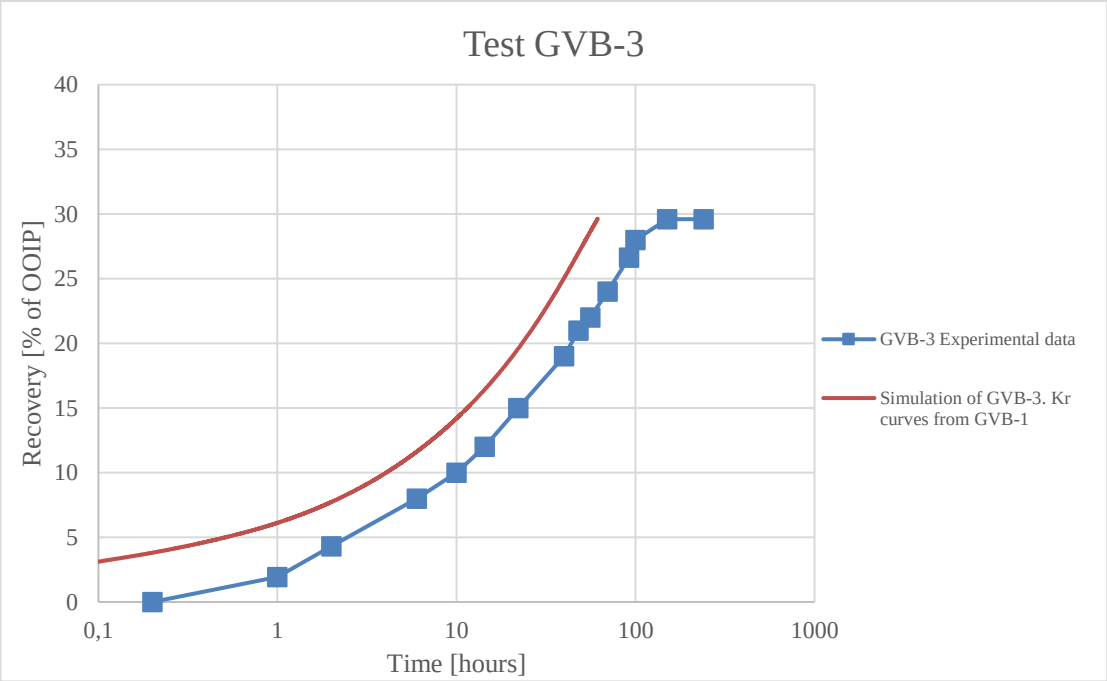

Figure 4.29: Comparison between experimental and simulated oil recovery curves for counter-current imbibition test GVB-3.

It was discussed in chapter 4.3 that several studies have been performed to investigate co-current and counter-current flow regimes. It was discovered by Bourbiaux & Kalaydjian in 1990 and experimentally confirmed by Standnes in 2004 that counter-current oil production is in general much slower than co-current production. The same conclusion was found by Pooladi-Darvish and Firoozabadi (2000). Hence, compared to these previous studies, the relationship between experimental and simulated oil recovery curves found in Figure 4.29 agrees with the theory. The simulation of test GVB-3 based on co-current relative permeability curves shows faster oil production. Yet, the shape of experimental data reproduced well and results are comparable to what was found by Bourbiaux & Kalaydjian. They discovered a 6 hour difference between experimental and simulated half-recovery time (when detailed petrophysical properties were considered). In comparison, with the model used in this thesis, the simulated half-recovery time was approximately 11 hours less than the experimental one. One explanation for this may be due to potential differences in the model used for simulations. Bourbiaux & Kalaydjian used a grid with 29 identical grid blocks whereas 8000 grid blocks was applied in this thesis.

4.8 Investigation of relative permeability curves

Bourbiaux & Kalaydjian investigated the origin of the difference between simulated and experimental oil recovery rates and found that good prediction could be achieved by decreasing the co-current relative permeabilities. The magnitude of reduction varied for oil and brine relative permeability. They concluded that a good match could be found by reducing the relative oil permeability values (k_{ro}) by 60

% of their co-current values, the brine relative permeabilities (k_{rw}) by 45 % or by reducing both k_{ro} and k_{rw} by 30 %. The latter option was considered to be the best approximate solution. To determine if a similar relationship between co-current and counter-current oil recovery curves exists for the model used in this thesis, the same reduction factors were applied for co-current relative permeability curves obtained from test GVB-1. Figure 4.30 shows the results of reduced relative permeability curves for oil and brine compared to counter-current experimental data.

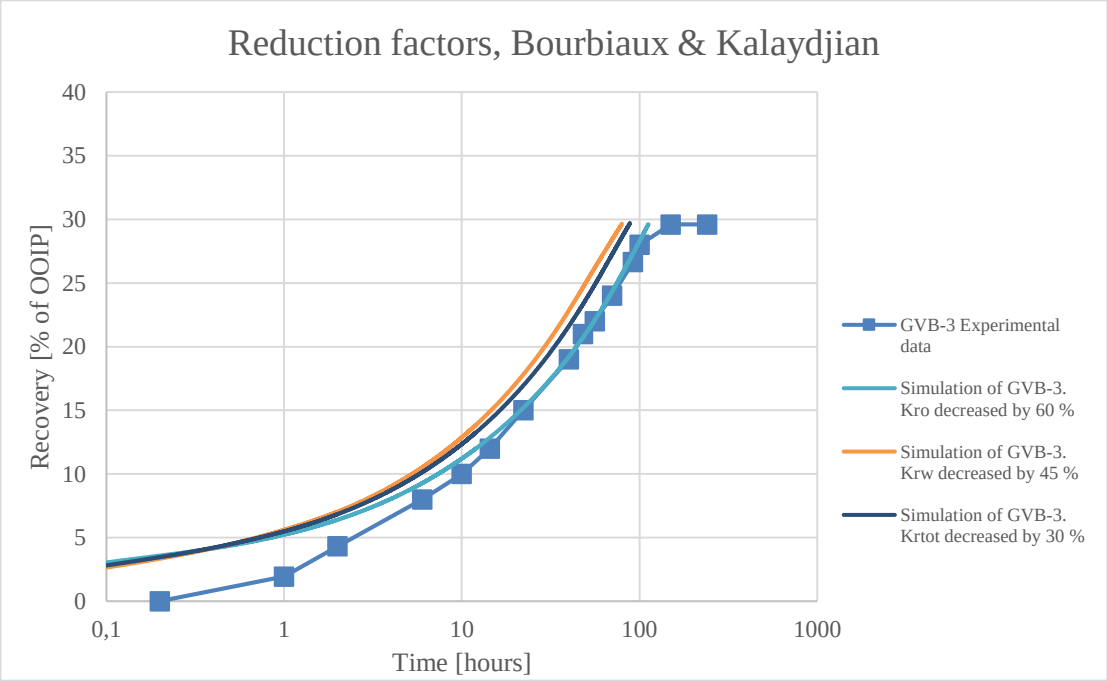

Figure 4.30: Comparison between experimental and simulated oil recovery curves for counter-current imbibition test GVB-3, with reduced co-current relative permeability curves. Reduction factors by Bourbiaux & Kalaydjian 1990.

A good reproduction of the experimental oil recovery rate was only obtained by reducing the oil relative permeabilities by 60 % of co-current values. The reason for this could be due to differences in the model used for simulations. It must be mentioned that Bourbiaux & Kalaydjian incorporated all local information in their numerical model including local porosities and local permeabilities estimated from micropermeability measurments. Such information was not included in the model used in this thesis. Consequently, identical results as found by Bourbiaux & Kalaydjian could not be expected. Therefore, it was decided to investigate how much the co-current relative permeability values from test GVB-1 had to be reduced in order to match experimental data. It was found that good reproduction was obtained by reducing oil relative permeabilities (k_{ro}) by 60 % of their co-current values, brine relative permeabilities (k_{rw}) by 60 % and both k_{ro} and k_{rw} by 50 %, Figure 4.31.

Further sensitivity analysis showed that oil relative permeability is most sensitive to adjustments for the model used in this thesis. This indicates that uncertainty in laboratory measurements of the oil relative permeability will have greater consequence than that for the water relative permeability. In other

words, this ranks the oil relative permeability as more important in terms of resources needed to adequately determine the parameter experimentally.

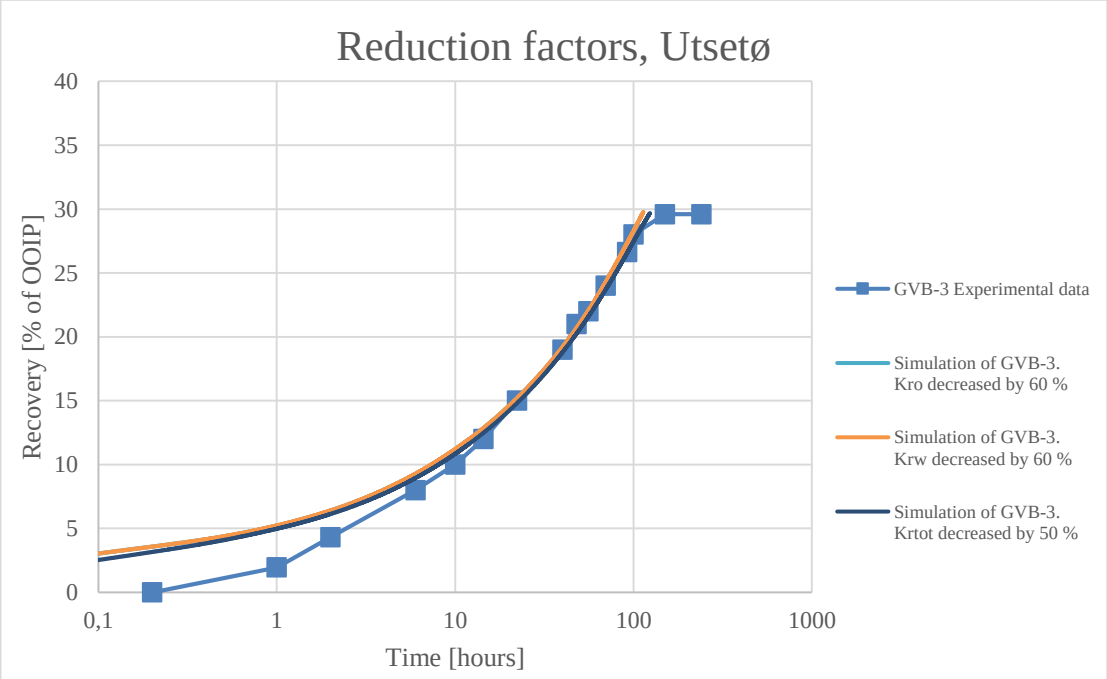

Figure 4.31: Comparison between experimental and simulated oil recovery curves for counter-current imbibition test GVB-3, with reduced co-current relative permeability curves. Reduction factors by Utsetø 2017.

4.8.1 Investigation of Corey exponents

Bourbiaux & Kalaydjian was able to reproduce counter-current experimental data by reducing the co-current relative permeability curves. However, instead of reducing the all values by a factor including the endpoint values, could a good match between simulated and experimental oil recovery curves also be obtained by solely adjusting the Corey exponents? In other words, keeping the endpoint values constant and only adjusting the shape of the relative permeability curves. Since the simulated counter-current oil recovery curves (test GVB-3) with co-current relative permeabilities (test GVB-1) experience faster production than the experimental data, the Corey exponents must be adjusted such that production time increases. This can be obtained by increasing the Corey-parameter for oil and water relative permeability, n_w and n_o. Figure 4.32 depicts the final best match between counter-current experimental data and co-current simulations with increased Corey exponents.

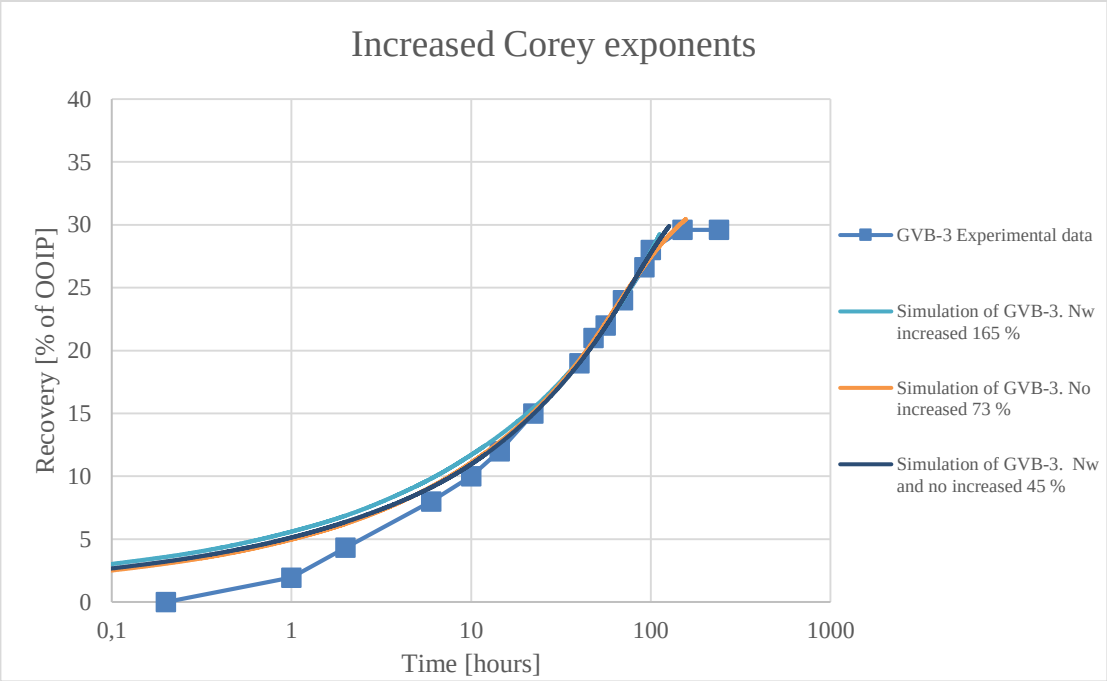

Figure 4.32: Comparison between experimental and simulated oil recovery curves for counter-current imbibition test GVB-3, with increased Corey exponents.

The effect of keeping the endpoint relative permeability values constant and increasing the Corey exponents is almost identical to the effect of reducing the entire relative permeability curve (including endpoints). However, the magnitude of which the Corey exponents needed to be increased was greater than the relative permeability curves had to be decreased. The Corey-parameter for water relative permeability, n_w, was increased as much as 165 % before a good reproduction of experimental data was obtained. Furthermore, a good match was obtained by increasing n_o (Corey-parameter for oil relative permeability) by 73 % and n_w and n_o by 45 %. Thus, if the two procedures of reducing co-current relative permeability values are compared, the Corey exponents show much more internal sensitivity to adjustments. The reason why n_w is much higher than n_o may be explained by the rock-fluid behaviour in a water-wet system. It was discussed in 2.4 that the water will fill all the smallest pores and move along the solid surface of the porous medium during displacement. Consequently, as the resistance of the medium to the flow of water will be greater than for oil, n_w needs to be increased more than n_o. Yet, for the scenario when both factors were adjusted simultaneously, the magnitude of adjustment is quite similar: a 50 % decrease in relative permeability curves compared to a 45 % increase in Corey exponents.

4.8.2 Sensitivity analysis of Corey exponents

To better understand the effect of adjusting the Corey exponents, it was decided to perform a sensitivity analysis for a range of selected Corey exponent values. A summary of the used values and corresponding increase in percentage is given in Table 12. Moreover, individual sensitivity plots for n_w, n_o and n_w & n_o are depicted in Figure 4.33 to Figure 4.35.

Table 12: A summary of Corey exponents used in sensitivity analysis.

Sensitivity of Corey exponents					
n_w		n_o		n_w & n_o	
4	100 %	2.25	50 %	2.5 & 1.875	25 %
5.3	165 %	2.6	73 %	2.9 & 2.175	45 %
6	200 %	3	100 %	3.3 & 2.475	65 %
8	300 %	3.75	150 %	3.7 & 2.775	85 %

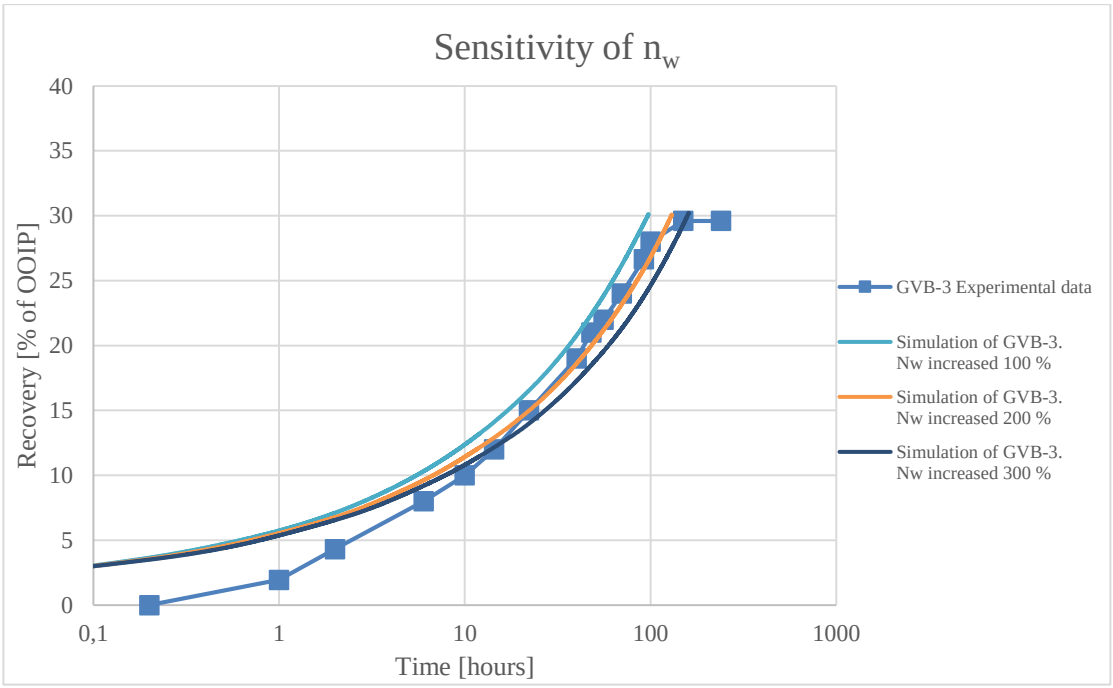

Figure 4.33: Sensitivity plot for increasing n_w values, illustrating the impact on oil recovery rates compared with experimental data.

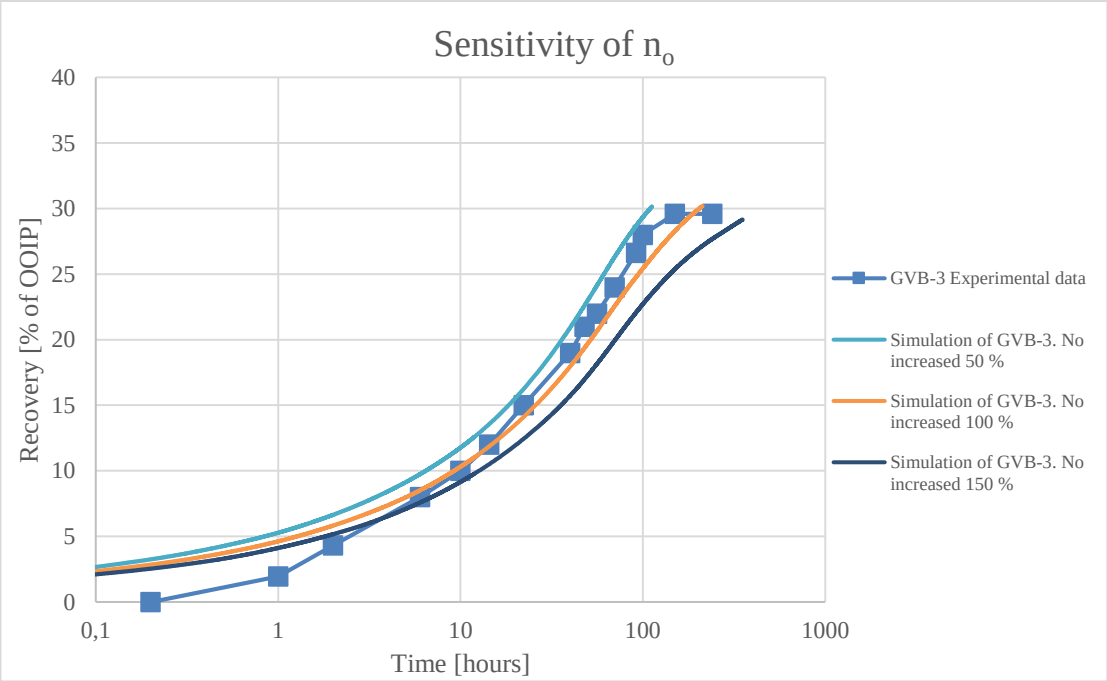

Figure 4.34: Sensitivity plot for increasing n_o values, illustrating the impact on oil recovery rates compared with experimental data.

The sensitivity analysis depicts varying sensitivity for adjustments of the Corey exponents. By plotting the two sensitivity plots with identical ranges for the x-axis and the y-axis, the sensitivity may be interpreted explicitly. The results show that similar responses (oil recovery curves) are obtained when n_w is increased 300 %, as when n_o is increased by 100 %. This clearly signifies that the Corey-parameter for oil relative permeability is the most sensitive in this thesis. It was mentioned in chapter 2.6 that the robustness of a reservoir simulator relies on the representativeness of input parameters. This signifies that experimental uncertainty ought to be minimized for parameters with high sensitivity attributes. Consequently, based on the sensitivity analyses in this thesis, measurements of the Corey-parameter for oil relative permeability should to be performed with extra accuracy as uncertainty will have correspondingly greater consequence.

It must be mentioned that the sensitivity analysis presented in Figure 4.33 presents the impact of adjusting the n_w, for a given value of n_o. Hence, it does not describe how n_w will vary for other n_o values. As the same procedure was used for the analysis in Figure 4.34, similarly, no information about the behaviour of n_o for other n_w values. Hence, a third sensitivity analysis was performed to observe the effect of adjusting n_w and n_o simultaneously. This provides a more detailed presentation of the Corey sensitivities as the impact of combining the two parameters can be observed. It was found that the effect on oil recovery curves when n_w and n_o are increased simultaneously, corresponds to the summed effect from increasing n_w and n_o individually. The sensitivity plot for increasing n_w and n_o simultaneously is depicted in Figure 4.35.

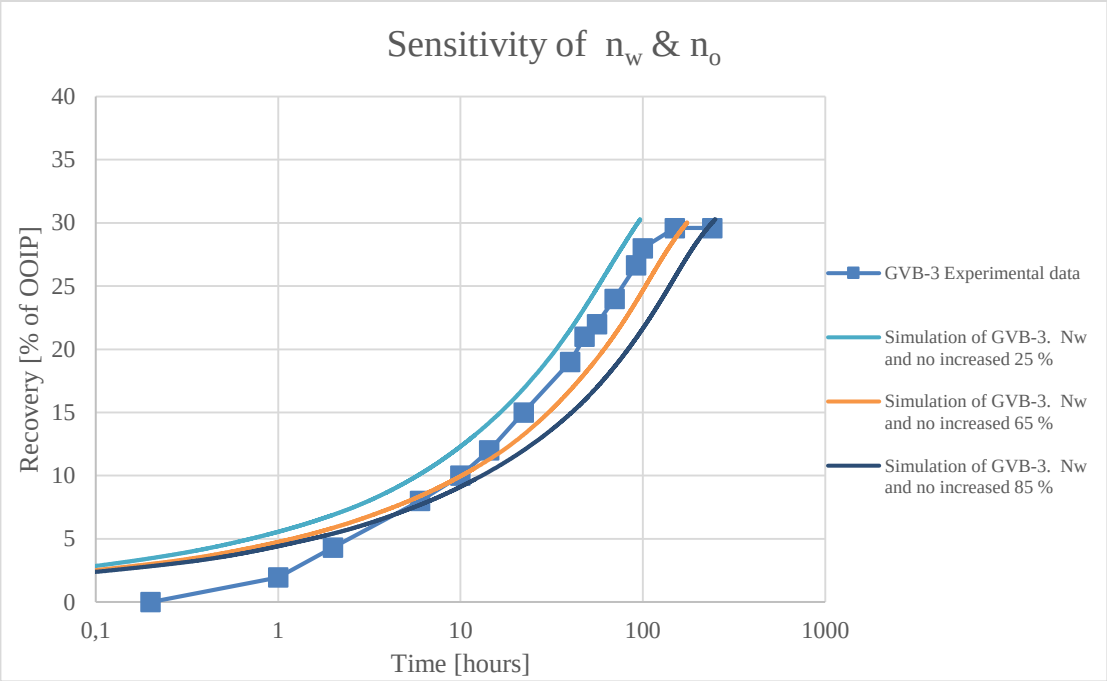

Figure 4.35: Sensitivity plot for increasing n_w & n_o values, illustrating the impact on oil recovery rates compared with experimental data.

4.8.3 Theoretical interpretation

It appears that adjusting co-current relative permeability curves to fit counter-current experimental data is possible, in more than one way. It has been found that good reproducibility of experimental data from simulations can be obtained by reducing the relative permeability curves by including endpoint values (k_{rw}* and k_{ro}*). Another possibility is to keep the endpoint values constant and adjust the shape of the relative permeability by increasing the Corey exponents. As almost identical results are obtained whether endpoints are included or kept constant, it suggests that the method of adjusting relative permeability curves is optional. According to literature, the subject of whether to include endpoints when relative permeability curves are adjusted, is widely discussed (Babchin et al., 1998; Bourbiaux & Kalaydjian, 1990; Kalaydjian, 1987, 1990). Yet, no agreement has been found and the subject remains to be further investigated.

The sensitivity analyses showed in both cases that the oil relative permeability parameter is most sensitive. Hence, it will be ranked more important than the water relative permeability parameter, in terms of resources needed to adequately determine the parameter experimentally.

It must be mentioned that the numerical investigation performed in this thesis considers a very simplified case. Boundary conditions are selected such that 1-D flow is obtained and the tests are assumed to involve only co-current or counter-current flows. However, as the conditions are much more complex in a real reservoir, the SI process will often involve both co-current and counter-current flow in more than 1 dimension. Since laboratory measurements in most cases are performed on co-current flow conditions, the reservoir recovery potential may be seriously overestimated. Consequently, in an

ideal world, tests ought to be performed under both co-current and counter-current conditions when evaluating the oil recovery potential on reservoir rocks experimentally. Though, due to limitations in resources, counter-current flow conditions are rarely experimentally investigated. Hence, to prevent overestimated oil recovery, a proposed approach is to use reduced relative permeabilities for parts of the field where co-current flow is dominant. In other words, implementing different relative permeability inputs for different grid sections in the ECLIPSE simulator.

4.9 Capillary diffusivity coefficient (CDC)

Sensitivity analyses are important to investigate both spread and response for a given parameter on the oil recovery curves. The capillary diffusivity coefficient (CDC) is investigated with the purpose of explaining the relationship between oil recovery curves and relative permeability curves for SI tests.

A study of spontaneous imbibition into cylindrical cores was performed by Standnes (2006), based on experiments from Standnes (2004). Here he proposed a theoretical model for analytically determining the normalized water saturation in the matrix block with specific boundary- and initial conditions. It was found that the 1-D radial counter-current SI could be modelled fairly well based on the assumption of a constant CDC (a kind of average CDC value which is independent of water saturation). The results were surprising since the CDC has been shown to exhibit a bell-shaped curve of water saturation, with maximum value at approximately S_w =0.5 (Gautam & Mohanty, 2004; Kashchiev & Firoozabadi, 2003). In this thesis, the process of spontaneous imbibition into cubic cores is also given by the capillary diffusivity coefficient, which is controlled by the Corey functions used to model relative permeability. Hence, the expression for $D(S_w)$ that was derived in chapter 2.5.2; equation (26), can be used to compare CDC values for the two methods used to adjust co-current relative permeability curves.

As Standnes (2006) found that 1-D radial counter-current SI could be modelled based on the assumption of a constant CDC, this investigation will qualitatively test if the same assumption can be made for 1-D counter-current SI into cubic core samples.

4.9.1 Calculation of CDC

The analysis of calculated CDC values was separated into two cases with respect to adjustment method: Case 1 - Reduction of relative permeability curves including endpoint values (k_{rw}* and k_{ro}*); Case 2 - Adjustments of the Corey exponents while keeping endpoint values fixed. The basecase (history match of co-current test GVB-1) was included for comparison of the CDC before and after adjusted relative permeability curves. The solid curve in Figure 4.36 depicts the $D(S_w)$ for test GVB-1, calculated from equation (31) in which the total area under the graph represents the capillary diffusivity coefficient. Since $D(S_w)$ normally exhibit a bell-shaped function of S_w, it was mathematically advantageous to use trapezoidal method to calculate the area under the graph.

$$\int_a^b D(S_w)\, dS_w \approx (b-a) * \left[\frac{f(a)+f(b)}{2}\right] \quad \textbf{(31)}$$

The trapezoidal rule approximates the region under the graph by a function $D(S_w)$, in which the approximation improves with more steps representing the domain [a,b] (Süli & Mayers, 2003). Consequently, the water saturation interval was divided into more steps by decreasing ΔS_w. This resulted in a good approximation of area under the curve, which can be seen from the fit of the columns occupying the area under the graph.

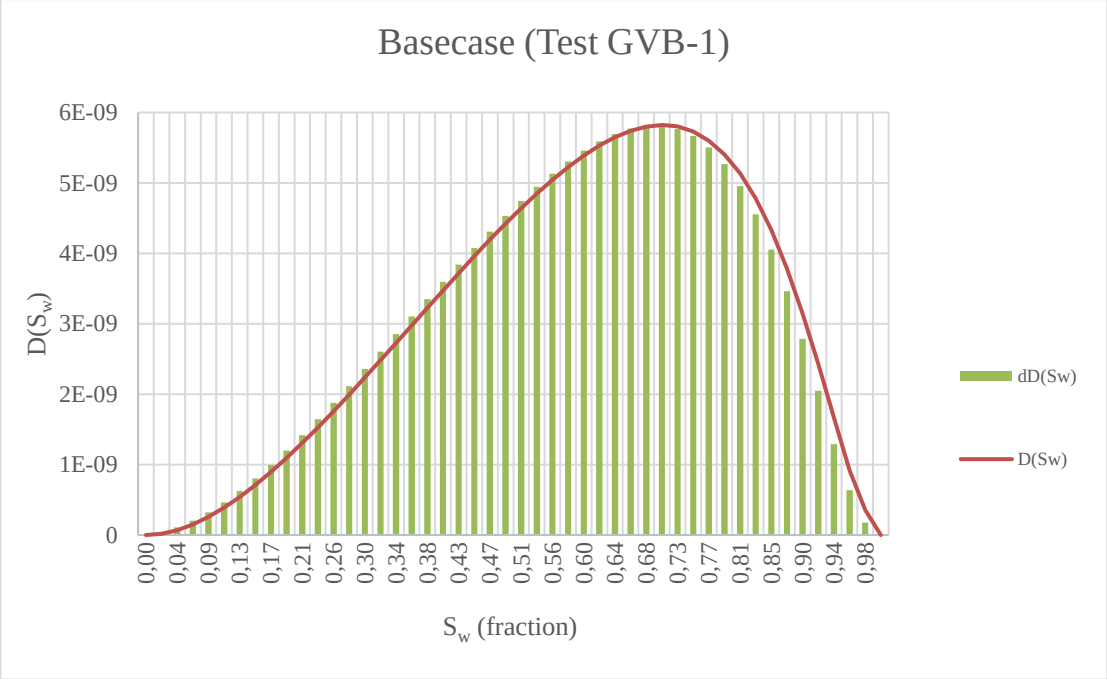

Figure 4.36: Capillary diffusion coefficient calculated as a function of normalized water saturation for the basecase (test GVB-1) with no reduction of relative permeability curves. Corey exponents: $n_w = 2$, $n_o = 1.5$.

4.9.1.1 Case 1

The column chart in Figure 4.37 shows the capillary diffusivity coefficients for each of the three reduction factors (k_{rw}, k_{ro} and k_{rw} & k_{ro}), compared with the basecase. The reduced relative permeability curves show consistently lower CDC values than for the basecase. This would be expected since the $D(S_w)$ is proportional to the relative permeability value, equation (26). It can be observed that some internal variation is found for the three reduction factors, yet noticing very similar results for k_{rw} reduced by 60 % and k_{rw} & k_{ro} reduced by 50 %. $D(S_w)$ is plotted as a function of normalized water saturation for the three reduction factors in Figure 4.38 to Figure 4.40, respectively.

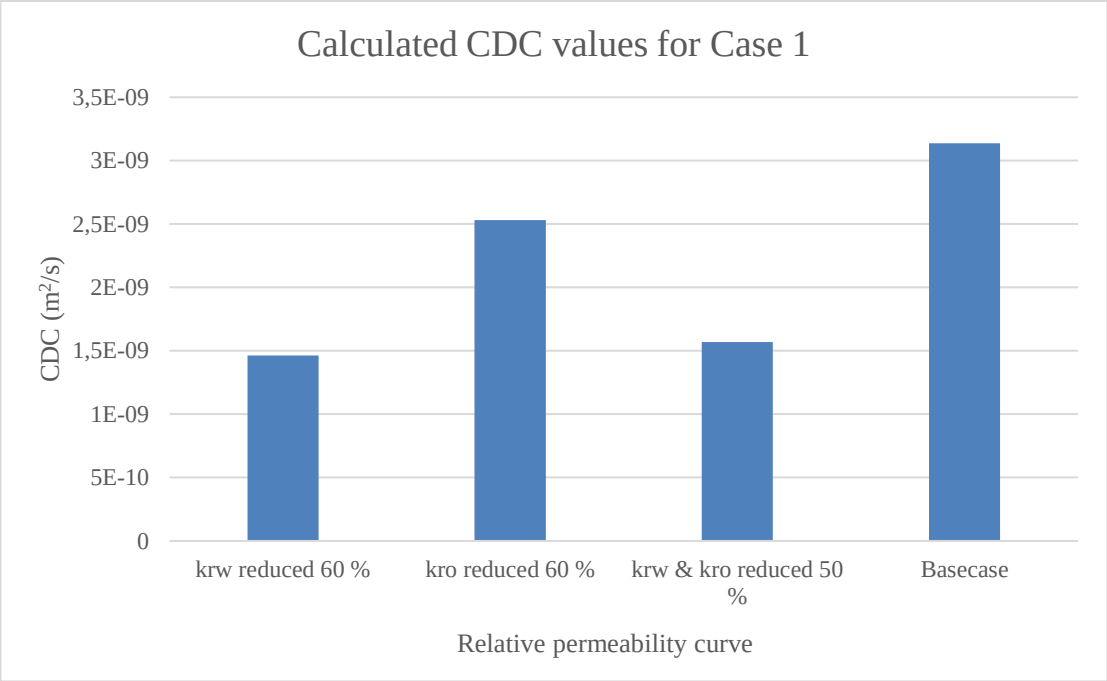

Figure 4.37: Capillary diffusivity coefficients for the corresponding reduction of relative permeability curves. Basecase is included for comparison.

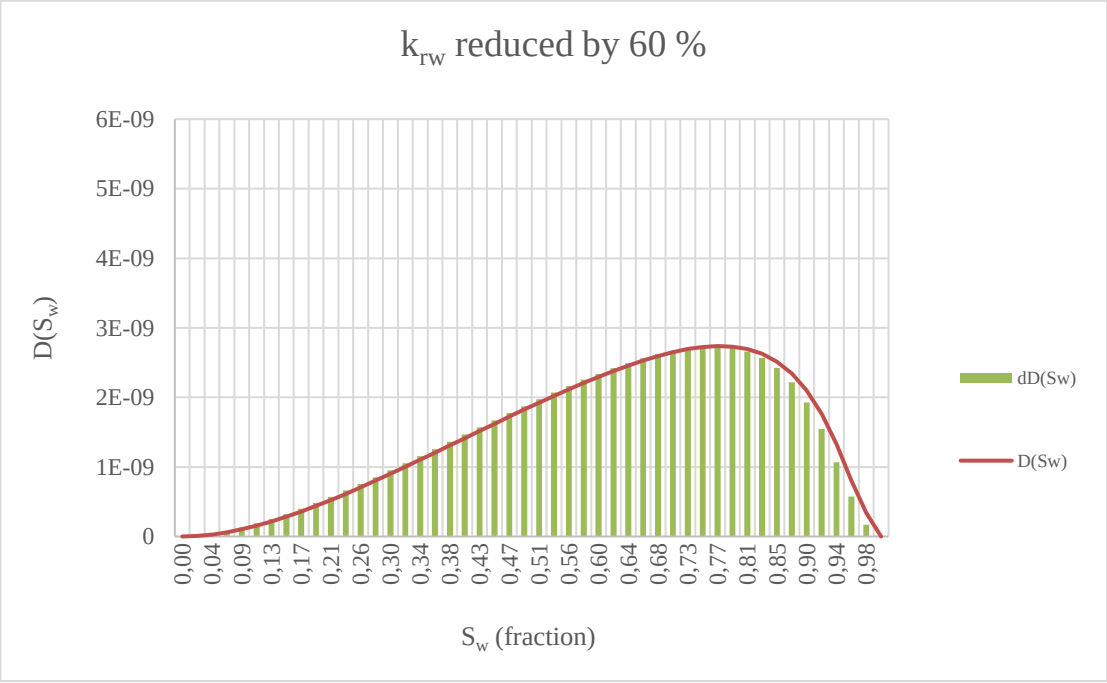

Figure 4.38: Capillary diffusion coefficient calculated as a function of normalized water saturation. K_{rw} reduced by 60 %.

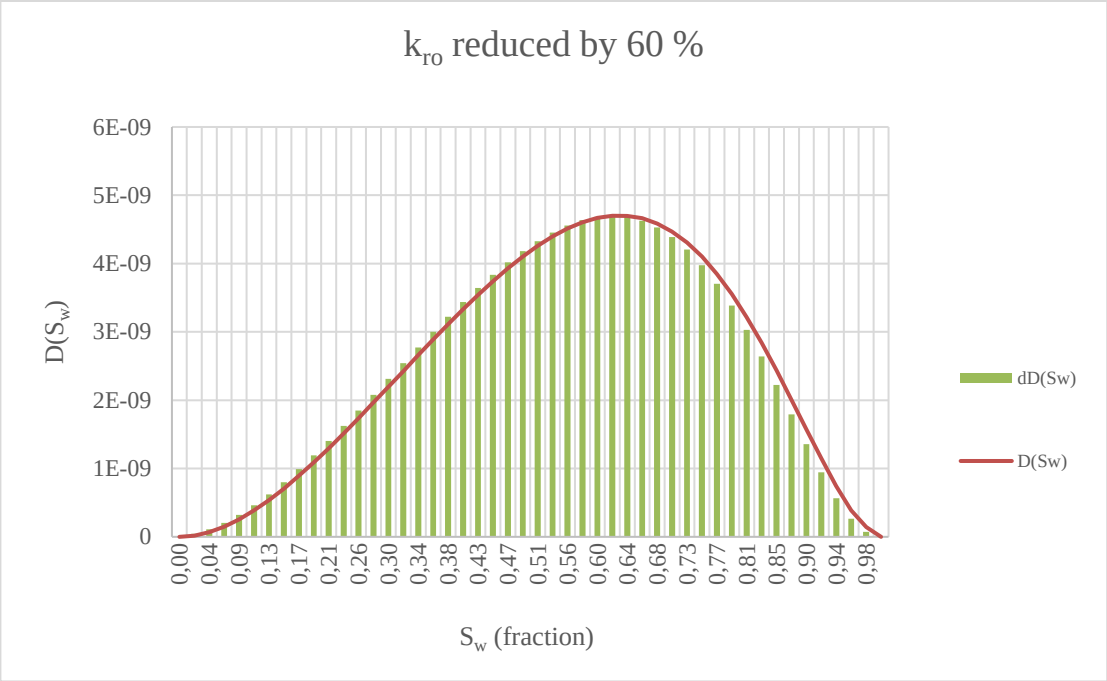

Figure 4.39: Capillary diffusion coefficient calculated as a function of normalized water saturation. K_{ro} reduced by 60 %.

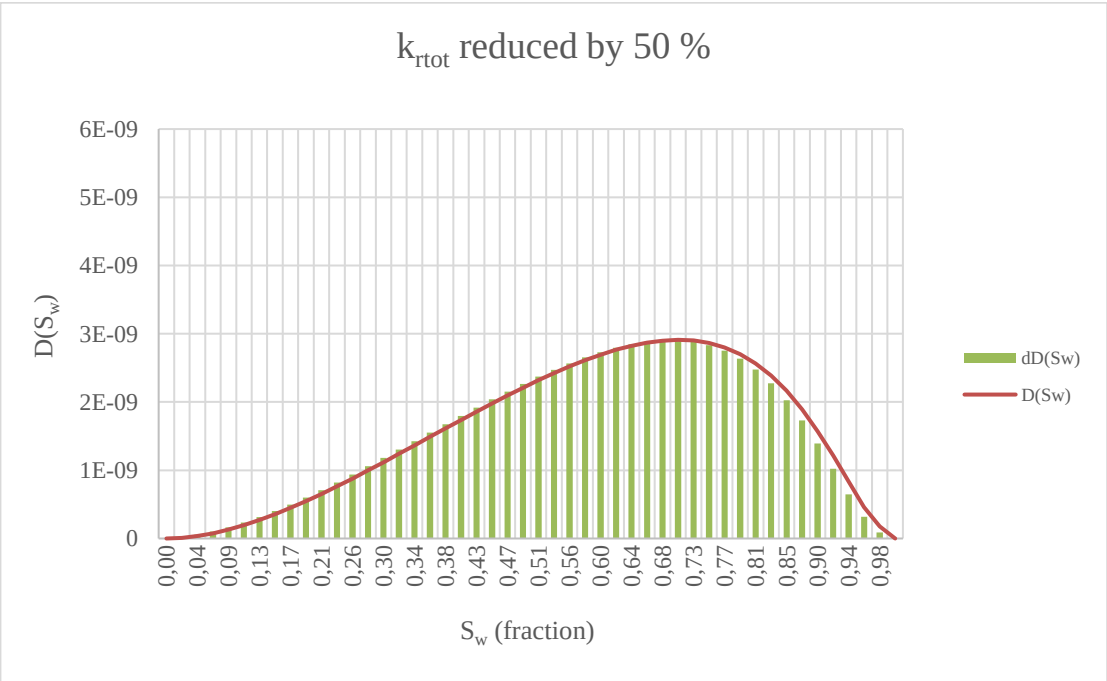

Figure 4.40: Capillary diffusion coefficient calculated as a function of normalized water saturation. K_{rtot} reduced by 50 %.

K_{rw} reduced by 60 % and k_{rw} & k_{ro} reduced by 50 % show very similar plots with a slight skewness to the right. In contrast, k_{ro} reduced by 60 % exhibits a more bell-shaped curve. It is interesting, however, that all the three reduced relative permeability curves gave almost identical oil recovery curves and reproduced counter-current experimental data with little deviation. This suggests that certain

combinations of CDC value and $D(S_w)$ curve shape will give the same oil recovery curve. If such a relationship exists, it would be expected to find similar results for Case 2.

4.9.1.2 Case 2

The column chart presented in Figure 4.41 shows lower capillary diffusivity coefficients for the adjusted Corey exponents (n_w, n_o and n_w & n_o), than for the basecase. The results are quite similar to what was found in case 1, however noticing slightly higher internal variation. Figure 4.42 to Figure 4.44 depict $D(S_w)$ plotted as a function of normalized water saturation for the three adjusted Corey exponents.

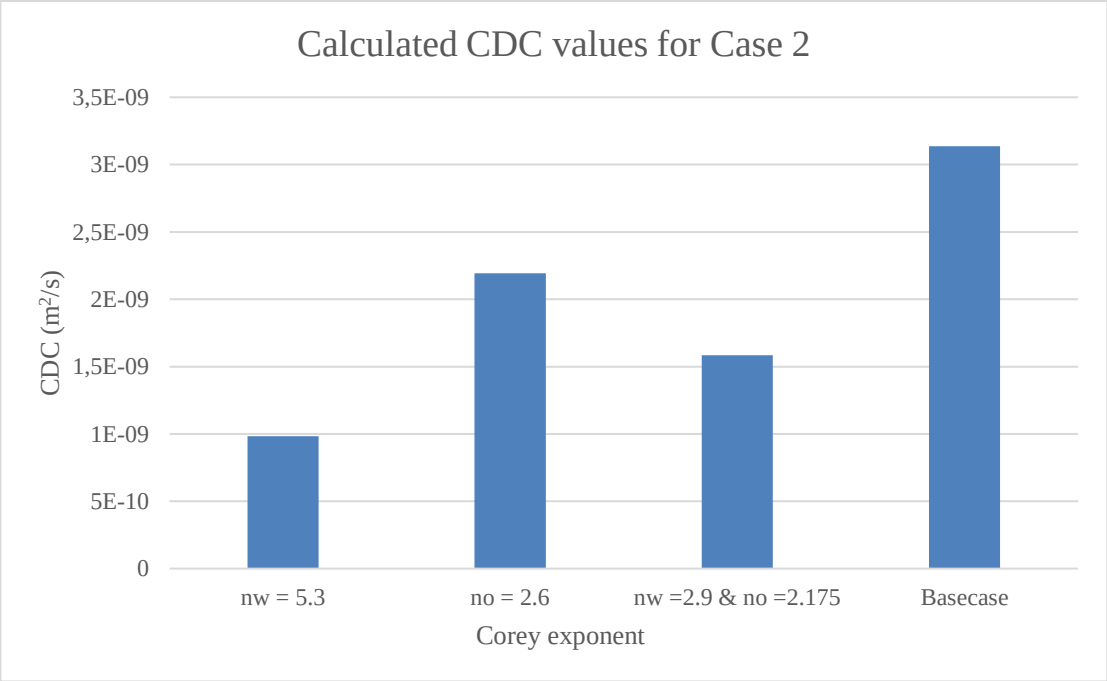

Figure 4.41: Capillary diffusivity coefficients for the corresponding Corey exponents. Basecase is included for comparison.

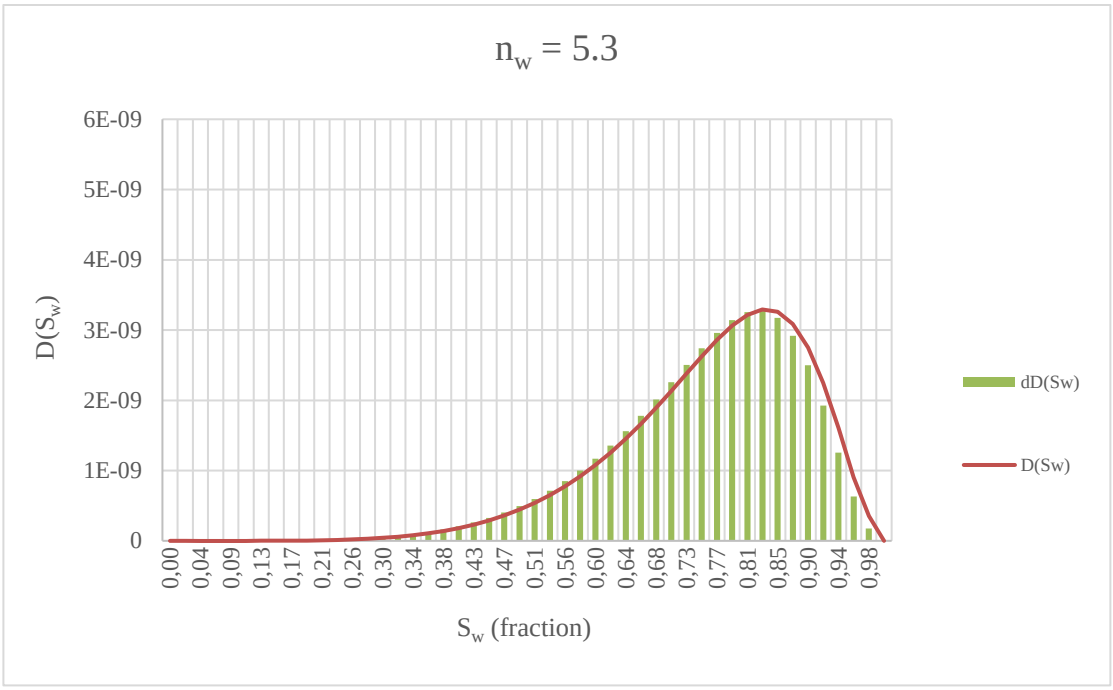

Figure 4.42: Capillary diffusion coefficient calculated as a function of normalized water saturation. Corey exponents: n_w = 5.3, n_o = 1.5.

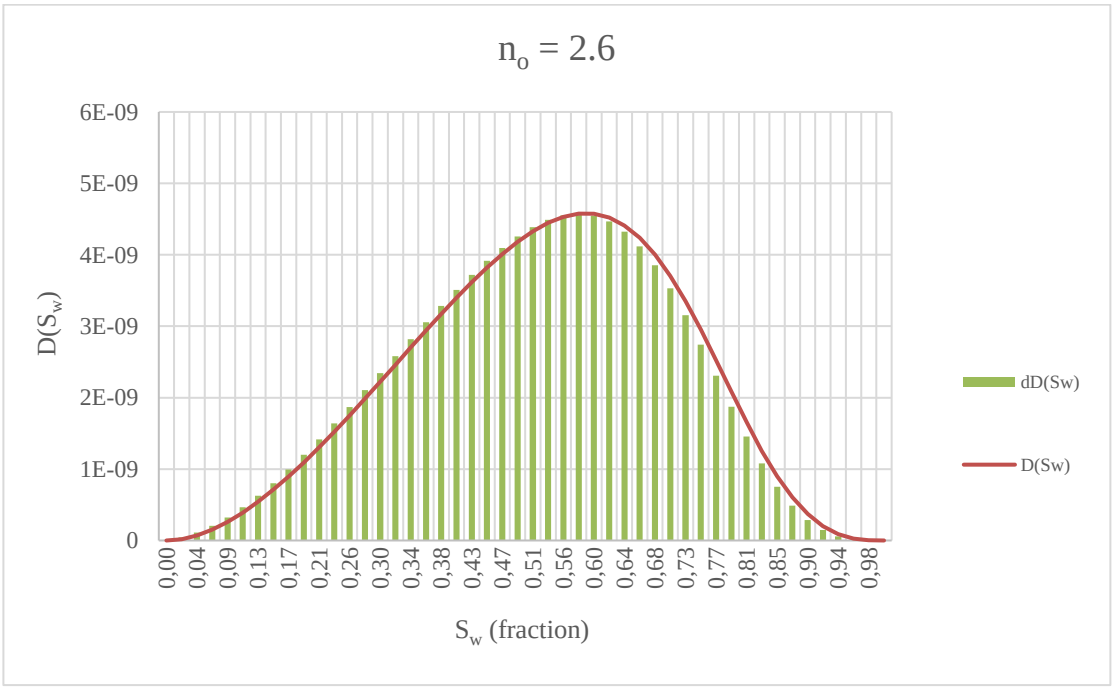

Figure 4.43: Capillary diffusion coefficient calculated as a function of normalized water saturation. Corey exponents: n_w = 2, n_o = 2.6.

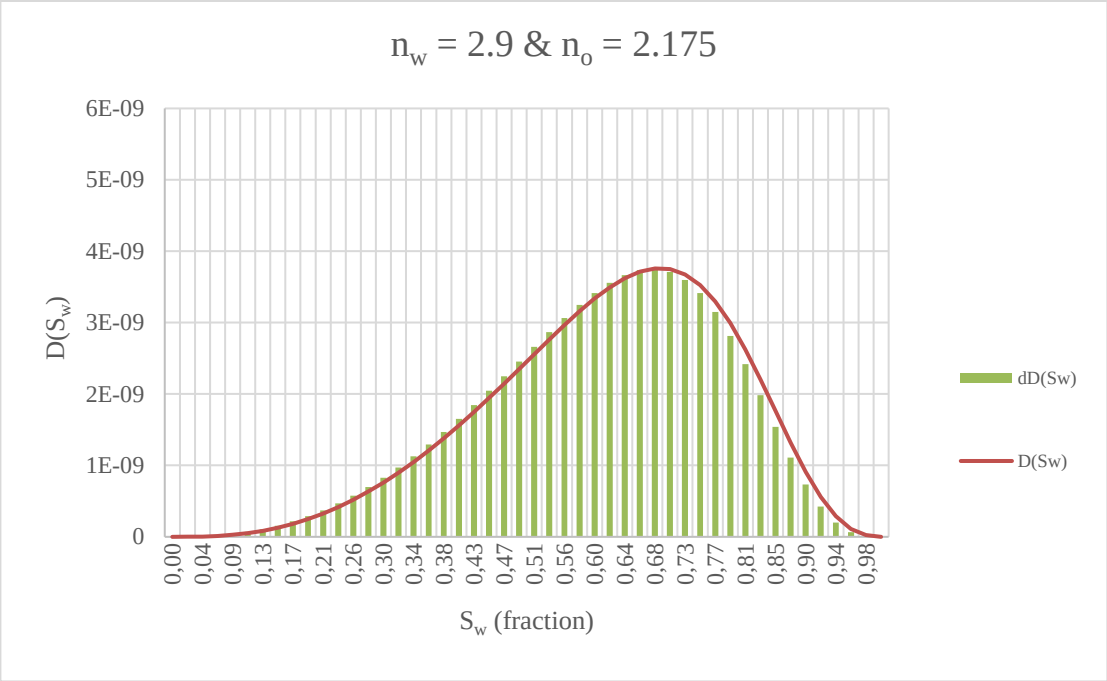

Figure 4.44: Capillary diffusion coefficient calculated as a function of normalized water saturation. Corey exponents: n_w = 2.9, n_o = 2.175.

The CDC value is lowest for n_w =5.3, which is also the case that exhibits most right skewness of the D(S_w) curve. A slightly higher CDC value can be found for n_w =2.9 & n_o =2.175, in which D(S_w) shows correspondingly less skewness to the right. As for Case 1, it is when adjusting the Corey-parameter for oil relative permeability, n_o = 2.6, that CDC is highest and the shape of D(S_w) is least right skewed (almost bell-shaped curve).

4.9.2 Comparison of results

Based on the results from Case 1 and Case 2, it can be observed that the combination of a low CDC value with a right skewed D(S_w) curve gives the same oil recovery curve as a high CDC value with a left skewed D(S_w) curve. Consequently, it can be argued that the right skewness compensates for small CDC values in the same way that left skewness will balance for high CDC values. These results can be compared with work by Joergensen (2017), which investigated the behaviour of CDC for SI into cylindrical cores. He found that the production rate and ultimate oil recovery decreases when the D(S_w) curve exhibits left skewness. It was also observed that high CDC values resulted in faster production and higher ultimate oil recovery. This agrees with the results found in this thesis and explains why different CDC values and D(S_w) curve shapes can give almost identical oil recovery curves.

A proposed relationship may be introduced to express the oil recovery curve as a function of CDC value and shape of D(S_w):

$$Oil\ recovery\ curve = F(CDC, Shape) \quad \textbf{(32)}$$

However, shape is not an easily quantified parameter and a system is needed to define the skewness of the $D(S_w)$ curve. Since D is a function of S_w, skewness may be defined by the water saturation of which $D(S_w)$ is highest. In other words, if a bell-shaped distribution has maximum $D(S_w)$ value at $S_w = 0.5$, left and right skewness may be defined for cases where the maximum $D(S_w)$ value is found for $S_w < 0.5$ and $S_w > 0.5$, respectively. This would give some indication of the shape of the $D(S_w)$ curve. Then, by using the definition of CDC from equation (31), the proposed relationship may be written on the following form:

$$Oil\ recovery\ curve = F\left[\left(\int_a^b D(S_w)\, dS_w\right), (Shape(D(S_w)^{max}))\right] \quad \textbf{(33)}$$

An investigation of the capillary diffusivity coefficient was performed with the purpose of finding an explanation for the results found in chapter 4.8. Even though the reduced relative permeability curves showed almost identical oil recovery curves, the CDC values were not constant. In other words, no direct relationship could be found between CDC value alone and oil recovery rate, by qualitative testing. Hence, another variable must be introduced to explain the fact that equal responses (oil recovery rates) were obtained with different CDC values, ergo the shape of $D(S_w)$. As Joergensen (2017) discovered increased production rates for higher CDC values and right skewed shape of $D(S_w)$, it supports the suggestion that certain combinations of the two variables may give identical responses. This point remains to be investigated more thoroughly to better understand the true relationship between oil recovery and capillary diffusivity coefficients.

5 Conclusions

The first objective of this thesis was to investigate the relationship between co-current and counter-current relative permeabilities for spontaneous imbibition. Considering theory of viscous coupling between fluid phases and experimental results from several authors, co-current relative permeabilities were expected to be higher. The second objective put forward a hypothesis that co-current relative permeability curves will reproduce counter-current experimental data, if reduced by some factor. For the experimental data investigated in this thesis, the following conclusions can be drawn:

Part 1.Experimental data by Standnes (2004)

- Numerical simulations showed that counter-current relative permeabilities could not give exact prediction of recovery rates for co-current SI.
- Too slow oil recovery curves are expected when counter-current relative permeabilities are used in the model. However, simulations showed reversed results.
    - An investigation of experimental inconsistency was performed, by which most factors indicated that certain tests are flawed.
- Further comparison of co-current and counter-current SI tests would give inconsistent results.
- As experimental data by Standnes (2004) did not give consistent results, a dataset by Bourbiaux and Kalaydjian (1990) was used for further investigations. By consequence, part 2 of this thesis was introduced.

Part 2. Experimental data by Bourbiaux and Kalaydjian (1990)

- Co-current relative permeabilities were used in counter-current simulations, in which too fast oil recovery rates were observed. The half-recovery time was underestimated by approximately 50 %, which is in agreement with results found by Bourbiaux and Kalaydjian (1990).
- Numerical investigation showed that exact prediction of counter-current recovery rates can be obtained by reducing both oil and water relative permeabilities (including k_{rw}* & k_{ro}*) by 50 %. For comparison, Bourbiaux and Kalaydjian (1990) obtained exact prediction when both curves were reduced by 30 %.
    - Further investigation showed that an equally good match was found by increasing the Corey exponents for oil and water (keeping k_{rw}* & k_{ro}* constant) by 45 %.
- Almost identical results in terms of oil recovery curves, are observed when:
    - Relative permeabilities are reduced including endpoints
    - Endpoints are kept constant and curvature is adjusted (by increasing Corey exponents)
- Sensitivity analyses showed that oil relative permeability exhibits higher sensitivity than that for water relative permeability, whether endpoints are reduced or kept constant.

    - Experimental uncertainty ought to be minimized for parameters with highest sensitivity attributes. In consequence, more resources are needed to adequately determine the parameter experimentally.
- A relationship between the capillary diffusivity coefficient and relative permeability curves for a given SI test was investigated.
    - Qualitative testing indicates that 1-D radial counter-current SI cannot be modelled based on the assumption of a constant CDC.
    - It was observed that certain combinations of CDC value and shape of the $D(S_w)$ can give equal production rates and ultimate oil recoveries.
    - It is proposed that oil recovery curve may be expressed as a function of the two factors, equation (33).

It has been found that relative permeabilities have great impact on production rates and ultimate oil recoveries. Relative permeabilities are lower for counter-current SI, because viscous coupling between fluid phases has opposite effects on co-current and counter-current flows. The numerical investigation showed that simulations based on co-current relative permeability curves will reproduce counter-current experimental data, if reduced by some factor.

The effect of gravity forces has not been investigated in this thesis because co-current gravity driven flow is mostly neglected when SI experiments are performed on small water-wet cores, by which capillary forces tend to dominate. However, as most carbonate fractured reservoirs exhibit less water-wet rock-fluid systems, different results will be expected regarding the contribution of gravity driven flow. For such conditions, oil will be produced both co-currently and counter-currently, in proportions depending on the magnitude of capillary forces compared to gravity forces. This points to inconsistencies that may arise when scaling up laboratory imbibition tests from matrix blocks with different contributions of co-current and counter-current flow. Ideally, to prevent incorrect estimation of production rate and ultimate oil recovery, tests ought to be performed under both co-current and counter-current conditions when evaluating the oil recovery potential on reservoir rocks experimentally. This will increase the robustness of the reservoir simulator and increase the validity of predicted reservoir behaviour.

5.1 Future work

As counter-current flow conditions rarely are experimentally investigated, an alternative approach may be introduced to prevent overestimated reservoir recovery potential. For a reservoir involving both co-current and counter-current flow, reduced relative permeability curves may be implemented for different grid sections in the ECLIPSE simulator, where counter-current flow is dominant. The extent that relative

permeabilities should be reduced will obviously vary greatly depending on the reservoir. Because the experimental study by Standnes (2004) showed inconsistency, results could not be used to compare potential reduction factors. The study by Bourbiaux and Kalaydjian (1990) appears to be the only reliable literature which investigates the subject of reducing co-current relative permeability curves to match counter-current data. Consequently, a new study of co-current and counter-current SI is needed to determine if the reduction factors found by Bourbiaux and Kalaydjian (1990) can be applied for other cases as well. If new studies show that counter-current experiments can be matched by reducing co-current curves by factors around 30 %, it would suggest that a quantifiable relationship exists between co-current and counter-current flow in porous media. On the other hand, if new studies show differing results, it would indicate that the relationship between co-current and counter-current relative permeabilities vary to such an extent that it cannot be quantified. Examples of future work are:

- Perform flow experiments involving 1-D co-current and counter-current SI of water into strongly water wet cubic core samples.
    - Use co-current relative permeability curves obtained from history matching in counter-current simulations of further SI tests.
    - Investigate to what extent co-current relative permeability curves must be adjusted to match counter-current experimental data.
    - Compare reduction factors with results by Bourbiaux and Kalaydjian (1990).
- Investigate the relationship between co-current and counter-current SI when boundary conditions enable 2-D and 3-D flow.
- Investigate the applicability of implementing reduced relative permeability curves for different grid sections in the ECLIPSE simulator, where counter-current flow is dominant.

Nomenclature

Symbols

A: Cross sectional area (m^2)

a_l: Pore size distribution index

C_l: Capillary entry pressure (atm)

f_w: Water fractional flow

g: Gravitational constant (m/s^2)

h: Height above free water level (m)

K: Absolute permeability (m^2, mD)

k_{rl}: Phase relative permeability

k_{rl}*: Endpoint relative permeability

k_{ww}: Transport coefficient 1, extended Darcy law

k_{wo}: Transport coefficient 2, extended Darcy law

k_{ow}: Transport coefficient 3, extended Darcy law

k_{oo}: Transport coefficient 4, extended Darcy law

L: Length of core sample (m)

n_o: Corey-parameter for oil relative permeability

n_w: Corey-parameter for water relative permeability

P_l: Phase pressure (atm)

P_c: Capillary pressure (atm)

P_{cd}: Reservoir threshold pressure (atm)

q_l: Phase flow rate (m^3)

R: Radius of interfacial tension surface

R_{tube}: Radius of capillary tube

R_{SI}: Ultimate oil recovery

S: Normalized water saturation (fraction)

S_l: Phase saturation (fraction)

S_{or}: Residual oil saturation (fraction)

S_{wir}: Irreducible water saturation (fraction)

S_{wi}: Initial water saturation (fraction)

t: Time (hr)

v_l: Phase velocity (m/s)

σ: Interfacial tension (mN/m)

ϕ: Porosity (m^3/m^3)

λ_l: Phase mobility

μ_l: Phase viscosity (Pa.s)

θ: Contact angle

ρ_l: Phase density (g/cm^3)

Abbreviations

AFO:	All face open
CDC:	Capillary diffusivity coefficient
CU:	Cubic rock sample
CY:	Cylindrical rock sample
IFT:	Interfacial tension
LGR:	Local grid refinement
OOIP:	Original oil in place
SI:	Spontaneous imbibition
WOAR:	Water-oil-area-ratio
1-D:	1-dimensional
2-D:	2-dimenisonal
3-D:	3-dimensional

ECLIPSE keywords

MULTX	Transmissibility multiplier in x-direction
MULTY	Transmissibility multiplier in y-direction
MULTZ	Transmissibility multiplier in z-direction
SWOF	Saturation function table for oil-water

References

Amott, E. (1959). ***Observations relating to the wettability of porous rock.*** Petroleum Transactions, AIME, *Vol. 216*, pp. 156-162.

Anderson, W. (1986). ***Wettability Literature Survey- Part 2: Wettability Measurement.*** Trans, AIME, pp. 1246-1262.

Babchin, A., Yuan, J., & Nasr, T. (1998). ***Generalized Phase Mobilities in Gravity Drainage Processes***. Paper presented at the Annual Technical Meeting, Calgary, Alberta, June 8-10.

Bourbiaux, B. J., & Kalaydjian, F. J. (1990). ***Experimental study of cocurrent and countercurrent flows in natural porous media.*** SPE Reservoir Engineering, *Vol. 5*, pp. 361-368.

Brownscombe, & Dyes. (1952). ***Water-imbibition displacement ... Can it release reluctant Spraberry oil?*** The Oil and Gas Journal, pp. 264-267.

Craig, F. F. (1971). ***The reservoir engineering aspects of waterflooding***. Society of Petroleum Engineers of AIME, Dallas, TX, US.

Cuiec, L. (1984). ***Rock/Crude-Oil Interactions and Wettability: An Attempt To Understand Their Interrelation***. Paper presented at the Annual Technical Conference and Exhibition, Housten, TX, USA, September 16-19.

Dean, R., & Lo, L. (1988). ***Simulations of naturally fractured reservoirs.*** SPE Reservoir Engineering, *Vol. 3*(02), pp. 638-648.

Espevold, I. (2015). ***Initial Fluid Distributions – The Importance for Simulation Results***. MSc thesis, Faculty of Science and Technology, University of Stavanger, Stavanger.

Fernø, M., Haugen, Å., Wickramathilaka, S., Howard, J., Graue, A., Mason, G., & Morrow, N. (2013). ***Magnetic resonance imaging of the development of fronts during spontaneous imbibition.*** Journal of Petroleum Science and Engineering, *Vol. 101*, pp. 1-11.

Fischer, H., & Morrow, N. R. (2005). ***Spontaneous imbibition with matched liquid viscosities***. Paper presented at the SPE Annual Technical Conference and Exhibition, Dallas, TX, October 9-12.

Gautam, P. S., & Mohanty, K. K. (2004). ***Matrix–Fracture Transfer through Countercurrent Imbibition in Presence of Fracture Fluid Flow.*** Transport in Porous Media, *Vol. 55*(3), pp. 309-337.

Gilman, J. R., & Kazemi, H. (1988). ***Improved calculations for viscous and gravity displacement in matrix blocks in dual-porosity simulators.*** Journal of petroleum technology, *Vol. 40*(01), pp. 60-70.

Glover, P. W. (2002). ***Formation evaluation***. Faculty of Science and Technology, Université Laval Québec, Canada. Retrieved from https://www.scribd.com/doc/187702058/Formation-Evaluation-MSc-Course-Notes-Paul-Glover

Hamon, G., & Vidal, J. (1986). ***Scaling-Up the Capillary Imbibition Process From Laboratory Experiments on Homogeneous and Heterogeneous Samples***. Paper presented at the European Petroleum Conference, London, UK, October 20-22.

Høgnesen, E., Standnes, D., & Austad, T. (2006). ***Experimental and numerical investigation of high temperature imbibition into preferential oil-wet chalk*****.** Journal of Petroleum Science and Engineering, *Vol. 53*(1), pp. 100-112.

Joergensen, K. (2017). ***A study of the diffusion coefficient term in counter current imbibition and its affect on production***. Msc thesis, Department of Petroleum Technology, University of Stavanger, Stavanger.

Kalaydjian, F. (1987). ***A macroscopic description of multiphase flow in porous media involving spacetime evolution of fluid/fluid interface*****.** Transport in Porous Media, *Vol. 2*(6), pp. 537-552.

Kalaydjian, F. (1990). ***Origin and quantification of coupling between relative permeabilities for two-phase flows in porous media*****.** Transport in Porous Media, *Vol. 5*(3), pp. 215-229.

Karimaie, H., Torsæter, O., Esfahani, M. R., Dadashpour, M., & Hashemi, S. M. (2006). ***Experimental investigation of oil recovery during water imbibition*****.** Journal of Petroleum Science and Engineering, *Vol. 52*(1–4), pp. 297-304.

Kashchiev, D., & Firoozabadi, A. (2003). ***Analytical solutions for 1D countercurrent imbibition in water-wet media*****.** SPE journal, *Vol. 8*(04), pp. 401-408.

Kazemi, H., Merrill Jr, L., Porterfield, K., & Zeman, P. (1976). ***Numerical simulation of water-oil flow in naturally fractured reservoirs*****.** SPE journal, *Vol. 16*(06), pp. 317-326.

Kleppe, H. (2014). ***Course compendium in reservoir simulation***. Faculty of Science and Technology, University of Stavanger Stavanger

Kleppe, J. (2014). ***Review of Relative Permeabilities and Capillary Pressure***. Faculty of Science and Technology, Norwegian University of Science and Technology, Trondheim, Norway. Retrieved from http://www.ipt.ntnu.no/~kleppe/TPG4150/krpc.pdf

Laplace, P. S. (1806). ***Méchanique céleste, Supplement to book 10***. Duprat, J. B. M, Paris, France.

Li, K., & Horne, R. N. (2006). ***Generalized scaling approach for spontaneous imbibition: an analytical model*****.** SPE Reservoir Evaluation & Engineering, *Vol. 9*(03), pp. 251-258.

Ma, Morrow, & Zhang. (1997). ***Generalized scaling of spontaneous imbibition data for strongly water-wet systems*****.** Journal of Petroleum Science and Engineering, *Vol. 18*(3), pp. 165-178.

Mattax, C. C., & Kyte, J. R. (1962). ***Imbibition Oil Recovery from Fractured, Water-Drive Reservoir*****.** SPE journal, *Vol. 2*(02), pp. 177-184.

Moe, M. (2016). ***Numerical investigation of the effect of sample shape and no-flow boundary conditions on the rate of spontaneous imbibition into short core samples*** BSc thesis, Department of Petroleum Technology, University of Stavanger, Stavanger.

Morrow, N. R., Li, Y., Fischer, H., Mason, G., Ruth, D., Yin, P., & Wo, S. (2006). ***Fundamentals of Reservoir Surface Energy as Related to Surface Properties, Wettability, Capillary Action and Oil Recovery from Fractured Reservoirs by Spontaneous Imbibition***. U. o. Wyoming, Leramie, Wyoming, 82071 DOE award No.: DE-FC26-03NT15408. Retrieved from https://www.netl.doe.gov/File%20Library/Research/Oil-Gas/enhanced%20oil%20recovery/NT15408_Semi-AnnJul-Dec2006.pdf

Nesvik, E. (2016). ***Numerical investigation of the effect of different boundary conditions on the rate of spontaneous imbibition into short core samples***. BSc thesis, Department of Petroleum Technology, University of Stavanger, Stavanger.

Pettersen, Ø. (2006). ***Basics of Reservoir Simulation with the Eclipse Reservoir Simulator***. Department of Mathematics, University of Bergen, Bergen, Norway. Retrieved from http://folk.uib.no/fciop/index_htm_files/ResSimNotes.pdf

Pinder, G. F., & Gray, W. G. (2008). ***Essentials of multiphase flow in porous media***. John Wiley & Sons Ltd, Hoboken, US.

Pooladi-Darvish, & Firoozabadi. (2000). ***Cocurrent and Countercurrent Imbibition in a Water-Wet Matrix Block.*** SPE journal, *Vol. 5*(01), pp. 3-11.

Pooladi-Darvish, & Firoozabadi, A. (1998). ***Experiments And Modelling of Water Injection In Water-wet Fractured Porous Media***. Paper presented at the Annual Technical Meeting, Calgary, Alberta, June 8-10

Rose, W. (1969). ***Transport through Interstitial Paths of Porous Solids.*** Journal of Pure & Applied Science, *Vol. 2*, pp. 117-132.

Rose, W. (1988). ***Measuring transport coefficients necessary for the description of coupled two-phase flow of immiscible fluids in porous media.*** Transport in Porous Media, *Vol. 3*(2), pp. 163-171.

Rossen, R., & Shen, E. (1989). ***Simulation of gas/oil drainage and water/oil imbibition in naturally fractured reservoirs.*** SPE Reservoir Engineering, *Vol. 4*(04), pp. 464-470.

Sherafati, M., & Jessen, K. (2017). ***Dynamic Relative Permeability and Simulation of WAG Injection Processes.*** Transport in Porous Media, *Vol. 117*(1), pp. 125-147.

Skjaeveland, S., Siqveland, L., Kjosavik, A., Hammervold, W., & Virnovsky, G. (1998). ***Capillary pressure correlation for mixed-wet reservoirs***. Paper presented at the SPE India Oil and Gas Conference and Exhibition, New Delhi, India, February 17-19.

Sonier, F., Souillard, P., & Blaskovich, F. (1988). ***Numerical simulation of naturally fractured reservoirs.*** SPE Reservoir Engineering, *Vol. 3*(04), pp. 1-122.

Spanos, P. (1981). ***Stochastic linearization in structural dynamics.*** Applied Mechanics Reviews, *Vol. 34*(1), pp. 1-8.

Standing, M. B. (1974). ***Notes on Relative Permeability Relationships***. Department of Petroleum Engineering and Applied Geophysics, The Norwegian institute of Technology, Trondheim, Norway. Retrieved from http://www.ipt.ntnu.no/~oletor/Standing-Relperm-Notes.pdf

Standnes, D. C. (2001). ***Enhanced Oil Recovery from Oil-Wet Carbonate Rock by Spontaneous Imbibition of Aqueous Surfactant Solutions***. PhD thesis, Department of Petroleum Technology, University of Stavanger, Stavanger.

Standnes, D. C. (2004). ***Experimental study of the impact of boundary conditions on oil recovery by co-current and counter-current spontaneous imbibition*****.** Energy & fuels, *Vol. 18*(1), pp. 271-282.

Standnes, D. C. (2006). ***Spontaneous imbibition of water into cylindrical cores with high aspect ratio: Numerical and experimental results*****.** Journal of Petroleum Science and Engineering, *Vol. 50*(2), pp. 151-160.

Süli, E., & Mayers, D. F. (2003). ***An introduction to numerical analysis***. Cambridge University press, Cambridge, UK.

Szymkiewicz, A. (2012). ***Modelling water flow in unsaturated porous media: accounting for nonlinear permeability and material heterogeneity***. Springer Science & Business Media, Berlin, Germany.

Thomas, L. K., Dixon, T. N., & Pierson, R. G. (1983). ***Fractured reservoir simulation*****.** SPE journal, *Vol. 23*(01), pp. 42-54.

Torsæter, O. a. S., J. (1985). ***The Effects of Sample Shape and Boundary Conditions on Capillary Imbibition***. Paper presented at the Norwegian Petroleum Directorate/Danish Energy Agency Chalk research program Symposium/seminar, Stavanger, Norway, May 21-22.

Uleberg, K., & Kleppe, J. (1996). ***Dual Porosity, Dual Permeability Formulation for Fractured Reservoir Simulation***. Paper presented at the RUTH Seminar, Stavanger, Norway, 1996.

Unsal, E., Mason, G., Morrow, N. R., & Ruth, D. W. (2009). ***Bubble snap-off and capillary-back pressure during counter-current spontaneous imbibition into model pores*****.** Langmuir (American Chemical Society publications), *Vol. 25*(6), pp. 3387-3395.

Ursin, J. R., & Zolotukhin, A. B. (1997). ***Fundamentals of petroleum reservoir engineering***. Høyskoleforlaget, Stavanger, Norway.

Warren, J., & Root, P. J. (1963). ***The behavior of naturally fractured reservoirs*****.** SPE journal, *Vol. 3*(03), pp. 245-255.

Young, T. (1805). ***An Essay on the Cohesion of Fluids - Philosophical Transactions***. Royal society London, 95,

Zhang, X., Morrow, N. R., & Ma, S. (1995). ***Experimental Verification of a Modified Scaling Group for Spontaneous Imbibition*****.** SPE Reservoir Engineering, *Vol. 11*(04), pp. 280-285.

Appendices

A. ECLIPSE file

A.1 - ECLIPSE DATA-file

The ECLIPSE simulator uses input data prepared in a DATA-file consisting of eight sections (some sections are optional), each with a range of available keywords to describe reservoir conditions. The following data organisation is based on Pettersen (2006):

RUNSPEC	Required. *Includes run specifications such as grid size, phases included, units, etc.*
GRID	Required. *Defines shape and grid dimensions, petrophysical properties (porosity, permeability, transmissibility).*
EDIT	Optional. *Enables the user to define changes to the grid data after ECLIPSE has processed them.*
PROPS	Required. *Fluid and rock properties (relative permutabilities, capillary pressure, density, etc)*
REGIONS	Optional. *Enables the user to define regions with different input values than generally defined (relative permeability curves).*
SOLUTION	Required. *Initialization data (initial pressures, fluid saturations).*
SUMMARY	Optional. *Enables user to specify which data items to write to report files.*
SCHEDULE	Required. *Well definitions, operating schedule, production specifications (rate- and pressure-restrictions, time steps).*

A.2 - Basecase code T12_CU5FC_MARCO.DATA

```
============================================================
RUNSPEC
============================================================

TITLE
SI of water into chalk saturated with decane

DIMENS
20   20   20  /

OIL

WATER

LAB

EQLDIMS
1 100 20 1 20 /

TABDIMS
2 1 60 4 2 2 /

NUPCOL
4 /

START
01 'JAN' 2016  /

NSTACK
50 /

UNIFOUT

UNIFIN

GRIDOPTS
YES  /


============================================================
GRID
============================================================

NOECHO

--The basic grid is a cube
DX
8000*0.038 /

DY
8000*0.038 /

DZ
8000*0.038 /
```

```
--Permeability in fracture area
PERMX
8000*100000 /

PERMY
8000*100000 /

PERMZ
8000*100000 /


--Permeability in matrix area
--IX1-IX2-JY1-JY2-KZ1-KZ2
BOX
6 15 6 15 6 15 /

PERMX
1000*2 /
PERMY
1000*2 /
PERMZ
1000*2 /

ENDBOX

--Porosity in fracture area
PORO
8000*0.99 /

-- Porosity in matrix area
--IX1-IX2-JY1-JY2-KZ1-KZ2
BOX
6 15 6 15 6 15 /

PORO
1000*0.423 /
ENDBOX

TOPS
400*0 /

MINPV
1E-10 /

INIT

--Closing of 5 sides of the cube
EQUALS
MULTX    0 5 5 6 15 6 15 /
MULTX    0 15 15 6 15 6 15 /
MULTZ    0 6 15 6 15 15 15 /
MULTY    0 6 15 5 5 6 15 /
MULTY    0 6 15 15 15 6 15 /
/

CARFIN
--Defining local grid refinement in outermost block in direction of flow
```

```
--LGRname  i1   i2   j1  j2   k1  k2   NX  NY  NZ    Max#WellsInLgr
'WP3HLGR' 6    15   6   6    6   15   50  5   50      0          /

CARFIN
--Defining local grid refinement in second block in direction of flow
-- LGRname  i1   i2   j1  j2   k1  k2   NX  NY  NZ    Max#WellsInLgr
'WP4HLGR' 6    15   7   7    6   15   30  3    30      0          /

AMALGAM
'WP3HLGR' 'WP4HLGR' /
/

ENDFIN


================================================================
PROPS
================================================================

SWOF
--Relative permeability and capillary pressure in matrix area
```

--Sw	krw	kro	Pc (atm)
0	0	1	8
0.02	5.08854E-06	0.96654021	4.3014632
0.04	4.07083E-05	0.933222089	3.259250674
0.06	0.000137391	0.900049439	2.770799395
0.08	0.000325667	0.867026287	2.469192334
0.1	0.000636068	0.834156911	2.25794868
0.12	0.001099125	0.801445861	2.098747569
0.14	0.001745369	0.76889799	1.972848347
0.16	0.002605333	0.736518485	1.869824598
0.18	0.003709546	0.704312903	1.783337647
0.2	0.005088541	0.672287212	1.709274656
0.22	0.006772848	0.640447843	1.644829911
0.24	0.008792998	0.608801748	1.588011279
0.26	0.011179524	0.577356461	1.537356813
0.28	0.013962955	0.546120186	1.491762984
0.3	0.017173825	0.515101886	1.450375692
0.32	0.020842662	0.484311398	1.412518223
0.34	0.025	0.453759578	1.377641693
0.36	0.029676369	0.423458461	1.345289427
0.38	0.0349023	0.393421482	1.315069831
0.4	0.040708325	0.363663735	1.286633997
0.42	0.047124975	0.334202317	1.259654869
0.44	0.05418278	0.305056761	1.233804645
0.46	0.061912274	0.276249624	1.208725775
0.48	0.070343985	0.247807265	1.183987684
0.5	0.079508447	0.219760936	1.15901391
0.52	0.08943619	0.192148332	1.132946766
0.54	0.100157745	0.165015903	1.104372175
0.56	0.111703643	0.138422427	1.070703133
0.58	0.124104417	0.11244492	1.026626226
0.6	0.137390596	0.087189146	0.959532884
0.62	0.151592713	0.062810502	0.832758127
0.64	0.166741299	0.03956291	0.497896562
0.66	0.182866884	0.017952049	-1.249265119
0.68	0.2	0	-6

```
/


--Relative permeability in fracture area
-- Straight line relperm and zero Pc
-- SW        krw       kro    Pcow (atm)
0.00000   0.00000    1.000  0.00000
1.00000   1.00000    0.000  0.00000 /

RSCONST
0   0.1 /

PVTW
1    1       4.4D-5          1.0          0 /
/

ROCK
1.05         4.2D-5         /
/

DENSITY
0.731   0.9982  0.0097  /
/

PVDO
1.0  1.0   0.95
10   0.9   0.95 /
/


============================================================
REGIONS
============================================================

EQUALS
FIPNUM             2   1    20  1   20   1   20 /
SATNUM             2   1    20  1   20   1   20 /
-- MATRIX IS REGION 1 AND FRACTURE IS REGION 2
FIPNUM 1           6   15   6   15   6   15 /
SATNUM             1   6   15   6   15   6   15 /
/


============================================================
SOLUTION
============================================================

--Water saturation in fracture area
SWAT
8000*1.00 /


--Defining initial water saturation and pressure in matrix area
----------IX1-IX2-JY1-JY2-KZ1-KZ2
BOX
6  15  6  15  6  15 /
```

```
SWAT
1000*0.00  /
ENDBOX

PRESSURE
8000*1  /

RPTRST
BASIC=5  NORST=1  FREQ=5 SOIL   SWAT   PRESSURE PCOW KRW  KRO   /


============================================================
SUMMARY
============================================================

ROEIW
1  /

ROFT
1  2  /
/

RWFT
1  2 /
/

ROE
1 /

RUNSUM

EXCEL


============================================================
SCHEDUELE
============================================================

RPTRST
BASIC=2 /

MESSAGES
9* 10000 2*  /

DRSDT
0  /

TUNING
0.00 10.25 0.005 0.005 /
/
50 1* 200  /

TSTEP
50*0.001  /

TSTEP
50*0.002  /
```

```
TSTEP
50*0.002 /

TSTEP
50*0.002 /

TSTEP
50*0.002  /

TSTEP
50*0.002 /

TSTEP
50*0.002  /

TSTEP
50*0.002  /

TSTEP
50*0.002  /

TSTEP
50*0.002  /

TSTEP
50*0.002  /

TSTEP
50*0.002  /

TSTEP
50*0.005  /

TSTEP
50*0.005  /

TSTEP
50*0.005  /

TSTEP
50*0.005  /

TSTEP
50*0.005  /

TSTEP
50*0.005  /

TSTEP
50*0.005  /

TSTEP
50*0.005 /

TSTEP
50*0.005 /
```

```
TSTEP
50*0.005 /

TSTEP
50*0.005  /

TSTEP
50*0.005 /

TSTEP
50*0.005 /

TSTEP
50*0.005 /

TSTEP
50*0.005  /

TSTEP
50*0.005 /

TSTEP
50*0.005 /

TSTEP
50*0.005 /

TSTEP
50*0.005  /

TSTEP
50*0.005 /

END
```

B. History match of test 23

Table 13: key input parameters used to generate final capillary pressure and relative permeability curves used in history matching of test 23.

Corey exponents and endpoint relative permeabilities		Capillary pressure constants and exponents		Endpoint saturations	
n_w	3	c_w	0.684	S_{wi}	0
n_o	1.14	c_o	-0.00152	S_{or}	0.32
k_{rw}*	0.2	a_w	0.304		
k_{ro}*	1	a_o	1.52		

Table 14: Tabulated values for Pc, k_{rw} and k_{ro} for different water saturations used in history match of test 23.

S_w [fraction]	K_{rw} [fraction]	K_{ro} [fraction]	P_c [atm]
0	0	1	8
0.02	5.08854E-06	0.96654	2.245099
0.04	4.07083E-05	0.933222	1.818159
0.06	0.000137391	0.900049	1.607036
0.08	0.000325667	0.867026	1.472227
0.1	0.000636068	0.834157	1.375452
0.12	0.001099125	0.801446	1.30108
0.14	0.001745369	0.768898	1.241306
0.16	0.002605333	0.736518	1.191713
0.18	0.003709546	0.704313	1.149576
0.2	0.005088541	0.672287	1.113108
0.22	0.006772848	0.640448	1.081073
0.24	0.008792998	0.608802	1.052587
0.26	0.011179524	0.577356	1.026997
0.28	0.013962955	0.54612	1.003805
0.3	0.017173825	0.515102	0.982624
0.32	0.020842662	0.484311	0.963146
0.34	0.025	0.45376	0.945122
0.36	0.029676369	0.423458	0.928346
0.38	0.0349023	0.393421	0.912641
0.4	0.040708325	0.363664	0.897856
0.42	0.047124975	0.334202	0.883853
0.44	0.05418278	0.305057	0.870501
0.46	0.061912274	0.27625	0.857671
0.48	0.070343985	0.247807	0.84522
0.5	0.079508447	0.219761	0.832979
0.52	0.08943619	0.192148	0.820724
0.54	0.100157745	0.165016	0.80812

0.56	0.111703643	0.138422	0.794616
0.58	0.124104417	0.112445	0.77918
0.6	0.137390596	0.087189	0.759595
0.62	0.151592713	0.062811	0.730107
0.64	0.166741299	0.039563	0.670636
0.66	0.182866884	0.017952	0.452731
0.68	0.2	0	-6

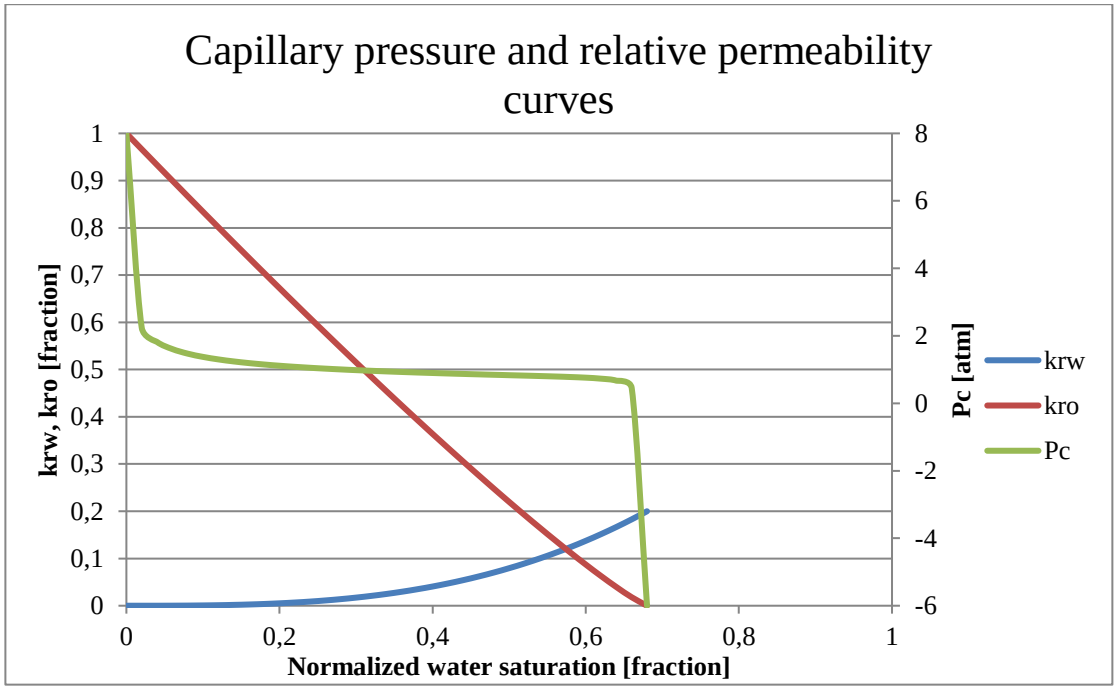

Figure B.1: Relative permeability curves (k_{rw}, k_{ro}) on the primary y-axis, capillary pressure curve on the secondary y-axis plotted against corresponding water saturation on the x-axis.

C. Co-current simulations based on test 23

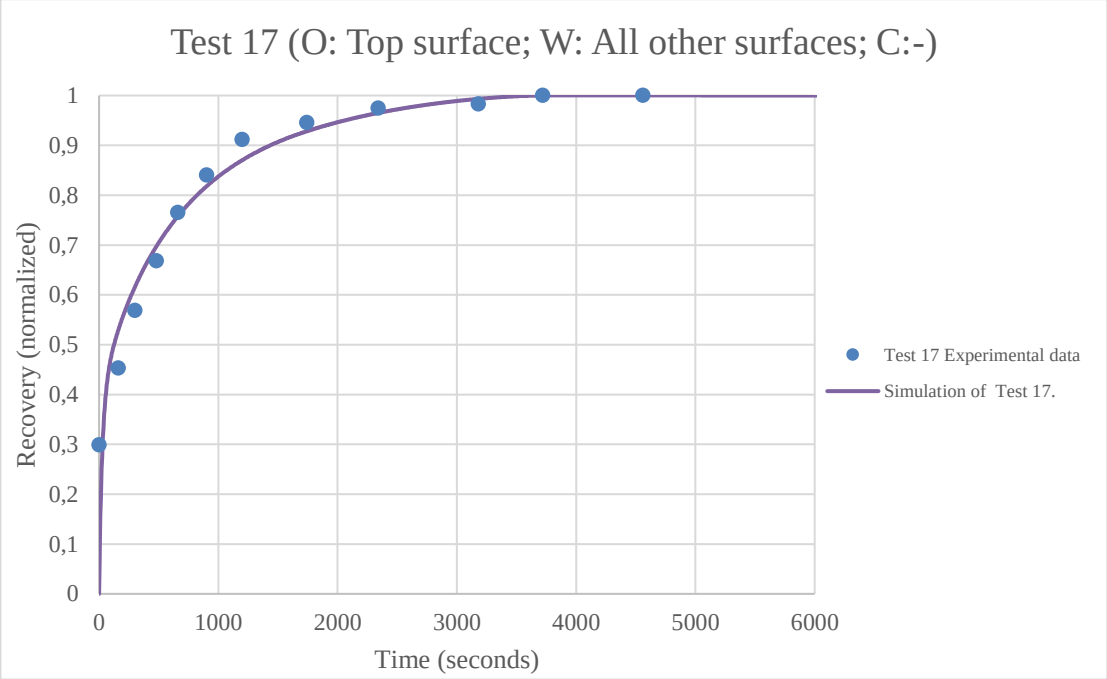

Figure C.1: Comparison between experimental and simulated oil recovery curves for co-current imbibition test 17.

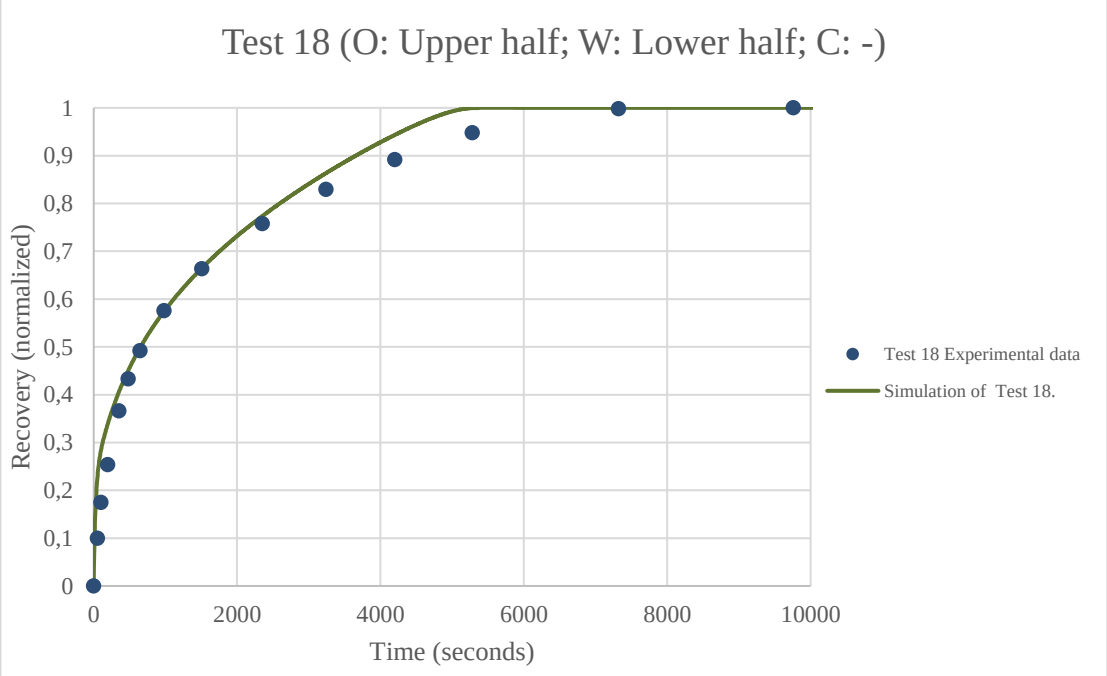

Figure C.2: Comparison between experimental and simulated oil recovery curves for co-current imbibition test 18.

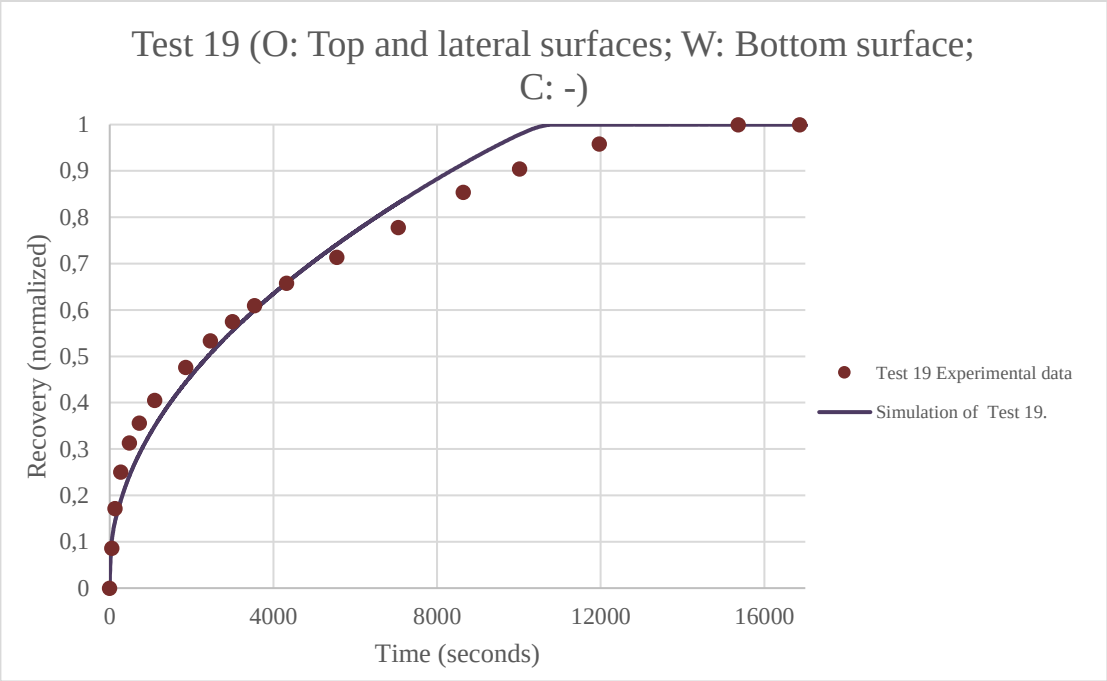

Figure C.3: Comparison between experimental and simulated oil recovery curves for co-current imbibition test 19.

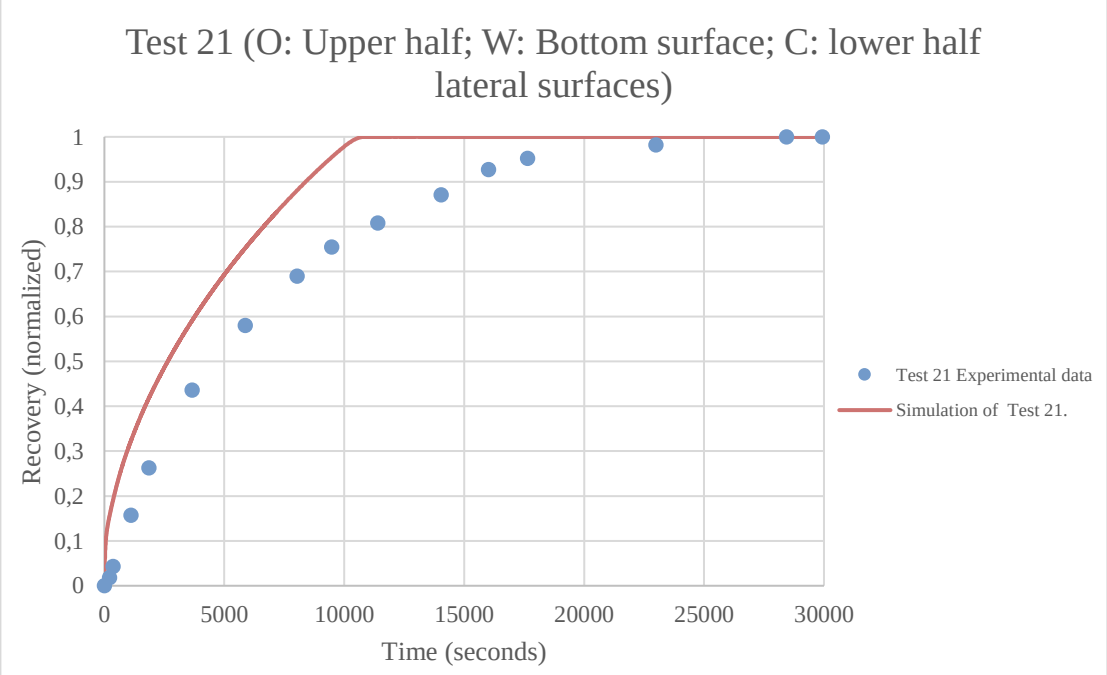

Figure C.4: Comparison between experimental and simulated oil recovery curves for co-current imbibition test 21.

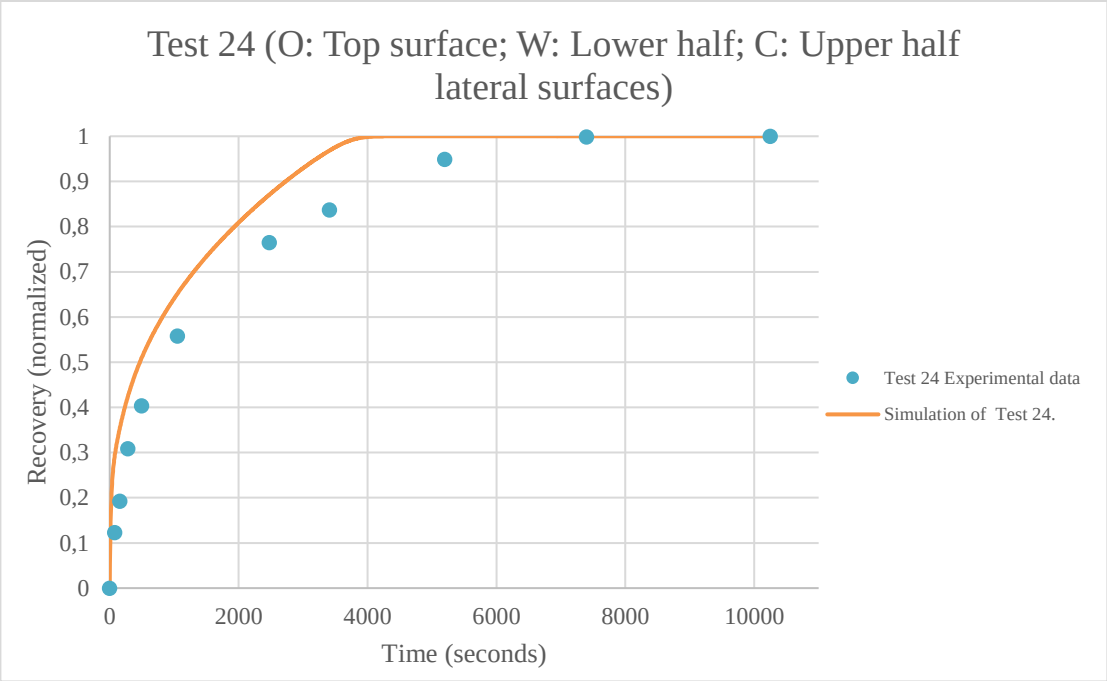

Figure C.5: Comparison between experimental and simulated oil recovery curves for co-current imbibition test 24.

D. History match of test 22

Table 15: key input parameters used to generate final capillary pressure and relative permeability curves used in history matching of test 22.

Corey exponents and endpoint relative permeabilities		Capillary pressure constants and exponents		Endpoint saturations	
n_w	3	c_w	0.375	S_{wi}	0
n_o	1.14	c_o	-0.00078	S_{or}	0.26
k_{rw}*	0.2	a_w	0.156		
k_{ro}*	1	a_o	2		

Table 16: Tabulated values for Pc, k_{rw} and k_{ro} for different water saturations used in history match of test 22.

S_w [fraction]	K_{rw} [fraction]	K_{ro} [fraction]	P_c [atm]
0	0	1	8
0.02	3.948E-06	0.96925	0.68953
0.04	3.159E-05	0.93862	0.61873
0.06	0.0001066	0.9081	0.5807
0.08	0.0002527	0.87772	0.55511
0.1	0.0004936	0.84746	0.53603
0.12	0.0008529	0.81734	0.5209
0.14	0.0013543	0.78735	0.50842
0.16	0.0020216	0.7575	0.49783
0.18	0.0028784	0.7278	0.48865
0.2	0.0039484	0.69824	0.48056
0.22	0.0052554	0.66884	0.47333
0.24	0.0068229	0.63959	0.4668
0.26	0.0086747	0.61051	0.46084
0.28	0.0108345	0.58159	0.45536
0.3	0.013326	0.55286	0.45027
0.32	0.0161728	0.5243	0.44553
0.34	0.0193987	0.49593	0.44106
0.36	0.0230273	0.46777	0.43683
0.38	0.0270823	0.43981	0.4328
0.4	0.0315875	0.41206	0.42893
0.42	0.0365664	0.38454	0.42517
0.44	0.0420429	0.35727	0.42149
0.46	0.0480406	0.33024	0.41784
0.48	0.0545831	0.30349	0.41417
0.5	0.0616943	0.27702	0.41041

0.52	0.0693977	0.25086	0.40645
0.54	0.077717	0.22503	0.40216
0.56	0.086676	0.19957	0.39732
0.58	0.0962983	0.17449	0.39158
0.6	0.1066077	0.14985	0.38431
0.62	0.1176278	0.1257	0.37437
0.64	0.1293823	0.10211	0.35933
0.66	0.1418949	0.07918	0.33337
0.68	0.1551892	0.05704	0.27961
0.7	0.1692891	0.03593	0.1295
0.72	0.2	0	-6

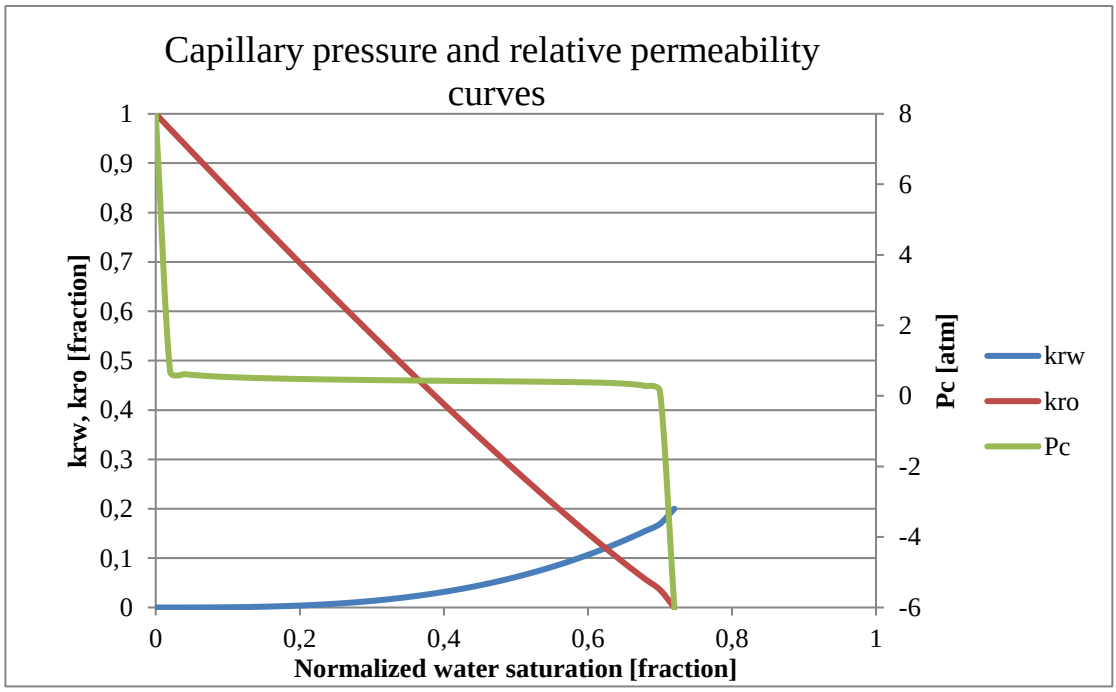

Figure D.1: Relative permeability curves (k_{rw}, k_{ro}) on the primary y-axis, capillary pressure curve on the secondary y-axis plotted against corresponding water saturation on the x-axis.